GBE

Genome Biology and Evolution

SMBE

Reticulate Speciation and Barriers to Introgression in the *Anopheles gambiae* Species Complex

Jacob E. Crawford[1,2,*], Michelle M. Riehle[3], Wamdaogo M. Guelbeogo[4], Awa Gneme[4], N'Fale Sagnon[4], Kenneth D. Vernick[5], Rasmus Nielsen[2,†] and Brian P. Lazzaro[1,†]

[1]Department of Entomology, Cornell University

[2]Department of Integrative Biology, University of California, Berkeley

[3]Department of Microbiology, University of Minnesota

[4]Centre National de Recherche et de Formation sur le Paludisme, Ouagadougou, Burkina Faso

[5]Unit of Insect Vector Genetics and Genomics, Institut Pasteur, Paris, France

*Corresponding author: E-mail: j.crawford@berkeley.edu.
[†]These authors contributed equally to this work.

Accepted: October 19, 2015

Data deposition: This project has been deposited at NCBI Short Read Archive under the accession BioProject ID PRJNA273873.

Abstract

Speciation as a process remains a central focus of evolutionary biology, but our understanding of the genomic architecture and prevalence of speciation in the face of gene flow remains incomplete. The *Anopheles gambiae* species complex of malaria mosquitoes is a radiation of ecologically diverse taxa. This complex is well-suited for testing for evidence of a speciation continuum and genomic barriers to introgression because its members exhibit partially overlapping geographic distributions as well as varying levels of divergence and reproductive isolation. We sequenced 20 genomes from wild *A. gambiae s.s.*, *Anopheles coluzzii*, *Anopheles arabiensis*, and compared these with 12 genomes from the "GOUNDRY" subgroup of *A. gambiae s.l.* Amidst a backdrop of strong reproductive isolation, we find strong evidence for a speciation continuum with introgression of autosomal chromosomal regions among species and subgroups. The X chromosome, however, is strongly differentiated among all taxa, pointing to a disproportionately large effect of X chromosome genes in driving speciation among anophelines. Strikingly, we find that autosomal introgression has occurred from contemporary hybridization between *A. gambiae* and *A. arabiensis* despite strong divergence (~5× higher than autosomal divergence) and isolation on the X chromosome. In addition to the X, we find strong evidence that lowly recombining autosomal regions, especially pericentromeric regions, serve as barriers to introgression secondarily to the X. We show that speciation with gene flow results in genomic mosaicism of divergence and introgression. Such a reticulate gene pool connecting vector taxa across the speciation continuum has important implications for malaria control efforts.

Key words: *Anopheles*, speciation, introgression, population genetics, gene flow.

Introduction

Speciation is a fundamental evolutionary process generating biodiversity and remains a central focus of evolutionary biology. Following The Modern Synthesis of Evolutionary Biology, speciation was commonly thought to require complete reproductive isolation of nascent taxa, often through geographic isolation (Dobzhansky 1937; Mayr 1942). Under this model, gene pools become separated by geography and diverge in reproductive isolation with no genetic exchange. However, an alternative, more fluid, view of species boundaries and divergence as a continuum may be more appropriate in some cases (reviewed in Harrison and Larson 2014). Both empirical examples and theory support the possibility that the process of speciation can include some gene flow either through intermittent hybridization in the early phases of divergence or through secondary contact (Bolnick and Fitzpatrick 2007; Nachman and Payseur 2012). This model deviates from the geographic isolation model in that it includes intermediate stages where reproductive isolation is incomplete between nascent taxa and hybridization results in genetic exchange between diverging gene pools.

Models of speciation with gene flow posit that speciation in the face of hybridization will result in regions of the genome that are differentiated while others introgress and mix between gene pools (Bazykin 1969; Wu 2001). A number of scenarios could lead to hybridization between taxa including secondary contact following a period of allopatric divergence, divergence in parapatry, sympatric speciation, or other similar models. The geographical details of the divergence process are likely associated with different genetic mechanisms. In the case of sympatric speciation, differentiated regions fail to introgress among taxa presumably due to natural selection against migrant alleles because of local natural selection against those alleles due to ecological misfit, while secondary contact models are more likely to involve selection against alleles that are neutral in the native genomic background but incompatible with the alternative genomic background (i.e., Bateson–Dobzhansky–Muller incompatibilities; Bateson 1909; Dobzhansky 1937; Muller 1940). Of course, these genetic mechanisms need not be mutually exclusive among speciation models. Regardless of the underlying genetic mechanisms, genomic regions in linkage disequilibrium (LD) with the incompatible loci also become differentiated over time, providing suitable genomic context for additional incompatible loci to accumulate, and the proportion of the genome that remains differentiated grows until reproductive isolation is complete. Building on the implied importance of recombination and LD in enabling this process, it has been suggested that genomic regions with restricted meiotic recombination, such as chromosomal inversions and centromeric regions, will facilitate this process and play an important role in speciation in the face of hybridization (Begun et al. 2007; McGaugh and Noor 2012; Mackay et al. 2012). Genomic regions with restricted meiotic recombination in hybrids are thought to be important in the formation and maintenance of species boundaries in the face of gene flow because the hitchhiking process involved in selection against maladaptive introgressed variants will affect larger genomic swaths in lowly recombining regions (Noor et al. 2001; Rieseberg 2001; Navarro and Barton 2003; Butlin 2005; Hoffmann and Rieseberg 2008). However, currently available empirical evidence supporting a role of centromeric regions is confounded by the effects of natural selection on linked sites (Charlesworth 1998; Noor and Bennett 2009; Cruickshank and Hahn 2014).

A number of studies have shown strong differences between sex chromosomes (X or Z) and autosomes in the rates of genetic divergence and introgression and therefore inferred a role for sex chromosomes in speciation among pairs of species in systems ranging from *Drosophila* to Hominids. Empirical and theoretical evidence also supports the hypothesis that the X chromosome may play an important role in maintaining species boundaries ("large-X effect"; Charlesworth et al. 1987; Coyne and Orr 1989; Garrigan et al. 2012; Sankararaman et al. 2014). Genetic divergence tends to be higher on sex chromosomes relative to autosomes and introgressed regions are underrepresented on the sex chromosomes, presumably owing to reduced recombination rates along sex chromosomes and exposure of recessive incompatible loci in the heterogametic sex (Coyne and Orr 1989; Geraldes et al. 2006; Sankararaman et al. 2014).

Unambiguously demonstrating differential gene flow along the genomes of diverging taxa is challenging for two reasons. First, most pairs of taxa that are most likely to hybridize tend to be very closely related, and may share substantial polymorphism either through inheritance from the ancestral population or due to ongoing genetic exchange, making it difficult to distinguish between the two (Hey 2006). Second, certain population genetic statistics used to measure differentiation are also sensitive to the population genetic effects of background or positive natural selection, thus confounding the signals of differential gene flow and natural selection (Charlesworth 1998; Noor and Bennett 2009). Indeed, many of the well-known empirical examples of genomic regions remaining differentiated in the face of gene flow have been called into question based on the possible confounding effects of selection in generating signals of differentiation (Cruickshank and Hahn 2014). Thus, further work is needed to understand the genomic architecture of speciation in the face of hybridization.

The *Anopheles gambiae* species complex in sub-Saharan Africa is well-suited for studying the genomic architecture of speciation. Prior to the 1940s, *A. gambiae* was considered a single biologically variable species, but crossing studies and genetic analysis led to the naming of nine morphologically similar species that vary in their geographic distribution, geographic overlap with other complex members, and ecology (reviewed in Coetzee et al. 2013). It is becoming increasingly appreciated from ecological distinctions and recent discoveries of additional genetic substructure that, even within species, *Anopheles* species frequently form partially reproductively isolated and differentiated subpopulations (Costantini et al. 2009; Gnémé et al. 2013; Lee et al. 2013). As an example of this dynamic, a new subgroup of *A. gambiae s.l.* named GOUNDRY was discovered in Burkina Faso that shares larval habitats with other subgroups, but prefers to rest outdoors as adults (Riehle et al. 2011). Although genetic distinctions are clear among most taxa within the species complex, both mixed mating swarms and hybrids have been documented (Marchand 1983; Diabaté et al. 2006), implying an absence of strict geographical isolation and an important role for postzygotic barriers to introgression in some cases.

Among taxa within this species complex, the most substantial effort has been dedicated to understanding the status, history, and genomic consequences of reproductive isolation between two members of the *A. gambiae* species complex, *Anopheles coluzzii* (previously the M molecular form of *A. gambiae*; Coetzee et al. 2013) and *A. gambiae* (previously the S molecular form of *A. gambiae*) (Turner et al. 2005; Lawniczak et al. 2010; Neafsey et al. 2010;

Weetman et al. 2012). These two taxa are mostly reproductively isolated in the field, although they are compatible in captivity (della Torre et al. 2001; Lawniczak et al. 2010). Internal subdivisions exist even within the molecular forms (Slotman et al. 2006, 2007) and recent evidence indicates an often high level of local *A. coluzzii–A. gambiae* hybridization (Lee et al. 2013), illustrating the potential for introgression within the *A. gambiae* group.

Firm conclusions regarding the degree of reproductive isolation and the age of these two taxa have been controversial. This is due in part to the fact that studies of *A. coluzzii–A. gambiae* were based on single nucleotide polymorphism (SNP) panels that preclude measurement of absolute sequence divergence, low-resolution sequencing data sets, and sequence data sets from small samples of laboratory mosquito colonies. In addition, they relied on statistical approaches that are incapable of distinguishing between multiple confounding population genetic processes. In particular, these analyses relied on measures of relative divergence, which are not robust to variation in recombination rates and natural selection across the genome and do not explicitly distinguish between lineage sorting of ancestral polymorphism and introgression (Charlesworth 1998; Noor and Bennett 2009; Hahn et al. 2012; Cruickshank and Hahn 2014). Relatively few studies have addressed divergence among other members of the species complex, and the same analytical concerns apply here as well (Wang-Sattler et al. 2007; Neafsey et al. 2010; O'Loughlin et al. 2014). A recent study used a phylogenetic approach to test for introgression among members of the *A. gambiae* species complex and found evidence for substantial introgression among many members of the complex, also arguing that the X chromosome has played an important role in speciation (Fontaine et al. 2015). However, additional questions remain about the nature of species boundaries and the genomic architecture of barriers to introgression in this system. In particular, it remains unclear whether signals of introgression reflect only historical hybridization or also signify the result of contemporary hybridization. In addition, whether certain autosomal genomic regions may also serve as barriers to introgression among a background of extensive autosomal introgression remains to be established. Understanding the nature of species boundaries in this system may reveal principles underlying the process of speciation in the absence of geographic isolation, but it also has relevance for public health because this complex includes several major vectors of malaria, which continues to place a devastating burden on local human populations (World Health Organization 2013).

In this study, we analyzed a panel of 32 newly generated and previously available genomes from wild-caught females from the *A. gambiae* species complex, representing multiple points along the speciation continuum within this complex. We conducted detailed population genetic analysis of these data to address questions regarding introgression among taxa of varying levels of divergence as well as questions regarding the genomic architecture of barriers to introgression.

Materials and Methods

Details regarding mosquito samples, DNA sequencing, next-generation sequencing bioinformatics, and standard population genetic analyses can be found as supplementary material, Supplementary Material online.

Introgression Analysis and D Statistics

To explicitly differentiate between introgression and ancestral lineage sorting, we used a modification of the ABBA-BABA test (Green et al. 2010; Durand et al. 2011). This test uses the *D* statistic to compare the distribution of alleles on the four taxon tree ((H1,H2),H3),O), where H1 and H2 are sister taxa and H3 and O are the outgroups. Under the null hypothesis of a perfect tree structure and no gene flow, the number of derived mutations that are shared only between the genomes of H2 and H3 (ABBA) is expected to equal the number of those that are shared only between H1 and H3 (BABA). *D* is then calculated as the standardized difference between the numbers of ABBAs and the number of BABAs with an expectation that *D* is zero under the null hypothesis (Green et al. 2010). Significant excess sharing of derived alleles between H3 and either H1 or H2 will result in a nonzero *D* and provides evidence of introgression. In our case, such tests are not appropriate because the alternative to no introgression is not only asymmetric introgression between an outgroup and one of the ingroups, but also potentially approximately equal amounts of introgression between the outgroup and each of the two ingroups (fig. 1). For that reason we use a modified test in which we instead consider the length distribution of fragments of shared ancestry. Because haplotypes are broken down by recombination over successive generations, the length distribution of shared haplotypes among populations is informative regarding the time since the most recent introgression event (Pool and Nielsen 2009; Gravel 2012). After *t* generations, the mean length of a shared haplotype is approximately $(r(1-m)(t-1))^{-1}$, where *r* is the recombination rate and *m* is the proportion of introgressed individuals in the population (Gravel 2012). Because *t* will be smaller for introgressed haplotypes than for shared ancestral haplotypes, the mean length of introgressed haplotypes will be longer resulting in longer clusters of excess ABBAs or BABAs. We used patterns of LD to approximate this expectation and deviations from it by calculating variance in the *D* statistic among genomic blocks, $\mathrm{Var}[D_{\mathrm{BLOCK}}]$, to detect physical clusters of correlated genomic segments consistent with an excess of long-shared haplotypes, and compared it with its null distribution generated by permuting fragments among blocks in order to manually break up possible correlations. If the observed value of $\mathrm{Var}[D_{\mathrm{BLOCK}}]$ is significantly larger than that predicted from permuted fragments of size, which

should be >10× the average length of the decay of LD, we conclude that the genomes harbor introgressed haplotypes.

We divided the genome into blocks of 500 informative sites (i.e., ABBAs and BABAs). These genomic blocks were then divided into 100 segments of 5 informative sites. We chose this block size because this number of sites corresponded to a physical size of ~100 × L_{LD}, where L_{LD} is the physical distance at which point LD decays to background levels. As a result, we could then divide the genomic blocks into 100 segments that would be larger in physical size than L_{LD}. Because introgressed haplotypes will be highly correlated over exceptionally high physical distances relative to ancestral haplotypes, we expect that the size of introgressed haplotypes would exceed L_{LD} while ancestral haplotypes would not. For the tests involving *A. gambiae* and *Anopheles arabiensis* as the H3 taxon, the mean genomic block length was ~250 and ~350 kb, respectively. Because L_{LD} is approximately 200 bp in this system (supplementary fig. S1, Supplementary Material online), and segments within the blocks were approximately 2.5 or 3.5 kb in size, segments exceeded L_{LD} by a factor of more than 10×. These analyses were conducted using pseudohaploidized genomes from the individuals from each population/species with the highest short-read coverage. In general, sites involved in calculating *D* are not entirely independent due to LD, so permutation and jackknife analyses are necessary to properly test for significance. We have used these corrected tests for significance in the following ways.

For the first test, we calculated the *D* statistic for each genomic block (hereafter D_{BLOCK}) and the variance among D_{BLOCK}, hereafter Var[D_{BLOCK}], to test for an excess in variance among genomic blocks that would be consistent with the presence of correlated genomic segments (haplotypes) with shared derived mutations. Under the null hypothesis of no introgression, Var[D_{BLOCK}] among true genomic blocks derives largely from relatively small ancestral haplotypes such that random permutation of segments among blocks will not affect the variance among blocks. If the genome contains introgressed haplotypes that are larger than the segments, Var[D_{BLOCK}] will be larger when these haplotypes are intact in the empirical data and smaller after random permutation that dissolves correlations among segments. We calculated Var[D_{BLOCK}] among genomic blocks in the empirical data. Then, for each comparison, we permuted the internal ~2.5 kb segments among genomic blocks and recalculated Var[D_{BLOCK}] for each permuted genome. Then Var[D_{BLOCK}] from the empirical data was compared to the distribution of Var[D_{BLOCK}] from permuted genomes to ask whether variance among genomic blocks is higher in the empirical data where true correlations remain intact relative to the permuted genomes where variance in *D* will be driven largely by segregating ancestral haplotypes.

For the second test, we established confidence intervals for estimates of the D_{BLOCK} statistic in order to identify individual genomic blocks with significant evidence for introgression. To do so, we conducted block jackknife analyses within each genomic block (Green et al. 2010) by dropping each genomic segment within a given block in turn and recalculating D_{BLOCK}. We calculated 95% confidence intervals for each genomic block using variance estimated from this jackknife procedure. These confidence intervals are presented as ribbons in figure 2.

For the third test, we established genome-wide thresholds corrected for multiple testing in order to identify genomic blocks exceeding these thresholds consistent with recent introgression. We conducted the permutation of segments within blocks procedure as above, but for each permuted genome, we calculated D_{BLOCK} and retained the maximum and minimum values of D_{BLOCK}. To determine whether any individual true genomic blocks showed evidence of significant excess sharing of derived alleles, we established 95% critical thresholds (table 1) from this permutation procedure and compared the value of D_{BLOCK} among true blocks. These genome-wide critical thresholds are presented as dashed lines in figure 2.

To determine whether introgression has been very recent between *A. arabiensis* and either *A. coluzzii* or GOUNDRY, we compared the proportion of the genome in windows with significant *D* values between sympatric *A. arabiensis* from Burkina Faso and allopatric *A. arabiensis* from Tanzania (Marsden et al. 2014). Because the standard assumption of introgression with only one of the two sister taxa holds for this test, we calculated the standard error of *D* for each comparison using the block jackknife approach and used a *Z*-test to assess significance (Green et al. 2010; Durand et al. 2011).

Comparing Genetic Divergence among Genomic Regions

To test hypotheses related to the role of recombination in determining the genomic architecture of reproductive isolation in this system, we divided the genome into regions based on expected levels of recombination in hypothetical hybrids. A fine-scale genetic map is not yet available for *Anopheles* mosquitoes, but it has been shown in *Drosophila* that recombination rates approach zero within several megabases on each side of the centromere and also near the telomeres (Fiston-Lavier et al. 2010; Chan et al. 2012). Although patterns of LD are also affected by processes other than local meiotic recombination rates, estimated recombination rates should give a rough approximation of expected LD across the genome. In fact, patterns of LD have been used to define genetic maps in some vertebrates and correspond approximately to genetic maps based on experimental crosses or pedigrees (McVean et al. 2004; Auton et al. 2013). We measured background LD (see Supplementary Material online for details) in our *A. coluzzii* and *A. arabiensis* samples, taking average r^2 values within 10 kb physical windows across the genome. We found that LD was relatively constant across the genome except for large increases near the autosomal

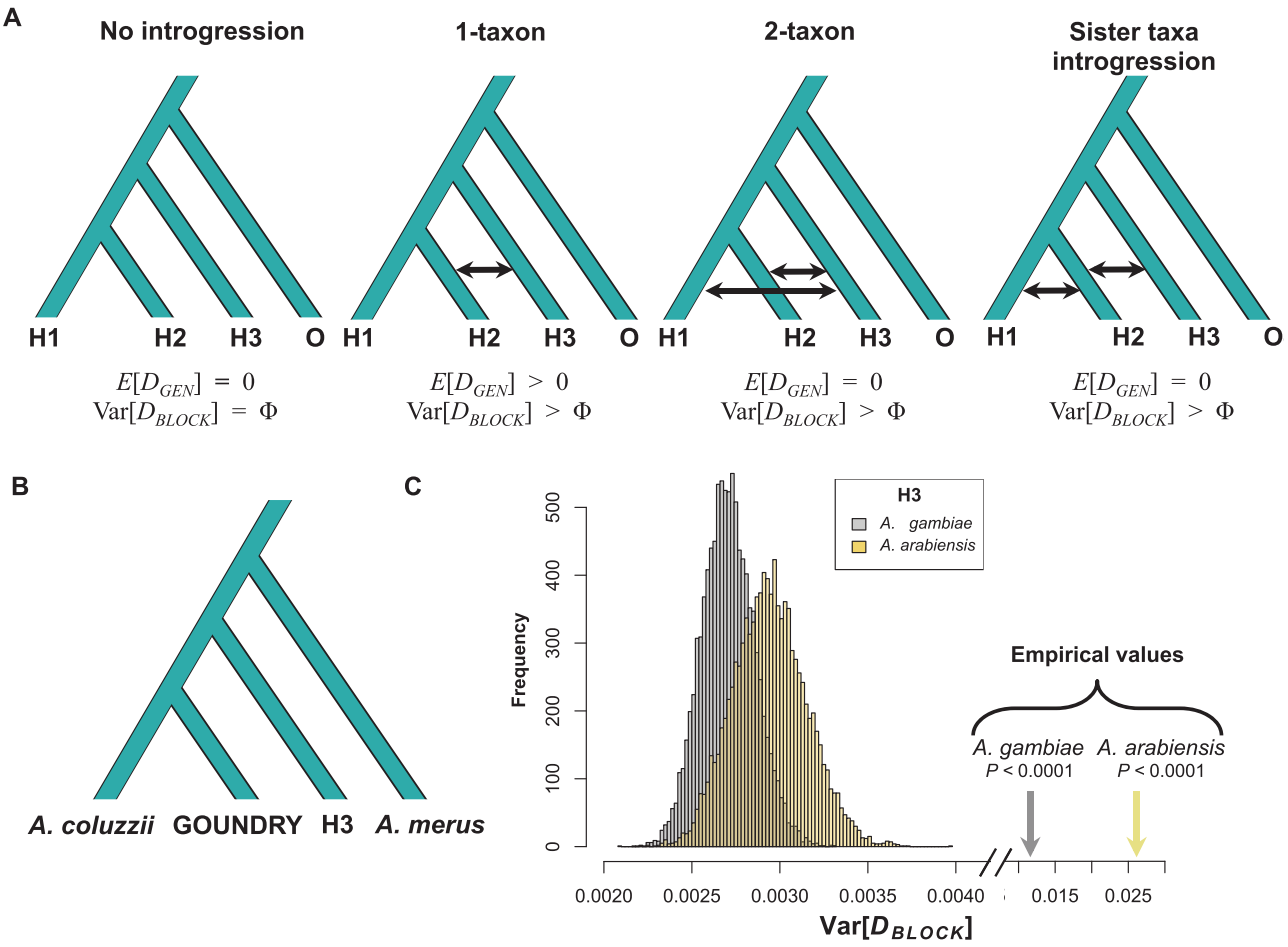

Fig. 1.—Excess variance in D_{BLOCK} indicates recent introgression. (*A*) Four-taxon trees used in ABBA-BABA tests with three alternative introgression models. The expected genome-wide value of the *D* statistic ($E[D_{GEN}]$) is presented below in addition to the expected variance among *D* statistics calculated in genomic blocks ($\mathrm{Var}[D_{BLOCK}]$). $\mathrm{Var}[D_{BLOCK}]$ under the "No introgression" model is unknown and indicated here by Φ for comparison in other models. The "2-taxon" and "Sister taxa introgression" models may result in $E[D_{GEN}]$ of 0 but are expected to have increased $\mathrm{Var}[D_{BLOCK}]$ relative to the No introgression model providing a test for introgression. (*B*) The four-taxon test tree used for analysis. (*C*) The distributions of $\mathrm{Var}[D_{BLOCK}]$ calculated from 10^4 permuted genomes (see Methods) for test trees with *Anopheles gambiae* (grey) and *Anopheles arabiensis* from Burkina Faso (yellow) as the H3 are presented. The true $\mathrm{Var}[D_{BLOCK}]$ values from each empirical data set, presented on a broken *x*-axis for comparison, are greater than all permuted genomes in each case consistent with the presence of introgressed haplotypes in these genomes.

centromeres and smaller increases near the telomeres (supplementary fig. S2, Supplementary Material online). Based on this pattern and the assumption that recombination rates in *Anopheles* correspond approximately to the *Drosophila* genetic map, we defined several broad recombinational categories for analysis. We first defined the "Pericentromeric–Telomeric" regions of the autosomes to be all windows within 10 MB on either side of the centromere or within 1 MB from the telomere. It should be noted that we assumed that the starting and ending coordinates of the *A. gambiae* PEST (Pink Eye STandard) reference chromosomal sequences were reliable indicators for distance from centromeres and telomeres. Unless a chromosomal inversion was present, all remaining regions on the autosomes were assigned to the "Freely Recombining" category. For the comparison between *A. gambiae* and *Anopheles merus*, we assigned all windows inside the 2R*op* chromosomal inversion complex to the "Autosomal-Inversion" category. We used the outer coordinates for 2R*o* and 2R*p* breakpoint regions estimated by Kamali et al. (2012).

The X chromosome was categorized for each comparison, according to species-specific conditions. We did not define a general Pericentromeric–Telomeric category for two reasons: 1) We did not observe an increase in LD in the euchromatic regions near centromeres and telomeres (supplementary fig. S2, Supplementary Material online) similar to increases observed on the autosomes. 2) In *Drosophila* (Fiston-Lavier et al. 2010; Chan et al. 2012), the pericentromeric reduction

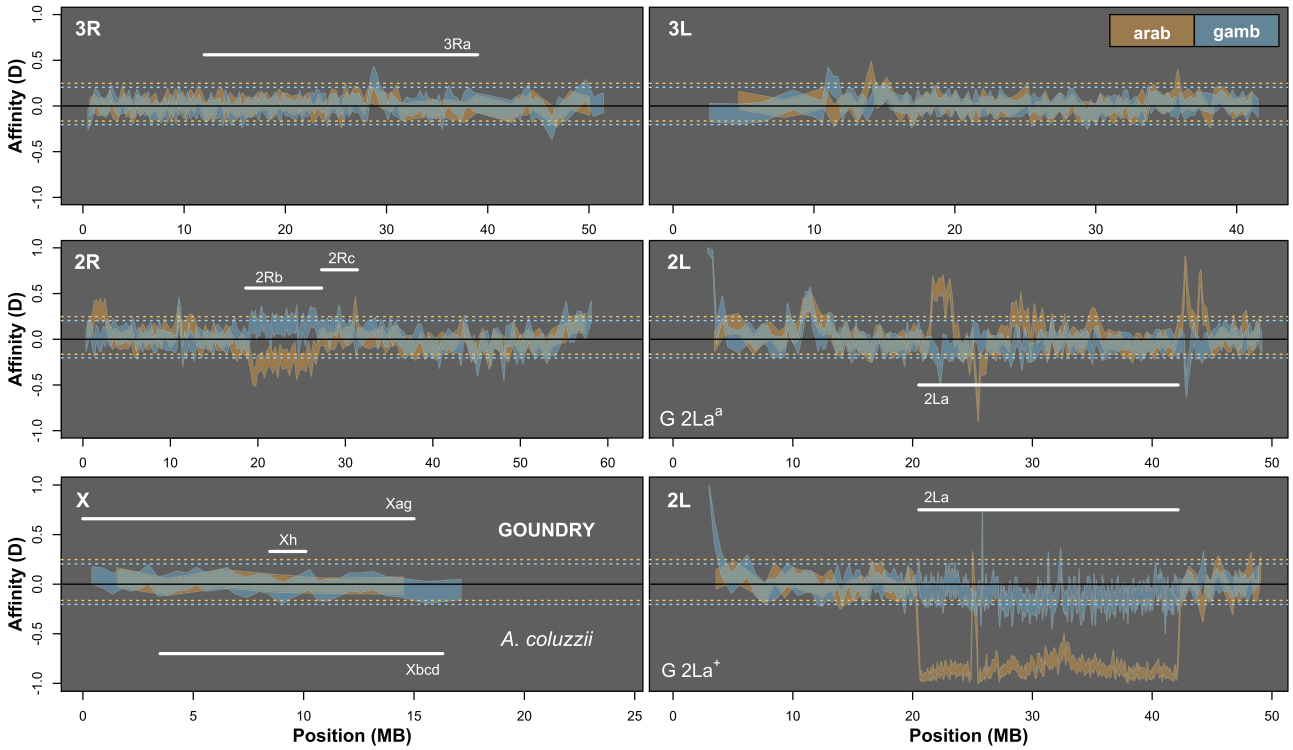

Fig. 2.—Significant autosomal introgression between pairs of *Anopheles* species and subspecies. ABBA-BABA statistics were calculated in nonoverlapping windows of 500 informative sites using *Anopheles merus* as the outgroup. Blue ribbon indicates 95% confidence region for introgression between *Anopheles gambiae* ($2La^{a/+}$) and GOUNDRY (positive *D*; $2La^{a/a}$ and $2La^{+/+}$; *3R+*; *Xag*) and *Anopheles coluzzii* (negative *D*; $2La^{a/a}$; *3R+*; *Xag*). Orange ribbon indicates 95% confidence region for introgression between *Anopheles arabiensis* ($2La^{a/a}$; *3Ra*; *Xbcd*) and GOUNDRY (positive *D*) and *A. coluzzii* (negative *D*). Horizontal dotted lines (orange = *A. arabiensis*; blue = *A. gambiae*) indicate genome-wide significance level after correction for multiple testing. Positions of relevant chromosomal inversions are indicated with horizontal white lines. A full list of genes within significant windows is given in supplementary table S2, Supplementary Material online.

Table 1
Modified Block-based ABBA-BABA Test of Introgression

H1[a]	H2[a]	H3[a]	Upper 95%[b]	Lower 95%[b]	Proportion of the genome in sig *Anopheles coluzzii* Windows[c]	Proportion of the genome in sig GOUNDRY Windows[c]
A. coluzzii	GOUNDRY	*Anopheles gambiae*	0.204	−0.204	0.0114	0.0325
A. coluzzii	GOUNDRY	*Anopheles arabiensis* (Burkina Faso)	0.248	−0.164	0.0364	0.0354
A. coluzzii	GOUNDRY	*A. arabiensis* (Tanzania)	0.256	−0.156	0.0323	0.0312

Note.—Genome-wide 95% thresholds and the proportions of the genome in significant windows are presented for three comparisons.
[a]Taxonomic assignment in the ABBA-BABA test tree ((H1,H2),H3),O).
[b]Boundaries of the genome-wide 95% threshold region estimated using block jackknife estimates of standard error within genomic regions after permutation ($n = 10^4$ replicates).
[c]For each comparison, windows exceeding the 95% thresholds were identified, and the sum of their length was compared with the total length of the *A. gambiae* PEST reference.

in recombination affects a relatively small region on the X relative to the autosomes, and we have excluded a large heterochromatic region around the centromere that likely encompasses the affected region in *Anopheles*. For the comparison between *A. gambiae* and *A. merus*, and the comparison between *A. coluzzii* and *A. gambiae*, the entire euchromatic region on the X was considered Freely Recombining because no inversions differentiate these groups on the X. For the comparison between *A. gambiae* and *A. arabiensis*, we assigned the entire euchromatic region of the X as "X-Inversion," because these species are differentiated across nearly 75% of the entire chromosome and introgression rates have been estimated to be 0 in laboratory crosses (Slotman et al. 2005). For the comparison between GOUNDRY and both A. *coluzzii* and *A. gambiae*, the entire euchromatic X was categorized as Freely Recombining except

for the region spanning 8.47–10.1 MB, which was categorized as X-Inversion. As described in Supplementary Material online, we were not able to identify inversion breakpoints for the GOUNDRY inversion, but these coordinates correspond to the outer boundaries of the region with reduced nucleotide diversity (fig. 3).

To identify regions that are barriers to introgression in the *A. gambiae* species complex, we compared genetic divergence among the four genomic categories using the following logic. Because genome-wide variation in mutation rate and the effects of linked selection could also lead to genomic variation in divergence among species even in the absence of introgression, we jointly analyzed absolute genetic divergence (D_{xy}) and nucleotide diversity (π) in 10 kb nonoverlapping windows and asked whether differences in genetic divergence among genomic regions are observed that cannot be explained by differences in nucleotide diversity (where diversity approximates the effects of linked selection or variation in mutation rate). D_{xy} is an estimate of $2\mu t + 4N_e\mu$, where N_e is the effective size of the ancestral population, μ is the mutation rate, and t is the divergence time. π provides an estimate of $4N_e\mu$, where N_e is the effective size of the current population. By jointly considering these, we can make comparisons among genomic regions that differ substantially in $4N_e\mu$ such that differences in D_{xy} largely reflect differences in $2\mu t$. We note that this analysis assumes that estimates of $4N_e\mu$ from current populations (or in most cases, average of the estimates from the two subgroups) are reliable estimates of $4N_e\mu$ in the ancestral population, and we believe this to be a reasonable assumption given the recency of radiation of the *A. gambiae* species complex. Under scenarios with gene flow among diverging subgroups or species, t will be smaller in regions that have introgressed, so regional barriers to gene flow are expected to have especially large values of t, and therefore values of D_{xy} that are larger than regions with similar $4N_e\mu$ but more introgression. In contrast, under a model of divergence in allopatry with no introgression, t is approximately equal among genomic regions such that divergence should be determined largely by $4N_e\mu$, and thus correlate well with nucleotide diversity, even if elevated. We made comparisons among genomic regions using this framework and assuming that most freely recombining autosomal regions will have been introgressed at some point in the history of divergence because high rates of recombination inhibit associations between barriers to introgression (e.g., hybrid sterility factors) and surrounding chromosomal regions. Therefore, we compared other genomic regions to freely recombining autosomal regions with respect to both divergence and nucleotide diversity to ask whether these other regions harbor excess divergence consistent with less introgression in these regions. Comparisons of distributions of genetic divergence and nucleotide diversity were made using the M–W test in R (R Development Core Team 2011).

For this analysis, we used only 10 kb windows containing at least 600 sequenced sites with data for the taxa involved. We chose to use a focal species comparison to minimize the number of comparisons for concise presentation, but we obtain similar results in other comparisons (e.g., GOUNDRY vs. *A. arabiensis*) because most variation in divergence depends on variance in coalescence in the ancestral population. We note that estimates of nucleotide diversity in GOUNDRY are not reliable estimates of the ancestral population because GOUNDRY is partially inbred and has the large swept region on the X (Crawford JE, et al. submitted), so we used estimates of nucleotide diversity from *A. coluzzii* only for the comparison with GOUNDRY.

Results

Genome Sequencing and Population Genetic Analysis

We have completely sequenced the genomes of 20 field-captured female *Anopheles* mosquitoes from Burkina Faso and Guinea using the Illumina HiSeq2000 platform. We sequenced *A. coluzzii* ($n = 10$), *A. gambiae* ($n = 1$), and *A. arabiensis* ($n = 9$) and compared these sequences with a panel of 12 *A. gambiae* GOUNDRY genomes. Most individuals were sequenced to an average read depth of 9.79 × (range 5.94–20.03 per individual), while one individual each from GOUNDRY, *A. coluzzii*, and *A. gambiae* was sequenced to at least 16.44 × (supplementary table S1, Supplementary Material online). We also used publicly available genome sequences from *A. merus* ($n = 6$) as an outgroup and an *A. arabiensis* genome from Tanzania for a geographically distinct comparison (Marsden et al. 2014). We conducted population genetic analysis of aligned short-read data using genotype likelihoods and genotype calls calculated using the probabilistic inference framework ANGSD (Korneliussen et al. 2014).

Broad-scale genetic relationships among the *Anopheles* included in this analysis were confirmed in a companion analysis (Crawford JE, et al. submitted). Briefly, a neighbor-joining tree based on genome-wide genetic distance shows that GOUNDRY is more closely related to *A. coluzzii* than to *A. gambiae*, and these three taxa are more closely related to *A. arabiensis* than to *A. merus*. This topology is consistent with other phylogenetic estimates for this species complex (Kamali et al. 2012; Fontaine et al. 2015).

Recent Autosomal Introgression

An important first step toward understanding the nature of species boundaries in *A. gambiae* species complex is to determine whether introgression has occurred among diverging *Anopheles* taxa and whether introgression is restricted to closely related taxa or occurs among more distant taxa. We tested for historical and contemporaneous introgression along the speciation continuum using a variance-based modification of the D statistic (Var[D_{BLOCK}]) that allows for

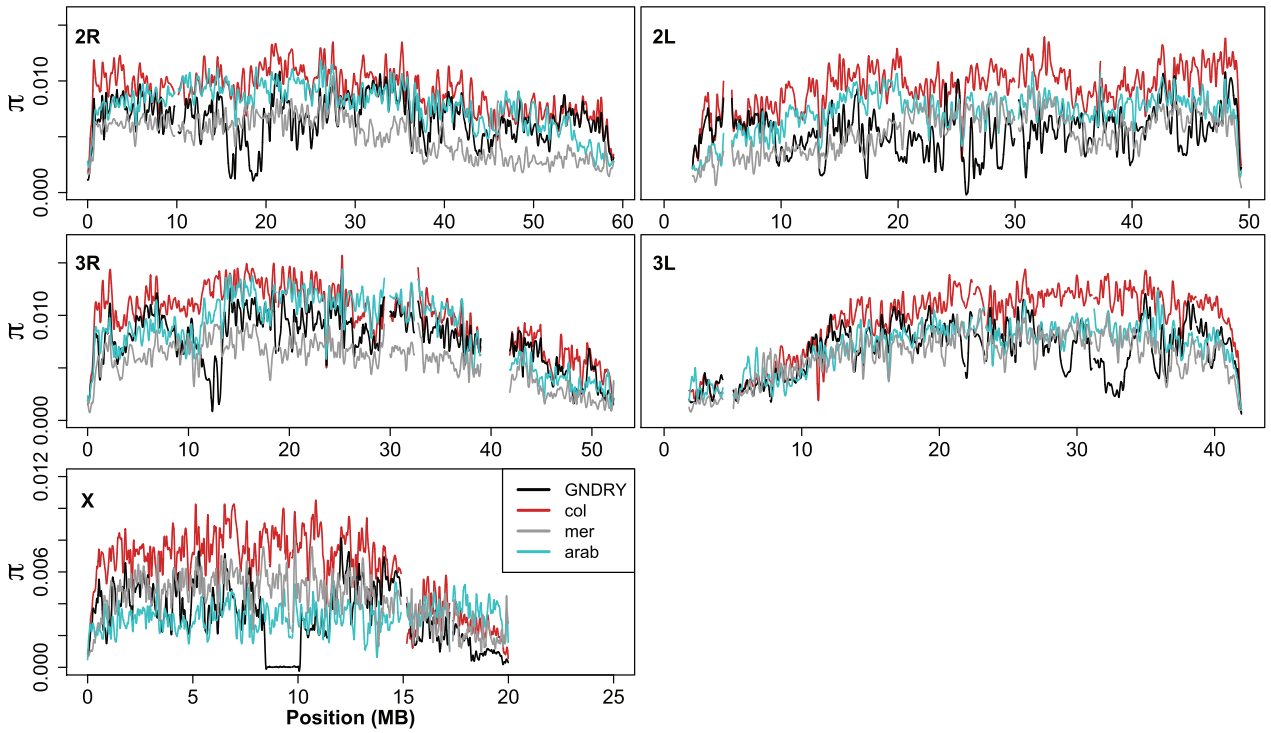

Fig. 3.—Chromosomal distributions of nucleotide diversity (π) at intergenic sites (LOESS-smoothed with span of 1% using 10 kb nonoverlapping windows). Low complexity and heterochromatic regions were excluded. col = *Anopheles coluzzii*; GNDRY = GOUNDRY ($2La^{+/+}$ individual excluded in 2 L estimate); mer = *Anopheles merus*; arab = *Anopheles arabiensis*.

introgression among multiple taxa in a four-taxon tree (Methods; fig. 1) by comparing the variance in *D* among genomic blocks with variance expected under the null hypothesis of shared ancestry due to lineage sorting. We applied this test using two four-taxon trees and find evidence for recent introgression among species and subgroups of the *A. gambiae* species complex. We calculated the *D* statistic using a four-taxon tree with *A. coluzzii* and GOUNDRY as the sister taxa (H1 and H2, respectively), *A. merus* as the outgroup (O), and either *A. gambiae* or *A. arabiensis* as the test group, H3. After comparing the Var[D_{BLOCK}] in the empirical data with Var[D_{BLOCK}] from 10^4 randomly permutated genomes, we find significant evidence for introgression between the *A. coluzzii*–GOUNDRY clade and *A. gambiae* ($P < 0.0001$, fig. 1). Using *A. coluzzii* and GOUNDRY as the ingroups again, but with *A. arabiensis* as the test taxon (H3), we also find that the Var[D_{BLOCK}] is significantly larger than all 10^4 permuted genomes ($P < 0.0001$, fig. 1). In fact, Var[D_{BLOCK}] is larger than the largest value of the 10^4 permuted genomes by a factor of 3.7 in the *A. gambiae* test (Var[D_{BLOCK}] = 0.0122) and by a factor of 6.7 in the *A. arabiensis* test (Var[D_{BLOCK}] = 0.0268) (fig. 1). These results indicate that the observation of shared polymorphism between these taxa can be attributed in part to introgression.

Contemporary Introgression between *Anopheles gambiae* and *Anopheles arabiensis*

Although the above analysis is sensitive to contemporary introgression, we used an additional approach comparing signals of introgression with sympatric and allopatric populations to explicitly ask whether introgression has occurred via contemporary hybridization. If introgression has occurred recently, we expect stronger affinity among sympatric populations relative to allopatric populations (Nosil et al. 2003; Grant et al. 2005; Noor and Bennett 2009). We tested whether introgression between *A. coluzzii* and *A. arabiensis* has been recent with sympatric *A. arabiensis* versus allopatric *A. arabiensis* from Tanzania. In this case, we used the standard ABBA-BABA test because we are explicitly testing a simple "1-taxon" model (fig. 1). We tested for introgression using a four-taxon tree of high-coverage individuals with the two *A. arabiensis* individuals as the ingroups (H1 and H2) and *A. coluzzii* as the test group (H3) and found a significant excess of shared derived mutations between *A. coluzzii* and sympatric *A. arabiensis* relative to allopatric *A. arabiensis* from Tanzania ($D = -0.0542$, Block Jackknife *Z*-score = −13.1533, $P = 1.63 \times 10^{-39}$; table 1). Similarly, we used GOUNDRY as H3 and found evidence for significant introgression between sympatric *A. arabiensis* and GOUNDRY ($D = -0.0441$,

Block Jackknife Z-score = −11.7559, $P = 6.58 \times 10^{-32}$; table 1). In line with recent evidence of contemporary hybridization between *A. gambiae* and *A. arabiensis* in Uganda (Weetman et al. 2014), our results provide strong evidence that introgression continues to occur via contemporary hybridization in Burkina Faso that has the potential to impact the evolution of both ecologically and epidemiologically relevant traits.

Introgressed Genes

Introgressed haplotypes may contain genes with potentially important phenotypic effects, and a local reduction in the concentration of introgressed haplotypes along the genome can be indicative of barriers to introgression, so we partitioned the signal of introgression across the genome to identify introgressed chromosomal segments. To do so, we compared each empirical D_{BLOCK} value with genome-wide significance thresholds established by analyzing the distribution of the most extreme D_{BLOCK} values from each of the 10^4 permuted genomes (Methods). Because each D_{BLOCK} statistic is polarized, we can identify windows that show significant introgression between each of the sister taxa (i.e., *A. coluzzii* and GOUNDRY) and H3 (fig. 2). After conservatively correcting for multiple testing by comparing the empirical values with a distribution of genome-wide extreme values from permutations, we find significant evidence of introgression between *A. coluzzii* and both *A. gambiae* and *A. arabiensis*, and the proportions of the genome that are represented by significant windows are 1.1% and 3.6% for *A. gambiae* and *A. arabiensis*, respectively. These introgressed chromosomal blocks include 97 annotated protein-coding sequences introgressed between *A. coluzzii* and *A. gambiae* and 543 introgressed between *A. coluzzii* and *A. arabiensis* (supplementay table S2, Supplementary Material online). Interestingly, we find strong evidence for introgression of the pericentromeric region on chromosome 2L between GOUNDRY and *A. gambiae*, which contrasts starkly with previous suggestions that this region may be a barrier to introgression and important for speciation between these taxa (Turner et al. 2005; Neafsey et al. 2010; Lawniczak et al. 2010). A recent study based on SNP genotype data identified a signal of introgression between *A. coluzzii* and *A. gambiae* in this genomic region and attributed the high frequency of the introgressed haplotype to the sharing of an adaptive insecticide resistance allele at the *kdr* locus (Clarkson et al. 2014).

One window that shows an exceptionally strong introgression signal between *A. coluzzii* and *A. arabiensis* harbors the GABA receptor gene, also known as the "resistance to dieldrin" locus because of the role of this receptor in conferring resistance to the insecticide dieldrin and related insecticides (Ffrench-Constant et al. 1993). Although any resistance phenotype conferred by introgressed alleles is unknown at this point, our finding that the *Rdl* locus has been introgressed between *A. coluzzii* and *A. arabiensis* would be contradictory to previous reports that these species have acquired resistance at this locus through independent but convergent mutations (Du et al. 2005). Moreover, introgression of an allele with adaptive value in the face of insecticide pressure further supports the occurrence of contemporary hybridization between these taxa.

We used the same approach to identify genomic blocks shared between GOUNDRY and two H3 taxa, *A. gambiae* and *A. arabiensis*. We find that windows representing 3.2% of the GOUNDRY genome and 369 protein-coding sequences share a significant excess of derived mutations with *A. gambiae* (table 1). In addition, we find that 3.5% of the GOUNDRY genome harboring 499 protein-coding sequences shares a significant excess of derived mutations with *A. arabiensis*. In line with results above showing evidence of more introgression with sympatric *A. arabiensis* relative to allopatric *A. arabiensis*, we find that the windows with significant evidence of introgression with sympatric (Burkina Faso) *A. arabiensis* cover slightly more of the genome than windows with significant evidence of introgression with allopatric (Tanzania) *A. arabiensis* (table 1). Although only relatively small percentages of these individual genomes show significant evidence of recent introgression, hundreds of protein-coding genes have been shared in each case such that homogenization of these genomic regions may have large effects on phenotypic evolution, exhibited most prominently by the sharing of presumably functional mutations at an insecticide locus in the *A. coluzzii* comparisons.

Although identifying introgressed regions provides insight into the homogenizing effects of hybridization, identifying genomic regions depauperate of recent introgression can provide evidence for genomic barriers to introgression. Despite evidence for considerable introgression on the autosomes, we find no evidence of recent introgression of X chromosome sequence among any subgroups or species, which suggests a disproportionately large role for the X in speciation among these taxa.

Excess Genetic Divergence on the X Chromosome

We hypothesized that long-term differences in introgression along the genome will be reflected in patterns of genetic divergence, because genetic divergence will be partially determined in part by selection for and against introgressed material. This pattern has been notoriously difficult to demonstrate, in part because measurable differences in divergence are slow to develop (Cruickshank and Hahn 2014). As such, we will focus largely on comparisons between more divergent species pairs (*A. coluzzii* vs. *A. arabiensis* and *A. coluzzii* vs. *A. merus*) where differences are most easily identified. To test for genomic barriers among taxa in the *A. gambiae* species complex, we asked whether sequence divergence (D_{xy}) between taxa differed among genomic regions as expected under a model of differential rates of introgression. However, D_{xy} is an

estimator of $2\mu t + 4N\mu$, where μ is the mutation rate, t is the number of generations since the species split, and N is the effective population size of the ancestral population, but $4N\mu$ can vary among genomic regions for reasons unrelated to differential introgression (i.e., variable mutation rate or effects of natural selection on linked sites; fig. 4). Therefore, we jointly analyzed nucleotide diversity (π) as a proxy for $4N\mu$ among genomic regions to avoid confounding intrapopulation effects with differential introgression (see Methods).

Hybrid male sterility maps to the X chromosome in *A. gambiae–A. arabiensis* crosses, and two large X-linked chromosomal inversion complexes (*Xag* and *Xbcd*) suppress recombination on the X in hybrids of these species, so we hypothesized that less frequent introgression may lead to exceptionally high sequence divergence on the X relative to other genomic regions. In support of this hypothesis, we found that nucleotide diversity on the X is significantly lower than on the autosomes (Mann–Whitney [hereafter M–W] $P < 2.2 \times 10^{-16}$), but genetic divergence is significantly higher on the X (M–W $P < 2.2 \times 10^{-16}$; fig. 3). Moreover, genetic divergence is significantly higher in the region harboring inversions (M–W $P < 2.2 \times 10^{-16}$) than in the surrounding chromosome. Nucleotide diversity, however, is also higher in the inverted region relative to the centromere-proximal region (M–W $P < 2.2 \times 10^{-16}$), where nucleotide diversity is especially low, presumably due to the effects of linked selection on neutral genetic variation. Although we cannot formally rule out an elevated mutation rate inside the inverted region, there is no reason to expect the inverted region to be more mutable. This excess genetic divergence on the X is consistent with our results in the ABBA-BABA analysis above showing that the X chromosome lacks evidence of recent introgression among these taxa. In general, these observations are in line with previous analyses of genetic differentiation among *A. arabiensis* and *A. gambiae*, as well as with laboratory backcrossing experiments (Slotman et al. 2005; Neafsey et al. 2010; O'Loughlin et al. 2014), indicating that introgression is particularly inhibited on the X chromosome, and that the X chromosome plays a disproportionately large role in driving speciation.

The X chromosomes of *A. coluzzii* and *A. gambiae* are collinear with that of *A. merus*, so recombination is not expected to be suppressed in contemporary or historical hybrids among these groups. To test whether sequence divergence is exceptionally high on the X relative to the autosomes in these comparisons despite the lack of inverted regions, we compared genetic divergence and nucleotide diversity among genomic regions as described above. We find that genetic divergence between *A. gambiaes.l.* (*A. coluzzii* used as proxy for ancestral population here) and *A. merus* does not scale with nucleotide diversity (fig. 3). Nucleotide diversity is lower on the X than on the autosomes (M–W $P < 2.2 \times 10^{-16}$), but genetic divergence is significantly higher on the X (M–W $P < 2.2 \times 10^{-16}$). This is strong evidence that the autosome continued to be homogenized by introgression after the X chromosome had become a barrier to introgression among these taxa.

Interestingly, despite the relatively recent split time (<0.5 N_e) between *A. coluzzii* and *A. gambiae* (Cruickshank and Hahn 2014; Fontaine et al. 2015), inspection of chromosomal distributions of divergence between *A. coluzzii* and *A. gambiae* reveals a slight elevation in genetic divergence in a chromosomal region where nucleotide diversity is low relative to the rest of the chromosome (~16–20 MB; figs. 4 and 5). Indeed, this particular region coincides with a genomic region recently shown to play a role in assortative mating between these taxa (Aboagye-Antwi et al. 2015), further supporting its role in speciation, especially the early stages. Such signals of excess divergence on the X provide further evidence for a large role of the X in driving speciation in *Anopheles* and suggests that inversions may facilitate speciation but are not required.

Autosomal Barriers to Introgression

Evidence for a large role of the X chromosome is strong, but it remains unclear which, if any, autosomal regions may serve as barriers to introgression. We divided the autosome into three classes based on expected levels of meiotic recombination (freely recombining, chromosomal inversions, pericentromeric and telomeric) and asked whether the regions where recombination may be restricted (i.e., inversions and pericentromeric/telomeric) harbor excess divergence consistent with barriers to introgression. In the comparison between *A. coluzzii* and *A. merus*, we find that pericentromeric and telomeric regions are significantly more diverged as a class than the freely recombining autosome (M–W $P < 2.2 \times 10^{-16}$), but nucleotide diversity is significantly lower in these regions (M–W $P < 2.2 \times 10^{-16}$). In the comparison between *A. coluzzii* and *A. arabiensis*, we generally find remarkably little evidence for elevated divergence across the autosome considering the level of divergence on the X, indicating a long history of introgression and few autosomal barriers. However, inspection of the genomic distribution of nucleotide diversity and divergence (figs. 4 and 5) reveals that the difference between nucleotide divergence and intraspecies diversity is especially high in the pericentromeric region of chromosome 3. Nucleotide diversity is reduced in this region, presumably resulting in part from the effects of intrapopulation positive and negative selection on linked sites. However, the relative increase in D_{xy}, which is not affected by positive selection, suggests that migrant alleles have been selected against in this region such that this region harbors both fewer shared polymorphisms as well as more private mutations relative to the nearby freely recombining regions.

Anopheles merus is fixed for a large private chromosomal inversion complex on chromosome 2 (2R*op*), while other members of the complex carry the alternative forms of the

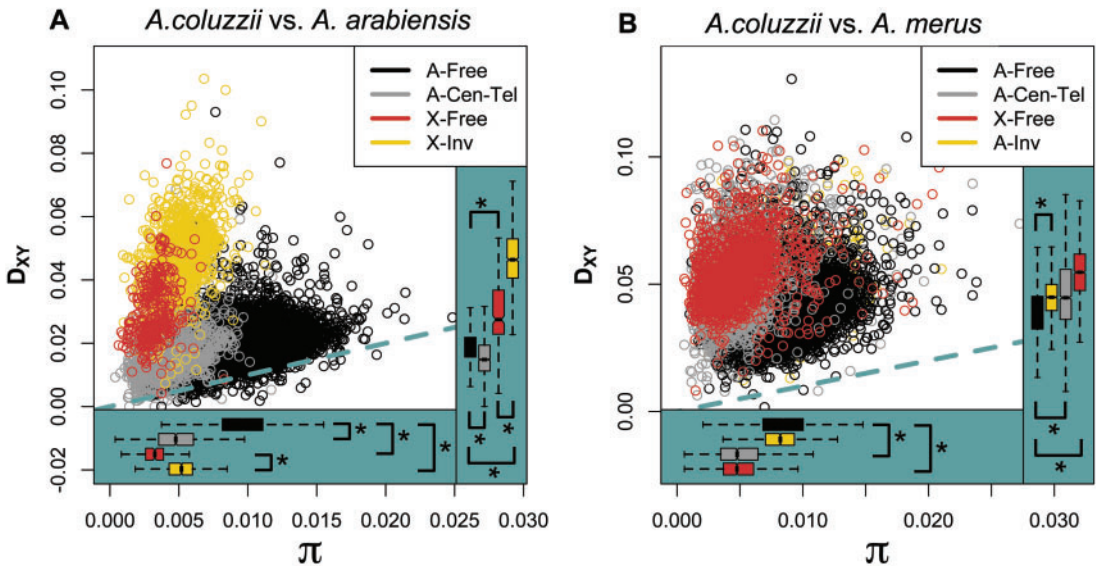

Fig. 4.—Patterns of genetic divergence (D_{xy}) between populations as a function of nucleotide diversity (π) reveal differential gene flow during speciation. Genomic regions defined by expected rates of recombination in hybrids (see Methods) differ in their distributions of nucleotide diversity and genetic divergence, but not always in the same direction, suggesting that gene flow has been restricted on the X and lowly recombining regions in some cases. (*A*) *Anopheles coluzzii* versus *Anopheles arabiensis*; (*B*) *A. coluzzii* versus *Anopheles merus*. Panel legends indicate colors corresponding to genomic location of each 10 kb window where "Free" indicates freely recombining regions, "Cen-Tel" indicates centromeric and telomeric autosomal regions, and "Inv" indicates chromosomal inversions. "A-" and "X-" indicate autosome or X chromosome. Dashed blue-green line indicates perfect correlation. Asterisks indicate M–W tests with $P < 3.92 \times 10^{-5}$ for comparisons indicated with brackets. Note that the *y*-axis scale differs among panels.

overlapping 2R*o* and 2R*p* inversions. We compared genetic divergence in this region with freely recombining autosomal regions and find that the inverted region is significantly more diverged than surrounding genomic regions (M–W $P < 2.2 \times 10^{-16}$; fig. 3). Within-population nucleotide diversity is also slightly higher within the inverted region, but only without correcting for multiple testing (M–W uncorrected $P = 0.0203$; fig. 3), implying that inherently higher levels of diversity in this region could explain increased divergence in this region. These results suggest that, while this inversion may serve as a more recent barrier to introgression, 2R*op* was not likely a primary barrier to introgression among these species, perhaps because it originated subsequent to the evolutionary periods with the highest rates of introgression between *A. gambiaes.l.* and *A. merus*.

Discussion

The permeability of species boundaries among species and subgroups of *Anopheles* has been controversial (Turner et al. 2005; Lawniczak et al. 2010; Neafsey et al. 2010; Turner and Hahn 2010; Cruickshank and Hahn 2014). The original observation of centromeric "islands of divergence" between the M and S (now *A. coluzzii* and *A. gambiae*, respectively) molecular forms led to the conclusion that gene flow among these species was extensive and ongoing, but these islands remained differentiated for reasons presumably related to their role in speciation among these taxa (Turner et al. 2005). Subsequent higher resolution studies observed especially high levels of differentiation in the islands of divergence against a background of differentiation across most of the genome, leading to the conclusion that reproductive isolation among these taxa is more advanced than previously thought (Lawniczak et al. 2010; Neafsey et al. 2010). However, these studies, like others claiming evidence of differential introgression along the genome, did not determine the relative roles of genetic drift, natural selection on linked sites, and introgression in determining the observed levels of differentiation (Cruickshank and Hahn 2014). A recent phylogenomic analysis made a strong case for extensive introgression among taxa within the *A. gambiae* species complex (Fontaine et al. 2015). In line with that conclusion, we use an alternative approach to show that chromosomal segments have introgressed among species at varying points on a speciation continuum (fig. 2). From these and previous results, a consensus is beginning to emerge that, rather than a radiation of discrete well-defined species, the *A. gambiae* species complex exists as a reticulate network of gene pools with offshoot populations and ancestral species remaining connected by periodic hybridization of differential efficiency across the genome. Such a model conflicts with traditional notions of species boundaries and raises questions about phenotypic evolution within a network of ecologically specialized gene pools.

Although the proportion of the individual genomes tested here that we identify with statistical evidence for recent

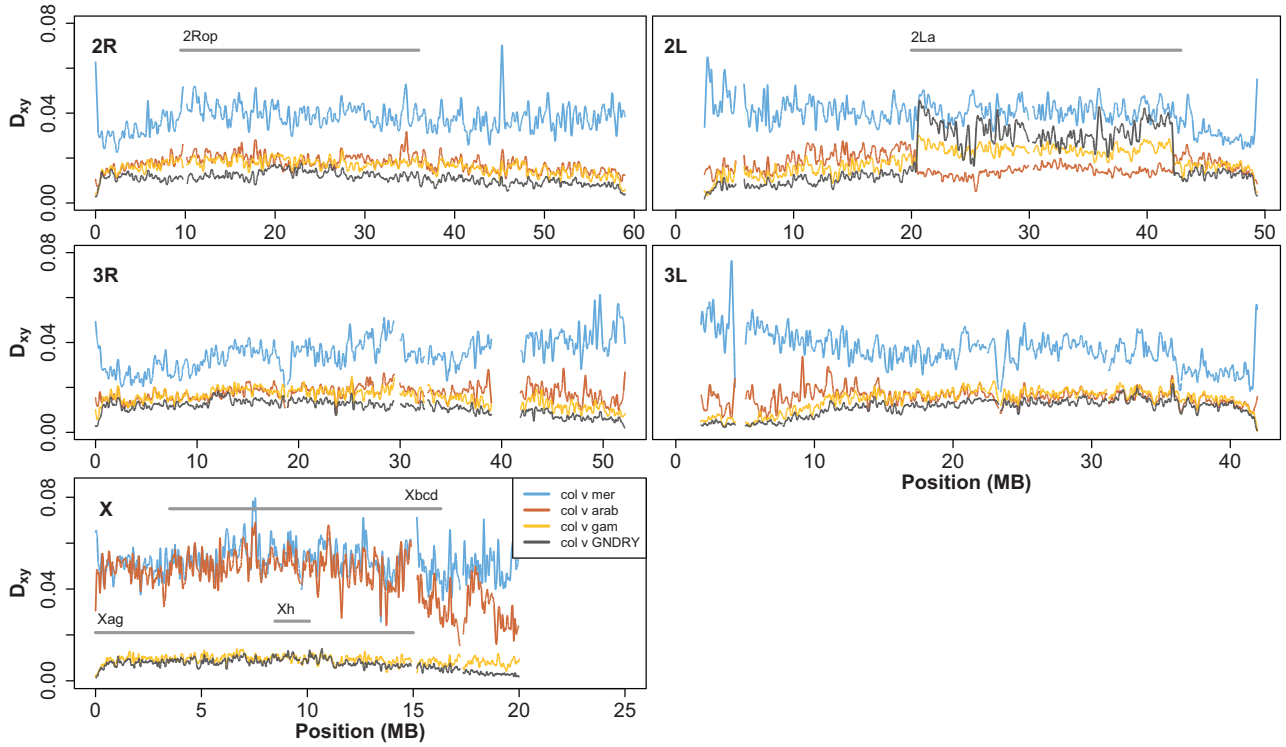

Fig. 5.—Patterns of divergence among subgroups of *Anopheles gambiae s.l.* follow similar curves (LOESS-smoothed with a span of 1% using 10 kb nonoverlapping windows), although differing slightly in magnitude. One exception to this pattern is an increase in the X chromosome pericentromeric region (~15–20 Mb) in the *Anopheles coluzzii* versus *A. gambiae* comparison and inside the 2L*a* inversion where these populations differ in karyotype (G-2L$a^{+/+}$, *A. coluzzii*–2L$a^{a/a}$, *A. gambiae*–2L$a^{a/+}$). Divergence between *A. coluzzii* and both *Anopheles arabiensis* and *Anopheles merus* is increased on the X chromosome, especially inside the inverted *Xag* and *Xbcd* region (*A. coluzzii* vs. *A. arabiensis*) and in pericentromeric regions (*A. coluzzii* vs. *A. merus*). Grey bars indicate locations of differentially fixed chromosomal inversions as well as the 2L*a* inversion and the large sweep on the GOUNDRY X (*Xh*). Low complexity and heterochromatic regions were excluded.

introgression is relatively small (~3%), the effect on the autosome is large over evolutionary time. The relationship between *A. gambiae* and *A. arabiensis* provides an extreme example of variation in the permeability of species boundaries, with evidence of autosomal introgression over the evolutionary history of these two species, including the putative sharing of an insecticide resistance allele in the last 60 years. In stark contrast to this pattern, the X chromosomes of these species remain highly diverged relative to the autosomes, implying that introgression has been ineffective on the X and that the X chromosome is the primary driver of speciation. A recent independent comparison between the *A. arabiensis* and *A. gambiae* genomes supports our conclusion that introgression is a major factor in the evolutionary history of the *A. gambiae* species complex (Fontaine et al. 2015).

Despite the homogenizing effects of extensive introgression among these taxa, distinct genetic clades can be identified implying that some genomic regions have remained differentiated and are incompatible with introgressing haplotypes. Over evolutionary time scales, we expect that natural selection will play a large role relative to drift in determining the composition of ancestry along the genome, resulting in a mosaic of introgressed segments along the genome, as has been observed for Neanderthal ancestry in modern humans (Sankararaman et al. 2014). To test for heterogeneity in ancestry that may reflect the action of natural selection and therefore barriers to introgression, we measured genetic sequence divergence among taxa and showed that long-term differential introgression has indeed shaped patterns of divergence among members of this species complex (figs. 3 and 5). By placing genomic patterns of divergence observed in our data into a phylogenetic context, a model of speciation and its genomic architecture emerges. In conjunction with known ecological differences between the species profiled here (Lehmann and Diabate 2008; Coetzee et al. 2013), our data point to a four-step speciation model in these mosquitoes in which 1) a small founder population expands into and adapts to an available ecological niche in the face of ongoing gene flow, 2) barriers to gene flow establish on the X chromosome, sometimes facilitated by suppressed recombination related to chromosomal inversions, 3) lowly recombining autosomal regions secondarily become restricted from gene flow, and 4) either pre- or postzygotic processes reduce effective gene flow entirely, and freely recombining autosomal

regions become reproductively isolated and accumulate genetic divergence. Implicit to this model is that different regions become barriers to introgression in stages while introgression continues to homogenize the remaining genomic regions as in standard speciation with gene flow models (Wu 2001).

We show that the X chromosome is the most diverged and harbors the least evidence for introgression, suggesting that it is likely a barrier to introgression in multiple *Anopheles* species (figs. 2 and 3). In some cases, chromosomal inversions seem to play an important role. The observation that the X chromosome plays a disproportionately large effect in driving speciation (large-X) is in line with studies from *Anopheles* as well as many other organisms ranging from *Drosophila* to mammals (Coyne and Orr 1989; Geraldes et al. 2008; Garrigan et al. 2012; Sankararaman et al. 2014), but a unifying explanation for this pattern has yet to emerge. Importantly, a recent study of mating behavior showed that assortative mating between *A. coluzzii* and *A. gambiae* is controlled by the pericentromeric region on the X chromosome, providing a functional role for this region in speciation (Aboagye-Antwi et al. 2015). From an evolutionary genetic perspective, however, multiple hypotheses have been posited to explain the underlying evolutionary mechanisms underlying this pattern including the "faster-X" hypothesis, sex ratio meiotic drive, and misregulation of X-linked genes in males (reviewed in Presgraves 2008). The faster-X hypothesis posits that X-linked loci adapt faster than autosomal loci because X-linked recessive mutations are exposed to selection in males that have only a single X chromosome, resulting in faster accumulation of hybrid sterility factors (Charlesworth et al. 1987; Coyne and Orr 1989). Another popular hypothesis involves sex ratio meiotic drive where species-specific sex ratio distorter suppressors are disrupted in hybrids causing hybrid sterility (Frank 1991; Hurst and Pomiankowski 1991). A third hypothesis to explain this pattern is that gene expression dosage compensation of X-linked genes is misregulated in hybrids, causing sterility in hybrids (Lifschytz and Lindsley 1972). Although data have accumulated in *Drosophila* allowing more detailed speculation about the mechanisms underlying the large-X effect (Presgraves 2008), more data are needed to fully understand this pattern in *Anopheles*.

We show that pericentromeric regions also harbor especially high levels of divergence among more distantly related species pairs. This pattern is most apparent in the comparison between *A. gambiae* (*A. coluzzii*) and *A. merus* (figs. 3 and 5) and provides strong evidence that both *A. arabiensis* as well as *A. merus* diverged from *A. gambiae* while continuing to hybridize at a nonnegligible rate in at least the early stages of speciation. Although we could not test for recent introgression among *A. gambiae* and *A. merus* using the ABBA-BABA tests, the pattern of excess divergence in some genomic regions is in contrast to what we would expect under a divergence in allopatry model and is more consistent with historical introgression in freely recombining autosomal regions among *A. gambiae* and *A. merus*, likely in the evolutionary period following the initial species split. In the case of *A. arabiensis*, we show that contemporary hybridization with *A. gambiae* continues to homogenize all autosomal regions except the pericentromeric region of 3L despite strong barriers to genetic introgression across the X chromosome. Similar patterns of elevated divergence in lowly recombining pericentromeric and telomeric regions have also been observed in comparisons between *Drosophila* species (Begun et al. 2007; Langley et al. 2012; Mackay et al. 2012; Garrigan et al. 2014), but our results are the first demonstration of this pattern of excess sequence divergence in *Anopheles*. It is important to note that our results, especially the observation of excess divergence between *A. gambiae* and *A. merus* in low-diversity pericentromeric regions, are robust to the issues confounding previous observations of high differentiation in these regions, because our results derive from absolute measures of divergence instead of relative divergence measures that are highly sensitive to other population genetic processes including natural selection (Charlesworth 1998; Noor and Bennett 2009; Cruickshank and Hahn 2014). Importantly, we conservatively excluded heterochromatic centromeric regions, so the signals we identify reach well into euchromatic autosomal regions that are more robust to bioinformatic artifacts that plague analyses of centromeric regions. These results provide a clear empirical example of the important role of lowly recombining regions as barriers to introgression among hybridizing species.

The ABBA-BABA test has become a preferred method for detecting introgression, but there are several caveats and concerns relating to both the standard test as well as our modified D_{BLOCK} test. First, it is possible that the signals of introgression we have detected are not from the species used in the test, but in fact we have detected introgression from an unsampled, or "ghost," species. Durand et al. (2011) showed that such introgression can affect the results of ABBA-BABA tests. The presence of ghost *Anopheles* species hybridizing with the species sampled here is certainly a possibility and could impact some of our results. However, the possibility of introgression from "ghost taxa" does not change our conclusion that introgression continues among *Anopheles* species, shaping patterns of divergence regardless of exactly which subgroup is the donor. Second, results from our divergence-based analysis suggest that *A. merus* introgressed with an ancestral population of the *A. gambiae* species complex, potentially compromising its use as an outgroup in the ABBA-BABA test. Although such historical introgression could contribute marginally to the false positive rate in our inference, it is not likely to change our conclusion of introgression among taxa because our analysis is focused on long-shared haplotypes that are not likely to be affected by such old introgression. And third, a recent analysis showing that a similar block-wise test of introgression lacked power to identify introgressed haplotypes (Martin et al. 2014) raises questions about the robustness of our D_{BLOCK} analysis. However, there are two

important differences between our approach and the one evaluated by Martin et al. (2014). First, these authors implemented the test based on constant-sized physical windows of the genome, but we used constant-sized blocks of informative sites that varied in their physical size. This is an important distinction because our approach controls for the amount of information in each window, while the number of ancestry informative sites is bound to vary greatly among physical windows in the approach of Martin et al., which is likely to impact the sensitivity of this approach. The second difference between the approaches is that our approach explicitly controlled for LD in the data. We chose block sizes of 500 informative sites because this resulted in average physical window sizes of ~ 250–350 kb (see Methods), which allowed each block to be divided into 100 segments larger in size than the expected distance that LD decays to background levels in this system. As a result, we believe that our approach is a robust approach for identifying introgressed genomic regions and is not likely to suffer from the same concerns raised by Martin et al. (2014).

In sum, our results suggest that species and subgroups in the *A. gambiae* species complex comprise a diffuse and interconnected gene pool that may confer access to beneficial genetic variants from a broad geographic and environmental range. Such genetic affinity has important implications for malaria control. On one hand, transgenes may spread more easily among subgroups and species of malaria vectors, which could reduce the effort needed to reach and manipulate all populations involved in disease transmission. On the other hand, our analysis suggests that certain genomic regions are less likely to cross species boundaries, especially the X chromosome, providing ideal settings for locating transgenes that are not intended for broad and general distribution across the species complex. In both cases, our results underscore the complexities involved in vector control on a continental scale.

Supplementary Material

Supplementary figures S1 and S2 and tables S1 and S2 are available at *Molecular Biology and Evolution* online (http://www.mbe.oxfordjournals.org/) .

Acknowledgments

We thank Matteo Fumagalli, Filipe Vieira, and Tyler Linderoth for assistance with next-generation sequence data analyses and ANGSD. We thank members of the Nielsen group for helpful discussions on various aspects of this work. We also thank Russ Corbett-Detig, Wynn Meyer, and three anonymous reviewers for helpful comments on an earlier version of this manuscript. We are thankful for the use of the Extreme Science and Engineering Discovery Environment, which is supported by National Science Foundation grant number OCI-1053575. This work was supported by National Institutes of Health grant AI062995. This work was also supported by a Cornell Center for Comparative and Population Genomics Graduate Fellowship and the National Institute Of General Medical Sciences of the National Institutes of Health under Award Number F32GM103258 (J.E.C.). The content is solely the responsibility of the authors and does not necessarily represent the official views of the National Institutes of Health.

Literature Cited

Aboagye-Antwi F, et al. 2015. Experimental swap of *Anopheles gambiae*'s assortative mating preferences demonstrates key role of X-chromosome divergence island in incipient sympatric speciation. PLoS Genet. 11:e1005141.

Auton A, et al. 2013. Genetic recombination is targeted towards gene promoter regions in dogs. PLoS Genet. 9:e1003984.

Bateson W. 1909. Heredity and variation in modern lights. In: Seward AC, editor. Darwin and modern science. Cambridge: Cambridge University Press. p. 85–101.

Bazykin AD. 1969. Hypothetical mechanism of speciation. Evolution 23:685–687.

Begun DJ, et al. 2007. Population genomics: whole-genome analysis of polymorphism and divergence in *Drosophila simulans*. PLoS Biol. 5:e310.

Bolnick DI, Fitzpatrick BM. 2007. Sympatric speciation: models and empirical evidence. Annu Rev Ecol Evol Syst. 38:459–487.

Butlin RK. 2005. Recombination and speciation. Mol Ecol. 14:2621–2635.

Chan AH, Jenkins PA, Song YS. 2012. Genome-wide fine-scale recombination rate variation in *Drosophila melanogaster*. PLoS Genet. 8:e1003090.

Charlesworth B. 1998. Measures of divergence between populations and the effect of forces that reduce variability. Mol Biol Evol. 15:538–543.

Charlesworth B, Coyne JA, Barton NH. 1987. The relative rates of evolution of sex chromosomes and autosomes. Am Nat. 130:113–146.

Clarkson CS, et al. 2014. Adaptive introgression between *Anopheles* sibling species eliminates a major genomic island but not reproductive isolation. Nat Commun. 5:4248.

Coetzee M, et al. 2013. *Anopheles coluzzii* and *Anopheles amharicus*, new members of the *Anopheles gambiae* complex. Zootaxa 3619:246–274.

Costantini C, et al. 2009. Living at the edge: biogeographic patterns of habitat segregation conform to speciation by niche expansion in *Anopheles gambiae*. BMC Ecol. 9:16.

Coyne JA, Orr HA. 1989. Patterns of speciation in *Drosophila*. Evolution 43:362–381.

Cruickshank TE, Hahn MW. 2014. Reanalysis suggests that genomic islands of speciation are due to reduced diversity, not reduced gene flow. Mol Ecol. 23:3133–3157.

della Torre A, et al. 2001. Molecular evidence of incipient speciation within *Anopheles gambiae* s.s. in West Africa. Insect Mol Biol. 10:9–18.

Diabaté A, et al. 2006. Mixed swarms of the molecular M and S forms of *Anopheles gambiae* (Diptera: Culicidae) in sympatric area from Burkina Faso. J Med Entomol. 43:480–483.

Dobzhansky TG. 1937. Genetics and the origin of species. New York: Columbia University Press.

Du W, et al. 2005. Independent mutations in the *Rdl* locus confer dieldrin resistance to *Anopheles gambiae* and *An. arabiensis*. Insect Mol Biol. 14:179–183.

Durand EY, Patterson N, Reich D, Slatkin M. 2011. Testing for ancient admixture between closely related populations. Mol Biol Evol. 28:2239–2252.

Ffrench-Constant RH, Rocheleau TA, Steichen JC, Chalmers AE. 1993. A point mutation in a *Drosophila* GABA receptor confers insecticide resistance. Nature 363:449–451.

Fiston-Lavier AS, Singh ND, Lipatov M, Petrov DA. 2010. *Drosophila melanogaster* recombination rate calculator. Gene 463:18–20.

Fontaine MC, et al. 2015. Mosquito genomics. Extensive introgression in a malaria vector species complex revealed by phylogenomics. Science 347:1258524.

Frank SA. 1991. Divergence of meiotic drive-suppression systems as an explanation for sex-biased hybrid sterility and inviability. Evolution 45:262–267.

Garrigan D, Kingan SB, Geneva AJ, Vedanayagam JP, Presgraves DC. 2014. Genome diversity and divergence in *Drosophila mauritiana*: multiple signatures of faster X evolution. Genome Biol Evol. 6:2444–2458.

Garrigan D, et al. 2012. Genome sequencing reveals complex speciation in the *Drosophila simulans* clade. Genome Res. 22:1499–1511.

Geraldes A, Ferrand N, Nachman MW. 2006. Contrasting patterns of introgression at X-linked loci across the hybrid zone between subspecies of the European rabbit (*Oryctolagus cuniculus*). Genetics 173:919–933.

Geraldes A, et al. 2008. Inferring the history of speciation in house mice from autosomal, X-linked, Y-linked and mitochondrial genes. Mol Ecol. 17:5349–5363.

Gnémé A, et al. 2013. Equivalent susceptibility of *Anopheles gambiae* M and S molecular forms and *Anopheles arabiensis* to *Plasmodium falciparum* infection in Burkina Faso. Malar J. 12:204.

Grant PR, Grant BR, Petren K. 2005. Hybridization in the recent past. Am Nat. 166:56–67.

Gravel S. 2012. Population genetics models of local ancestry. Genetics 191:607–619.

Green RE, et al. 2010. A draft sequence of the Neandertal genome. Science 328:710–722.

Hahn MW, White BJ, Muir CD, Besansky NJ. 2012. No evidence for biased co-transmission of speciation islands in *Anopheles gambiae*. Philos Trans R Soc Lond B Biol Sci. 367:374–384.

Harrison RG, Larson EL. 2014. Hybridization, introgression, and the nature of species boundaries. J Hered. 105(Suppl. 1):795–809.

Hey J. 2006. Recent advances in assessing gene flow between diverging populations and species. Curr Opin Genet Dev. 16:592–596.

Hoffmann AA, Rieseberg LH. 2008. Revisiting the impact of inversions in evolution: from population genetic markers to drivers of adaptive shifts and speciation? Annu Rev Ecol Evol Syst. 39:21–42.

Hurst LD, Pomiankowski A. 1991. Causes of sex ratio bias may account for unisexual sterility in hybrids: a new explanation of Haldane's rule and related phenomena. Genetics 128:841–858.

Kamali M, Xia A, Tu Z, Sharakhov IV. 2012. A new chromosomal phylogeny supports the repeated origin of vectorial capacity in malaria mosquitoes of the *Anopheles gambiae* complex. PLoS Pathog. 8:e1002960.

Korneliussen T, Albrechtsen A, Nielsen R. 2014. ANGSD: Analysis of Next Generation Sequencing Data. BMC Bioinformatics 15:356.

Langley CH, et al. 2012. Genomic variation in natural populations of *Drosophila melanogaster*. Genetics 192:533–598.

Lawniczak MKN, et al. 2010. Widespread divergence between incipient *Anopheles gambiae* species revealed by whole genome sequences. Science 330:512–514.

Lee Y, et al. 2013. Spatiotemporal dynamics of gene flow and hybrid fitness between the M and S forms of the malaria mosquito, *Anopheles gambiae*. Proc Natl Acad Sci U S A. 110: 19854–19859.

Lehmann T, Diabate A. 2008. The molecular forms of *Anopheles gambiae*: a phenotypic perspective. Infect Genet Evol. 8:737–746.

Lifschytz E, Lindsley DL. 1972. The role of X-chromosome inactivation during spermatogenesis (*Drosophila*-allocycly-chromosome evolution-male sterility-dosage compensation). Proc Natl Acad Sci U S A. 69:182–186.

Mackay TFC, et al. 2012. The *Drosophila melanogaster* genetic reference panel. Nature 482:173–178.

Marchand RP. 1983. Field observations on swarming and mating in *Anopheles Gambiae* mosquitoes in Tanzania. Neth J Zool. 34:367–387.

Marsden CD, et al. 2014. Diversity, differentiation, and linkage disequilibrium: prospects for association mapping in the malaria vector *Anopheles arabiensis*. G3 (Bethesda) 4:121–131.

Martin SH, Davey JW, Jiggins CD. 2014. Evaluating the use of ABBA-BABA statistics to locate introgressed loci. Mol Biol Evol. 32:244–257.

Mayr E. 1942. Systematics and the origin of species, from the viewpoint of a zoologist. New York: Columbia University Press.

McGaugh SE, Noor MAF. 2012. Genomic impacts of chromosomal inversions in parapatric *Drosophila* species. Philos Trans R Soc Lond B Biol Sci. 367:422–429.

McVean GAT, et al. 2004. The fine-scale structure of recombination rate variation in the human genome. Science 304:581–584.

Muller HJ. 1940. Bearing of the *Drosophila* work on systematics. In: Huxley JS, editor. The new systematics. Oxford: Clarendon Press. p. 185–268.

Nachman MW, Payseur BA. 2012. Recombination rate variation and speciation: theoretical predictions and empirical results from rabbits and mice. Philos Trans R Soc Lond B Biol Sci. 367:409–421.

Navarro A, Barton NH. 2003. Accumulating postzygotic isolation genes in parapatry: a new twist on chromosomal speciation. Evol Int J Org Evol. 57:447–459.

Neafsey DE, et al. 2010. SNP genotyping defines complex gene-flow boundaries among African malaria vector mosquitoes. Science 330:514–517.

Noor MA, Grams KL, Bertucci LA, Reiland J. 2001. Chromosomal inversions and the reproductive isolation of species. Proc Natl Acad Sci U S A. 98:12084–12088.

Noor MAF, Bennett SM. 2009. Islands of speciation or mirages in the desert? Examining the role of restricted recombination in maintaining species. Heredity 103:439–444.

Nosil P, Crespi BJ, Sandoval CP. 2003. Reproductive isolation driven by the combined effects of ecological adaptation and reinforcement. Proc Biol Sci. 270:1911–1918.

O'Loughlin SM, et al. 2014. Genomic analyses of three malaria vectors reveals extensive shared polymorphism but contrasting population histories. Mol Biol Evol. 31:889–902.

Pool JE, Nielsen R. 2009. Inference of historical changes in migration rate from the lengths of migrant tracts. Genetics 181:711–719.

Presgraves DC. 2008. Sex chromosomes and speciation in *Drosophila*. Trends Genet. 24:336–343.

R Development Core Team. 2011. R: a language and environment for statistical computing. Vienna (Austria): R Foundation for Statistical Computing.

Riehle MM, et al. 2011. A cryptic subgroup of *Anopheles gambiae* is highly susceptible to human malaria parasites. Science 331:596–598.

Rieseberg LH. 2001. Chromosomal rearrangements and speciation. Trends Ecol Evol. 16:351–358.

Sankararaman S, et al. 2014. The genomic landscape of Neanderthal ancestry in present-day humans. Nature 507:354–357.

Slotman MA, della Torre A, Calzetta M, Powell JR. 2005. Differential introgression of chromsomal regions between *Anopheles gambiae* and *An. arabiensis*. Am J Trop Med Hyg. 73:326–335.

Slotman MA, et al. 2006. Genetic differentiation between the BAMAKO and SAVANNA chromosomal forms of *Anopheles gambiae* as indicated by amplified fragment length polymorphism analysis. Am J Trop Med Hyg. 74:641–648.

Slotman MA, et al. 2007. Evidence for subdivision within the M molecular form of *Anopheles gambiae*. Mol Ecol. 16:639–649.

Turner TL, Hahn MW. 2010. Genomic islands of speciation or genomic islands and speciation? Mol Ecol. 19:848–850.
Turner TL, Hahn MW, Nuzhdin SV. 2005. Genomic islands of speciation in *Anopheles gambiae*. PLoS Biol. 3:e285.
Wang-Sattler R, et al. 2007. Mosaic genome architecture of the *Anopheles gambiae* species complex. PLoS One. 2:e1249.
Weetman D, Wilding CS, Steen K, Pinto J, Donnelly MJ. 2012. Gene flow-dependent genomic divergence between *Anopheles gambiae* M and S forms. Mol Biol Evol. 29:279–291.
Weetman D, et al. 2014. Contemporary gene flow between wild *An. gambiae* s.s. and *An. arabiensis*. Parasit Vectors. 7:345.
World Health Organization. 2013. World malaria report. Geneva (Switzerland): World Health Organization.
Wu CI. 2001. The genic view of the process of speciation. J Evol Biol. 14:851–865.

Associate editor: Geoff McFadden

Genome Biology and Evolution SMBE

Supplementary Text

Mosquito samples

Mosquito sample collection and species/subgroup identification was previously described for *A. coluzzii*, GOUNDRY, and *A. arabiensis* samples (Riehle et al. 2011). Briefly, larvae and adults were collected from three villages in Burkina Faso in 2007 and 2008 (Table S3). Larvae were reared to adults in an insectary, and both field caught adults and reared adults were harvested and stored for DNA collection. One *A. gambiae* individual was also included in this study. This sample was collected indoors as an adult in the village of Korabo in the Kissidougou prefecture in Guinea in October 2012. Individuals were typed for species, molecular form and *2*L*a* karyotype using a series of standard molecular diagnostics (Fanello et al. 2002; White et al. 2007; Santolamazza et al. 2008). All *A. coluzzii* and *A. arabiensis* samples are $2La^{a/a}$ homokaryotypes and the A. gambiae sample typed as a heterokaryotype ($2La^{a/+}$). Eleven of the twelve GOUNDRY samples typed as $2La^{+/+}$ homokaryotypes, but one sample (GOUND_0446) typed as a $2La^{a/a}$ homokaryotype.

DNA extractions and genome sequencing

DNA was extracted from female carcasses using standard protocols. Genomic DNA samples were diluted in purified water and sent to BGI (Shenzhen, China) for paired-end sequencing on the Illumina HiSeq2000 platform. We sequenced 10 females from *A. coluzzii* and 9 female *Anopheles arabiensis*. Sequence reads were filtered if they 1) contained more than 5% Ns or polyA structure, 2) contained 20% or more low quality (Q<20) bases, 3) contained adapter sequence, or 4) contained overlap between pairs. After quality filtering, each sample was represented by an average of 47.91 million reads with an expected insert size of 500 base pairs, except two samples that were sequenced to deeper read depth (Table S1).

In a separate sequencing effort, we also sequenced one individual *A. gambiae* female. The sequencing library was prepared using the Nextera kit (Illumina Inc., San Diego, CA) according to manufacturer's specifications and sequenced on the Illumina HiSeq2000 platform (Illumina Inc., San Diego, CA) at the University of Minnesota Genomics Center core facility for a total of 125.88 million reads. All Illumina reads used generated for this study and our companion study have been submitted to the Short Read Archive at NCBI under BioProject ID PRJNA273873.

We obtained publicly available *Anopheles merus* and *Anopheles arabiensis* short read Illumina data from NCBI SRA. We downloaded *A. merus* accessions ERR022713-8 that were generated and deposited by The Sanger Center. Individual accessions are paired-end 76 bp read

fastq files representing whole genome sequence from single individual *A. merus* individuals collected in Kenya and sequenced on the Illumina GAII platform. In addition, we downloaded *A. arabiensis* accession SRX377561, representing an individual collected in Minepa, Tanzania (Marsden et al. 2014). These data are paired-end 100 bp reads generated on the Illumina HiSeq2000 platform. This sample is the individual sequenced to 'high coverage' from the Marsden et al. Tanzania population sample.

Illumina short read alignment and subgroup specific references

At the time of this analysis, the only genome reference sequence with scaffolds mapped to chromosomes for any *Anopheles* mosquito was the *Anopheles gambiae* PEST AgamP3 assembly [(Holt et al. 2002); vectorbase.org], so we used this reference for mapping reads from all groups and species in this study. Since an unknown subset of the short reads generated for this experiment were expected to be substantially diverged from the PEST reference, we conducted short read alignment iteratively in two steps. First, we conducted paired-end mapping of all available reads to the *Anopheles gambiae* PEST reference genome (Holt et al. 2002) using the BWA *mem* algorithm [(Li 2013); bio-bwa.sourceforge.net] with default settings except applying the –M flag, which marks shorter hits as secondary. We then generated new 'Subgroup-Specific' references (hereafter SPEC) for *A. coluzzii*, *Anopheles gambiae* GOUNDRY, *Anopheles arabiensis*, and *Anopheles merus* separately. To do so, we combined sequence reads for each Subgroup and generated a pseudo-consensus sequence for each Subgroup. We used the software package ANGSD (version 0.534; (Nielsen et al. 2012); popgen.dk/wiki) to generate a read pileup, count reads and bases at each site, and identify the major allele at all sites. Then for every site that was covered by 1) at least 4 sequence bases that pass filtering, 2) fewer than a Subgroup-specific threshold number reads (mean read depth plus two standard deviations), and 3) a major allele that was segregating at a frequency of at least 0.5 across all reads, we assigned the new reference base to the major allele and to 'N' otherwise.

After alignment to the PEST reference, the mean total read depth for the autosomal arms was 136.14 for *A. arabiensis*, 136.63 for *A. coluzzii*, 157.42 for *A. gambiae* GOUNDRY, and 52.94 for *A. merus*. Mean total read depth on the X chromosome was 124.27 for *A. arabiensis*, 145.63 for *A. coluzzii*, and 168.75 for *A. gambiae* GOUNDRY, and 44.37 for *A. merus*. The proportion of unknown bases ('N's) increased in the new references (0.12, 0.11, 0.05, 0.14 for the autosomes of *A. arabiensis*, *A. coluzzii*, GOUNDRY, and *A. merus*, respectively, and 0.22, 0.05, 0.06, 0.25 for the X) relative to PEST (0.02 for autosomes, 0.04 for X). The differences between Subgroups in read depth and proportion of sites missing data can be attributed in part to

differences in the number of individuals sequenced (n = 9,10,12, 6 for *A. arabiensis*, *A. coluzzii*, GOUNDRY, *A. merus*, respectively). However, the differences between autosomes and the X likely reflect difficulties in mapping divergent reads to the PEST reference. The proportion of sites missing data were higher on the X relative to the autosomes for alignments of data from *A. arabiensis* and *A. merus* to both the PEST reference and the Subgroup specific references (Table S4). Two other studies found a similar discrepancy when mapping these species to the *A. gambiae* PEST reference (Marsden et al. 2014; O'Loughlin et al. 2014), indicating that it is not unique to our pipeline and likely reflects the relatively higher divergence on the X that proves to be a higher barrier to read mapping.

Following the generation of new reference sequences for *A. coluzzii*, GOUNDRY, *A. arabiensis,* and *A. merus*, short read datasets for each Subgroup were then aligned back to the new subgroup specific (hereafter SPEC) reference using the BWA *mem* algorithm with default settings. The A. gambiae individual was aligned to the A. coluzzii reference sequence. Local realignment around indels was then performed for each subgroup separately using GATK (DePristo et al. 2011). Duplicates were removed using the SAMtools (Li et al. 2009) *rmdup* function.

Although the read mapping rate was consistently lower for the SPEC reference relative to rates when mapping to PEST, the proportion of mapped reads with a quality score of 20 increased for all groups except the *A. coluzzii* where it decreased slightly. The reduction in mapping rate when using the SPEC reference reflects the greater number of ambiguous bases ('N') in the SPEC reference relative to PEST and thus a smaller mapping target. Importantly, the proportion of mapped reads with quality score of 20 on the X chromosome increased from 0.6961 (PEST) to 0.7775 (SPEC) when mapping the *A. merus* data to the PEST and SPEC references. A similar increase was also observed for *A. arabiensis*, with the proportion of Q20 reads increasing from 0.7604 (PEST) to 0.8241 (SPEC), indicating that the Subgroup specific reference is especially helpful for mapping X-chromosome reads. As discussed above, mapping non-*A. gambiae* reads to the PEST X chromosome is expected to be difficult. Mapping biases may lead to underestimates of diversity and genetic divergence, but such downward biases do not change the main conclusions regarding *A. arabiensis* and *A. merus*.

Data Filtering

The data were filtered in two steps. First, we used SAMtools to generate a pileup and genotype likelihoods for each site. We calculated a series of alignment and read statistics and then applied a series of filters to obtain a set of sites considered reliable for downstream analysis.

Filters were applied using the SNPcleaner Perl Script from the ngsTools package (Fumagalli et al. 2014). Those filters are as follows.

1. *Read distribution among individuals*: No more than one individual is allowed to have fewer than 2 reads covering the site.
2. *Maximum read depth*: The site must not be covered by more than 350, 350, and 400 reads for A. coluzzii, *A. arabiensis*, and GOUNDRY, respectively, in each combined sample.
3. *Mapping Quality*: Only reads with a BWA mapping quality of at least 10 were included.
4. *Base Quality*: Only bases with Illumina base quality of 20 or more were included.
5. *Proper pairs*: Only reads the mapped in the proper paired-end orientation and within the expected distribution of insert lengths were included.
6. *Hardy-Weinberg proportions*: Expected genotype frequencies were calculated for each variable site based on allele frequencies based on genotypes called with SAMtools. Any site with an excess of heterozygotes were considered potential mapping errors and excluded.
7. *Heterozygous biases*: Sites with heterozygous genotype calls were evaluated with SAMtools for several biases using exact tests. If one of the two alternative alleles was biased with respect to the read base quality (minimum $P=1x10^{-100}$), read strand (minimum $P=1x10^{-4}$), or distance from the end of the read (minimum $P=1x10^{-4}$), the site was excluded.

The next filter was intended to exclude regions of the genome where short-read alignment may be compromised, such as low-complexity and regions with a high concentration of 'N' bases in the reference. The goal was to avoid edge effects and regions where mapping becomes ambiguous. To identify such regions, we scanned each Subgroup specific reference calculating the proportion of Ns in every 100-basepair window. All sites that fell within windows that contained 50 or more Ns were excluded. Since short read alignment is likely to be unreliable in highly repetitive genomic regions such as heterochromatic regions, we also excluded regions that have been identified as heterochromatic in *A. gambiae*, including both pericentric and intercalary heterochromatic regions (Sharakhova et al. 2010) to be conservative in our analyses.

A final list of sites-to-exclude was compiled for each subgroup-specific reference that included any site excluded by any of the above filters. This resulted in a different number and set of sites available for downstream analysis for each Subgroup (Table S5). In addition to these

138 excluded sites, we identified a series of regions that exhibited exceptionally high nucleotide
139 diversity even after front-end filtering. These sites were not excluded from ANGSD analyses
140 (see below), but were excluded from all other population genetic analyses (Table S5).
141
142 ***Site-frequency spectrum inference***
143 Population genetic inference from next-generation sequencing data was performed using
144 a statistical framework implemented in the software package Analysis of Next-Generation
145 Sequencing Data (ANGSD, (Nielsen et al. 2012), popgen.dk/wiki). Much of the BAM
146 manipulation and read-filtering functionality implemented in SAMtools is also implemented in
147 ANGSD and several functions were utilized in all of the following analyses with ANGSD.
148 Minimum map quality and base quality thresholds of 10 and 20 were used. Probabilistic
149 realignment for the computation of base alignment quality (BAQ) was enabled throughout with a
150 downgrading coefficient of 50. Reads that were not aligned as proper pairs or had bitwise flags
151 above 255 were excluded.
152 The first step in the pipeline was to infer the site-frequency spectrum (SFS) directly from
153 genotype likelihoods estimated from the read data. The global SFS was estimated in two steps.
154 The first step was to obtain a maximum likelihood estimate of per-site allele frequencies by
155 calculating multi-sample genotype likelihoods using the SAMtools model ((Li et al. 2009); -GL 1
156 in ANGSD) and estimating the minor allele frequency using the –realSFS 1 function in ANGSD
157 (Nielsen et al. 2012). Files containing the per-site estimates of allele frequencies were then used
158 as input for optimization of the global SFS across all sites using a BFGS optimization algorithm
159 implemented in the optimSFS program within ANGSD. Unfolded spectra were obtained by
160 including ancestral polarization assigned by a synthetic ancestral sequence described below.
161 Sites without ancestral assignment were excluded from SFS estimation. The optimized global
162 SFS was estimated for each chromosomal arm separately and the results from 2R, 3L, and 3R
163 were averaged to obtain an autosomal SFS. Autosomal and X chromosome site frequency spectra
164 were obtained for *A. coluzzii*, GOUNDRY, and *A. arabiensis* separately. These spectra were used
165 as priors for downstream analyses within ANGSD.
166
167 ***Genotype calling***
168 Genotypes were called in two steps at all sites that passed filtering. For both the
169 population samples (*A. coluzzii*, GOUNDRY, *A. arabiensis, A. merus*) as well as the *A. gambiae*
170 individual, genotype likelihoods were calculated using the SAMtools model as described above.
171 Then genotype posterior probabilities were calculated for each individual at each site. For the

population samples, posterior probabilities were calculated using maximum likelihood estimates of allele frequencies as a prior (Kim et al. 2011). For the single individual samples, a uniform prior was assumed for calculation of the posterior probabilities. For all samples, diploid genotypes were called only at sites with posterior probabilities of 0.9 or greater. Genotypes for GOUNDRY sample were obtained using a slightly different approach since this Subgroup is partially inbred (see below).

Genetic divergence

We measured absolute genetic divergence as the average number of pairwise differences between alleles from different subgroups, or D_{xy} (Nei 1987). We calculated D_{xy} as

$$D_{xy} = \frac{h+2H}{2L}$$

where h is the number of sites where one or both individuals carry heterozygous genotypes, H is the number of sites where the two individuals are homozygous for different alleles, and L is the number of sites where both individuals have called genotypes. As with our estimates of within-population diversity, we excluded all sites within 200 bp of the outer coordinates of annotated protein coding sequences in the AgamP3.8 gene set (vectorbase.org). For subgroups where we have sequences from multiple individuals (*A. coluzzii*, GOUNDRY, *A. arabiensis, A. merus*), we estimated D_{xy} calculated from the number of pairwise differences between each individual from every other subgroup and then averaged across comparisons for each subgroup to obtain an average D_{xy} value for each pair of subgroups. For comparisons made to *A. gambiae*, D_{xy} was calculated between the individual A. gambiae sequence and the individual sequence with the highest average read depth from each of the other subgroups.

For chromosomal plots (Figure 5) and boxplot analysis (Figure 4), each chromosomal arm was divided into 10 kb windows and D_{xy} was calculated across each window. Windows with fewer than 200 sites with data for comparison were excluded. Chromosomal curves were LOESS-smoothed using a span of 1% and degree of 2 with the loess.smooth function in R (R Development Core Team 2011). For the boxplot analysis, chromosome 2L was excluded to avoid the large effects of the *2La* inversion. Comparisons were made between categories using a Mann-Whitney test implemented in the wilcox.test function in R (R Development Core Team 2011).

Linkage disequilibrium

We measured LD using Haploview (Barrett et al. 2005) applied to genotype and SNP calls made using ANGSD as described above for *A. coluzzii*, GOUNDRY, and *A. arabiensis*. LD was calculated independently on each chromosomal arm and comparisons were made only between SNPs separated by 10 kb or less. For all analyses, we used the r^2 statistic generated by Haploview. For computational tractability, we reduced the number of SNP-by-SNP comparisons by randomly sampling comparisons down to either 1%, 10% or 20% of the total number of comparisons depending on the total number of comparisons for each subgroup. To obtain LD decay curves, we binned r^2 values for each subgroup based on physical distance in the PEST reference, and then averaged within each bin and plotted as a function of physical distance (Figure S1). We combined measures for chromosomal arms 2R, 3R, and 3L to obtain an autosomal curve while avoiding the effects of the 2L*a* inversion. We estimated a curve for the X chromosome separately. In all three subgroups, LD decays to background levels within several hundred basepairs on both the autosomes and on the X, consistent with previous analyses in these species (Harris et al. 2010; Weetman et al. 2010; Marsden et al. 2014). Interestingly, background levels of LD differ substantially among subgroups. Background LD is slightly higher in *A. arabiensis* than in *A. coluzzii*, which is consistent with a small effective population size and perhaps some greater degree of population substructure in *A. arabiensis* than in *A. coluzzii*. GOUNDRY exhibits very high levels of background LD, but this is due to the high levels of inbreeding-related homozygosity. In all cases, LD decay curves suggest bootstrapping can be conducted on 200 kb regions with confidence.

We generated background LD chromosomal plots (Figure S2) by dividing each chromosome into 10kb windows, identifying all SNPs inside each window, and taking the average r^2 value for all comparisons after thinning (see above) between SNPs inside the window and SNPs greater than 1 kb but less than 10 kb away on the PEST reference sequence. Only windows with at least 100 comparisons were included. Background LD was measured for *A. coluzzii* and *A. arabiensis* only since inbreeding has skewed measures of LD in GOUNDRY. LOESS-smoothed curves were generated using a span of 1% and a degree of 2 in the loess.smooth function in R (R Development Core Team 2011).

Nucleotide diversity

To enrich our data set for neutrally evolving sequence, we excluded sites within 200 bp of a coding sequence annotated in the AgamP3.8 gene set for the *A. gambiae* PEST reference available on VectorBase.org from our estimates of nucleotide diversity. If only a single individual was available for a group (*A. gambiae*), nucleotide diversity was estimated simply as

the fraction of sites with genotypes that were called as heterozygous. If a population sample was available (GOUNDRY, *A. coluzzii* and *A. arabiensis, A. merus*), we estimated nucleotide diversity directly from the read data using a maximum likelihood approach based on posterior probabilities of per-site allele frequencies (Korneliussen et al. 2013). The method is implemented under the –doThetas function within ANGSD and takes a global SFS as a prior to calculate posterior probabilities of allele frequencies. We chose to use Tajima's π statistic (Tajima 1989) as our estimate for nucleotide diversity. For all downstream analyses, nucleotide diversity was calculated as an average within 10 kb non-overlapping windows. The comparison of nucleotide diversity between genomic regions (see below) included only 10 kb windows containing at least 500 sequenced sites from 2R, 3L, 3R, and X chromosomal arms. The distribution of nucleotide diversity was compared between genomic regions using a Mann-Whitney test implemented in the wilcox.test function in R (R Development Core Team 2011).

References:

Barrett JC, Fry B, Maller J, Daly MJ. 2005. Haploview: analysis and visualization of LD and haplotype maps. Bioinformatics 21:263–265.

DePristo MA, Banks E, Poplin R, Garimella KV, Maguire JR, Hartl C, Philippakis AA, del Angel G, Rivas MA, Hanna M, et al. 2011. A framework for variation discovery and genotyping using next-generation DNA sequencing data. Nat. Genet. 43:491–498.

Fanello C, Santolamazza F, della Torre A. 2002. Simultaneous identification of species and molecular forms of the Anopheles gambiae complex by PCR-RFLP. Med. Vet. Entomol. 16:461–464.

Fumagalli M, Vieira FG, Linderoth T, Nielsen R. 2014. ngsTools: methods for population genetics analyses from next-generation sequencing data. Bioinforma. Oxf. Engl. 30:1486–1487.

Harris C, Lambrechts L, Rousset F, Abate L, Nsango SE, Fontenille D, Morlais I, Cohuet A. 2010. Polymorphisms in Anopheles gambiae immune genes associated with natural resistance to Plasmodium falciparum. PLoS Pathog. 6:e1001112.

Holt RA, Subramanian GM, Halpern A, Sutton GG, Charlab R, Nusskern DR, Wincker P, Clark AG, Ribeiro JMC, Wides R, et al. 2002. The genome sequence of the malaria mosquito Anopheles gambiae. Science 298:129–149.

Kim SY, Lohmueller KE, Albrechtsen A, Li Y, Korneliussen T, Tian G, Grarup N, Jiang T, Andersen G, Witte D, et al. 2011. Estimation of allele frequency and

association mapping using next-generation sequencing data. BMC Bioinformatics 12:231.

Korneliussen TS, Moltke I, Albrechtsen A, Nielsen R. 2013. Calculation of Tajima's D and other neutrality test statistics from low depth next-generation sequencing data. BMC Bioinformatics 14:289.

Li H. 2013. Aligning sequence reads, clone sequences and assembly contigs with BWA-MEM. ArXiv13033997 Q-Bio [Internet]. Available from: http://arxiv.org/abs/1303.3997

Li H, Handsaker B, Wysoker A, Fennell T, Ruan J, Homer N, Marth G, Abecasis G, Durbin R. 2009. The Sequence Alignment/Map format and SAMtools. Bioinforma. Oxf. Engl. 25:2078–2079.

Marsden CD, Lee Y, Kreppel K, Weakley A, Cornel A, Ferguson HM, Eskin E, Lanzaro GC. 2014. Diversity, differentiation, and linkage disequilibrium: prospects for association mapping in the malaria vector Anopheles arabiensis. G3 Bethesda Md 4:121–131.

Nei M. 1987. Molecular Evolutionary Genetics. New York, NY: Columbia University Press

Nielsen R, Korneliussen T, Albrechtsen A, Li Y, Wang J. 2012. SNP calling, genotype calling, and sample allele frequency estimation from New-Generation Sequencing data. PloS One 7:e37558.

O'Loughlin SM, Magesa S, Mbogo C, Mosha F, Midega J, Lomas S, Burt A. 2014. Genomic analyses of three malaria vectors reveals extensive shared polymorphism but contrasting population histories. Mol. Biol. Evol. 31:889–902.

R Development Core Team. 2011. R: A language and Environment for Statistical Computing. Available from: http://www.R-project.org/

Riehle MM, Guelbeogo WM, Gneme A, Eiglmeier K, Holm I, Bischoff E, Garnier T, Snyder GM, Li X, Markianos K, et al. 2011. A cryptic subgroup of Anopheles gambiae is highly susceptible to human malaria parasites. Science 331:596–598.

Santolamazza F, Mancini E, Simard F, Qi Y, Tu Z, della Torre A. 2008. Insertion polymorphisms of SINE200 retrotransposons within speciation islands of Anopheles gambiae molecular forms. Malar. J. 7:163.

Sharakhova MV, George P, Brusentsova IV, Leman SC, Bailey JA, Smith CD, Sharakhov IV. 2010. Genome mapping and characterization of the Anopheles gambiae heterochromatin. BMC Genomics 11:459.

310 Tajima F. 1989. Statistical method for testing the neutral mutation hypothesis by
311 DNA polymorphism. Genetics 123:585.

312 Weetman D, Wilding CS, Steen K, Morgan JC, Simard F, Donnelly MJ. 2010.
313 Association Mapping of Insecticide Resistance in Wild Anopheles gambiae
314 Populations: Major Variants Identified in a Low-Linkage Disequilbrium
315 Genome. PLoS ONE 5:e13140.

316 White BJ, Santolamazza F, Kamau L, Pombi M, Grushko O, Mouline K, Brengues C,
317 Guelbeogo W, Coulibaly M, Kayondo JK, et al. 2007. Molecular karyotyping of
318 the 2La inversion in Anopheles gambiae. Am. J. Trop. Med. Hyg. 76:334–339.

319

Supplementary Figure Legends:

Figure S1: Decay of Linkage Disequilibrium (LD) in *A. coluzzii* and *A. arabiensis*. LD (r^2) between SNPs separated by no more than 5 kb binned, averaged, and plotted as a function of physical distance. Low complexity regions were excluded. Chromosomal arms 2R, 3L, and 3R were included for the autosome curves and the X plotted separately. Note different X and autosome y-axis scales**.**

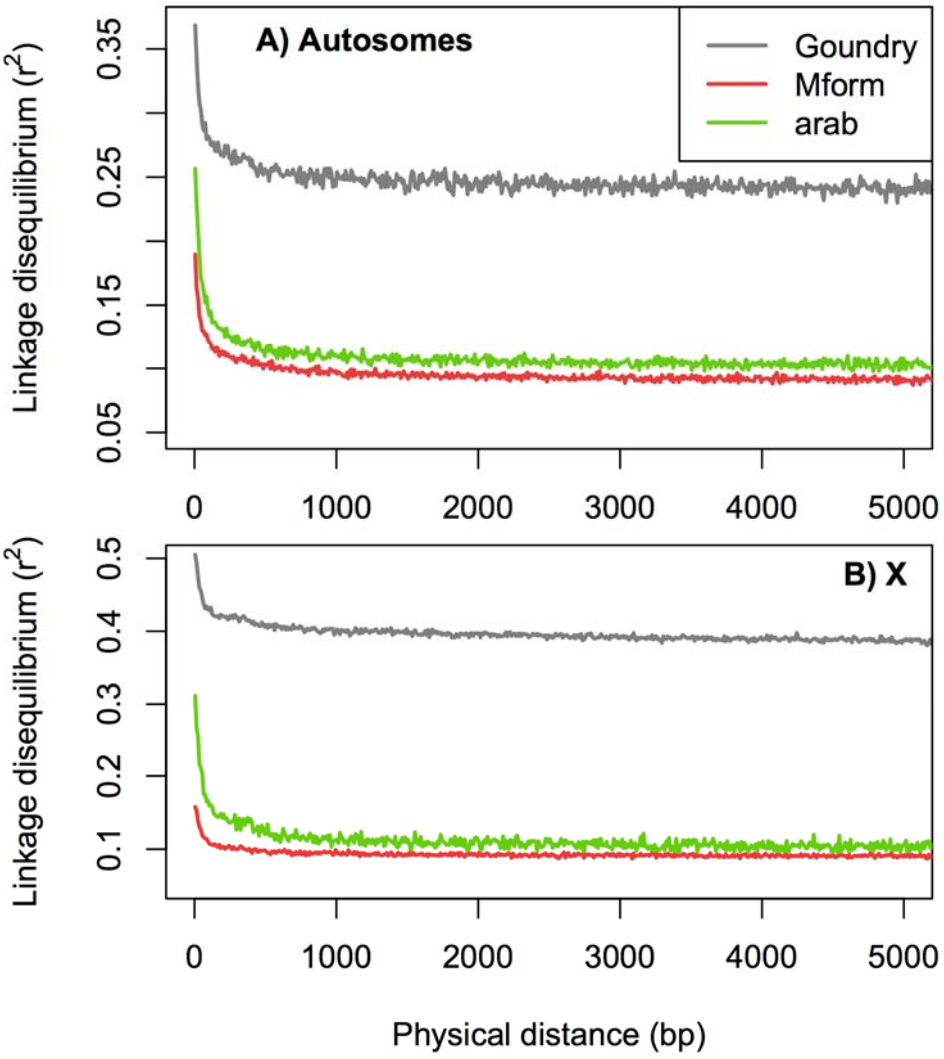

Figure S2: Background Linkage Disequilibrium (LD) for each chromosomal arm in *A. coluzzii* (*Ac*) and *A. arabiensis* (*Aa*). LD (r^2) between SNPs separated by at least 1kb (10 kb maximum) was averaged in 10 kb non-overlapping windows and LOESS-smoothed using a span of 1%. Low complexity and heterochromatic regions have been excluded. The large spikes on 2L and X (noted with vertical blue shaded bars) also coincide with reductions in nucleotide diversity and are thus likely to be recent selective sweeps. Additionally, there are a number of long distance increases (noted with horizontal grey bars) in LD in both *A. coluzzii* and *A. arabiensis* that coincide approximately with the locations of known chromosomal inversions segregating in these subgroups (Coluzzi et al. 2002).

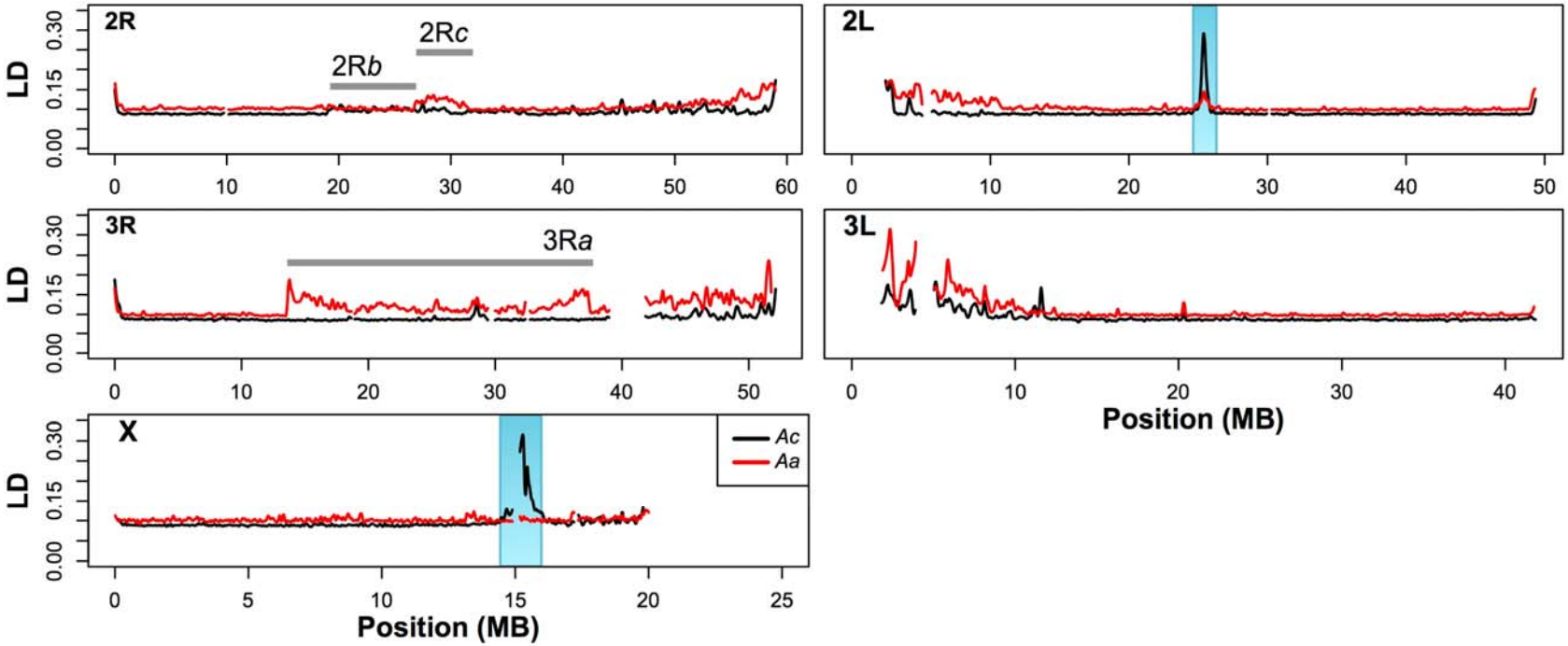

Table S1: Next-generation sequencing statistics for mosquito samples.

Taxon	Sample ID	Raw Reads (M) Clean data	Mean read depth
GOUNDRY	AG08-350	42.53	10.99
	AG07-136	44.99	8.75
	AG08-345	44.81	10.67
	AG08-366	45.00	10.96
	AG08-365	42.87	9.86
	AG07-317	44.67	10.85
	AG07-117	45.00	9.32
	AG07-235	45.00	11.61
	AG08-355	42.51	10.62
	AG08-359	44.14	11.15
	GOUND-0352	61.18	14.15
	GOUND-0446	110.86	20.03
A. coluzzii	GOUND-0021	39.81	8.26
	GOUND-0027	49.76	9.01
	GOUND-0030	48.89	9.46
	GOUND-0068	47.29	7.91
	GOUND-0135	55.07	9.46
	KODOU-0063	49.45	8.02
	KODOU-0064	43.05	9.21
	KODOU-0066	62.15	8.65
	KODOU-0068	54.38	11.14
	KODOU-0070	108.15	16.44
A. gambiae	GUIN-0001	125.88	19.09
A. arabiensis	GOUND-0101	51.23	12.76
	GOUND-0103	53.05	11.32
	GOUND-0105	47.88	10.97
	GOUND-0112	44.09	9.92
	GOUND-0137	62.54	9.04
	GOUND-0022	38.37	8.52
	GOUND-0024	44.70	5.94
	KODOU-0009	60.19	12.30
	GOUND-0069	34.83	7.66
	MINE-0001	124.5	10.58
A. merus	AK0012-C	43.34	9.72
	AK0013-C	46.31	10.74
	AK0014-C	43.41	8.88
	AK0015-C	34.01	7.77
	AK0016-C	37.41	8.36

Table S3: Collection site and date information for mosquito samples.

Sample ID	Site	Year	Date	Group
GOUND_0022	GOUNDRY	2008	November	*A. arabiensis*
GOUND_0024	GOUNDRY	2008	November	*A. arabiensis*
GOUND_0069	GOUNDRY	2008	November	*A. arabiensis*
GOUND_0101	GOUNDRY	2008	November	*A. arabiensis*
GOUND_0103	GOUNDRY	2008	November	*A. arabiensis*
GOUND_0105	GOUNDRY	2008	November	*A. arabiensis*
GOUND_0112	GOUNDRY	2008	November	*A. arabiensis*
GOUND_0137	GOUNDRY	2008	November	*A. arabiensis*
KODOU_0009	Kodougou	2008	November	*A. arabiensis*
AG07_136	GOUNDRY	2007	17-Nov	GOUNDRY
AG07_117	GOUNDRY	2007	17-Nov	GOUNDRY
AG07_235	GOUNDRY	2007	1-Dec	GOUNDRY
AG07_317	GOUNDRY	2007	1-Dec	GOUNDRY
AG08_359	Koupela	2008	November	GOUNDRY
AG08_365	Koupela	2008	November	GOUNDRY
AG08_366	Koupela	2008	November	GOUNDRY
AG08_345	Koupela	2008	November	GOUNDRY
AG08_350	Koupela	2008	November	GOUNDRY
AG08_355	Koupela	2008	November	GOUNDRY
GOUND_0352	GOUNDRY	2008	November	GOUNDRY
GOUND_0446	GOUNDRY	2008	November	GOUNDRY
GOUND_0021	GOUNDRY	2008	November	*A. coluzzii*
GOUND_0027	GOUNDRY	2008	November	*A. coluzzii*
GOUND_0030	GOUNDRY	2008	November	*A. coluzzii*
GOUND_0068	GOUNDRY	2008	November	*A. coluzzii*
GOUND_0135	GOUNDRY	2008	November	*A. coluzzii*
KODOU_0063	Kodougou	2008	November	*A. coluzzii*
KODOU_0064	Kodougou	2008	November	*A. coluzzii*
KODOU_0066	Kodougou	2008	November	*A. coluzzii*
KODOU_0068	Kodougou	2008	November	*A. coluzzii*
KODOU_0070	Kodougou	2008	November	*A. coluzzii*
GUIN_0001	Korabo	2012	October	*A. gambiae*

Table S4: Summary statistics for mapping to *A. gambiae* PEST reference and subgroup SPEC reference.

	PEST	**Pop Specific**
A. coluzzii		
Proportion 'N'[a]	0.0756	0.1514
Prop reads mapped[b]	0.8040	0.7850
Prop mapped reads Q20[c]	0.6971	0.6824
GOUNDRY		
Proportion Ns	0.0756	0.1127
Prop reads mapped	0.9586	0.9552
Prop mapped reads Q20	0.7837	0.8038
A. arabiensis		
Proportion Ns	0.0756	0.2006
Prop reads mapped	0.8912	0.8705
Prop mapped reads Q20	0.7408	0.7487
A. merus		
Proportion Ns	0.0756	0.2453
Prop reads mapped[d]	0.8325	0.8519
Prop mapped reads Q20[d]	0.8262	0.8492

[a] Proportion of bases across all chromosomes including UNKN and Y_unplaced that remain ambiguous 'N' base in reference sequence.
[b] Proportion of all reads that were mapped to reference.
[c] Proportion of mapped reads that were assigned a mapping quality phred score of at least 20.

Table S5: Genomic sites included and excluded from analysis in all subgroups.

Chromosomal arm	**Included *A. coluzzii*[a]**	**Included GOUNDRY[b]**	**Included *A. arabiensis*[c]**	**Number of sites excluded[d]**
X	17,771,610	17,488,872	13,500,342	4,915,713
2L	35,544,277	40,431,873	37,408,491	3,600,733
2R	47,883,360	50,489,876	46,304,728	3,063,230
3L	27,117,039	33,421,571	29,181,317	3,151,773
3R	34,646,563	39,071,752	36,247,383	5,102,107
Total	162,962,849	180,903,944	162,642,261	19,833,556

[a] Number of sites included in the .keep file used in ANGSD for the *A. coluzzii* population sample. This file includes only sites that passed the SNPcleaner, are found in euchromatic regions, and did not fall in 'low-complexity' regions.

[b] Same criteria as for M form, but specific to GOUNDRY sample.

[c] Same criteria as for M form, but specific to *A. arabiensis* sample.

[d] Sites that fell in heterochromatic regions, fell inside 'low-complexity' windows, or were identified manually as problematic. These sites were excluded from analysis in all samples.

Table S2: Genes located inside introgressed windows with genome-wide significant values of *D.* Introg - Introgression between indicated subgroups; G_Abf – Introgression between GOUNDRY and Burkina Faso population of *A. arabiensis*; Ac_Abf - Introgression between *A. coluzzii* and Burkina Faso population of *A. arabiensis*; Ac_Ag - Introgression between *A. coluzzii* and *A. gambiae*; G_Ag - Introgression between GOUNDRY and *A. gambiae*; Chr – chromosomal location; Gene start bp – basepair coordinate of start in coding gene sequence; Gene end bp – basepair coordinate of end in coding gene sequence; Gene name, ImmunoDB ID, and Gene description from Vectorbase.org.

Introg	Chr	Gene stable ID	Gene start bp	Gene end bp	Gene name	ImmunoD ID	Gene description
G_Abf	2L	AGAP005158	10651450	10734138			
G_Abf	2L	AGAP005159	10768635	10770047			adenosine deaminase [Source:VB External Description;Acc:AGAP005158]
G_Abf	2L	AGAP005160	10773905	10775953			Ras-related protein Rap-1b [Source:VB External Description;Acc:AGAP005159]
G_Abf	2L	AGAP005161	10785074	10811531			Ras homolog gene family, member A [Source:VB External Description;Acc:AGAP005160]
G_Abf	2L	AGAP005162	10811841	10816977			polynucleotide 5'-hydroxyl-kinase GRC3/NOL9 [Source:VB External Description;Acc:AGAP005161]
G_Abf	2L	AGAP005163	10820811	10847221			dystroglycan 1 [Source:VB External Description;Acc:AGAP005162]
G_Abf	2L	AGAP005164	10907702	10909701			Glucosyl/glucuronosyl transferases [Source:VB External Description;Acc:AGAP005163]
G_Abf	2L	AGAP005165	11054076	11119385			

G_Abf	2L	AGAP005166	11131877	11241906			
G_Abf	2L	AGAP005167	11186428	11190856			
G_Abf	2L	AGAP005168	11192031	11193411			Short chain dehydrogenase/3-oxoacyl-(acyl-carrier protein) reductase [Source:VB External Description;Acc:AGAP005167]
G_Abf	2L	AGAP005169	11195971	11200471			
G_Abf	2L	AGAP005170	11274226	11275949			
G_Abf	2L	AGAP005171	11284393	11334901			
G_Abf	2L	AGAP005172	11337707	11346317			Tctex1 domain-containing protein 4 [Source:VB External Description;Acc:AGAP005171]
G_Abf	2L	AGAP005173	11340609	11341921			
G_Abf	2L	AGAP005174	11368159	11374909			Px serine/threonine kinase [Source:VB External Description;Acc:AGAP005173]
G_Abf	2L	AGAP005175	11376450	11378030			nucleoporin SEH1 [Source:VB External Description;Acc:AGAP005174]
G_Abf	2L	AGAP005176	11378371	11405181			acetyl-CoA carboxylase / biotin carboxylase [Source:VB External Description;Acc:AGAP005175]
G_Abf	2L	AGAP005177	11407606	11409098			cell division control protein 6 [Source:VB External Description;Acc:AGAP005176]

G_Abf	2L	AGAP005178	11409421	11410687			Intraflagellar transport 46 homolog [Source:VB External Description;Acc:AGAP005177]
G_Abf	2L	AGAP005179	11410730	11414253			
G_Abf	2L	AGAP005180	11414718	11415633			
G_Abf	2L	AGAP005181	11415914	11416886			
G_Abf	2L	AGAP005182	11479150	11496824			
G_Abf	2L	AGAP005183	11685185	11686024	OBP41		odorant binding protein [Source:VB Community Annotation;Acc:AGAP005182]
G_Abf	2L	AGAP007237	11847212	11849149			
G_Abf	2L	AGAP005878	44471352	44503960	HPX4	HPX4	heme peroxidase [Source:VB Community Annotation;Acc:AGAP007237]
G_Abf	2L	AGAP005809	23058812	23061695			POU domain transcription factor, class 3 [Source:VB External Description;Acc:AGAP005878]
G_Abf	2L	AGAP005810	21508765	21610766			
G_Abf	2L	AGAP005811	21620403	21623334			protein phosphatase inhibitor 2 [Source:VB External Description;Acc:AGAP005809]
G_Abf	2L	AGAP005812	21624117	21626855			

G_Abf	2L	AGAP005813	21627556	21630573			protein xylosyltransferase [Source:VB External Description;Acc:AGAP005811]
G_Abf	2L	AGAP005814	21631168	21632196			
G_Abf	2L	AGAP005815	21632619	21633346			FeS cluster assembly scaffold IscU [Source:VB External Description;Acc:AGAP005813]
G_Abf	2L	AGAP005816	21634351	21636655			ecdysoneless homolog [Source:VB External Description;Acc:AGAP005814]
G_Abf	2L	AGAP005817	21638346	21640590			
G_Abf	2L	AGAP005818	21761237	21821057			BAI1-associated protein 3 [Source:VB External Description;Acc:AGAP005816]
G_Abf	2L	AGAP005819	21826613	21829719			cyclin-dependent kinase 4 [Source:VB External Description;Acc:AGAP005817]
G_Abf	2L	AGAP005820	21831271	21832371			nurim homolog [Source:VB External Description;Acc:AGAP005818]
G_Abf	2L	AGAP005822	21832968	21835239			
G_Abf	2L	AGAP005823	21835318	21836802			
G_Abf	2L	AGAP005824	21865434	21867120			
G_Abf	2L	AGAP005825	22049966	22051521			ubiquitin-related modifier 1 homolog [Source:VB External Description;Acc:AGAP005823]

G_Abf	2L	AGAP005826	22051819	22052908			presqualene diphosphate phosphatase [Source:VB External Description;Acc:AGAP005824]
G_Abf	2L	AGAP005828	22052936	22054542			acylglycerol kinase [Source:VB External Description;Acc:AGAP005825]
G_Abf	2L	AGAP005829	22057270	22066474			
G_Abf	2L	AGAP005830	22068864	22086035			Alpha-tubulin N-acetyltransferase [Source:VB External Description;Acc:AGAP005828]
G_Abf	2L	AGAP005831	22088475	22089755			microtubule-associated protein, RP/EB family, member 1, like [Source:VB External Description;Acc:AGAP005829]
G_Abf	2L	AGAP005832	22091909	22094208			
G_Abf	2L	AGAP005833	22279213	22283130			E3 ubiquitin-protein ligase Topors [Source:VB External Description;Acc:AGAP005831]
G_Abf	2L	AGAP005834	22284707	22295257			
G_Abf	2L	AGAP005835	22295976	22297899	COEJHE1E		carboxylesterase juvenile hormone esterase [Source:VB Community Annotation;Acc:AGAP005833]
G_Abf	2L	AGAP005836	22298997	22304146	COEJHE2E		carboxylesterase [Source:VB Community Annotation;Acc:AGAP005834]
G_Abf	2L	AGAP005837	22310958	22312826	COEJHE3E		carboxylesterase juvenile hormone esterase [Source:VB Community Annotation;Acc:AGAP005835]
G_Abf	2L	AGAP005838	22313684	22315544	COEJHE4E		carboxylesterase juvenile hormone esterase [Source:VB Community Annotation;Acc:AGAP005836]

G_Abf	2L	AGAP005839	22316476	22318579	COEJHE5E		carboxylesterase [Source:VB Community Annotation;Acc:AGAP005837]
G_Abf	2L	AGAP005840	22321985	22327760			
G_Abf	2L	AGAP005841	22337247	22358013			MFS transporter, FLVCR family, feline leukemia virus subgroup C receptor-relat [Source:VB External Description;Acc:AGAP005839]
G_Abf	2L	AGAP005842	22376630	22417899			
G_Abf	2L	AGAP005843	22418105	22419345			
G_Abf	2L	AGAP005844	22420222	22420962			
G_Abf	2L	AGAP005845	22422914	22423937			
G_Abf	2L	AGAP005846	22424221	22425368			
G_Abf	2L	AGAP005847	22427237	22434841			V-type H+-transporting ATPase subunit C [Source:VB External Description;Acc:AGAP005845]
G_Abf	2L	AGAP005848	22436100	22438204			alpha-galactosidase [Source:VB External Description;Acc:AGAP005846]
G_Abf	2L	AGAP005849	22441282	22442694			hydroxymethylglutaryl-CoA synthase [Source:VB External Description;Acc:AGAP005847]
G_Abf	2L	AGAP005850	22488407	22489811		FREP44	ficolin A [Source:VB External Description;Acc:AGAP005848]

G_Abf	2L	AGAP005851	22501623	22534076			colmedin [Source:VB External Description;Acc:AGAP005849]
G_Abf	2L	AGAP005852	22596794	22598098			growth arrest-specific protein 8 homolog [Source:VB External Description;Acc:AGAP005850]
G_Abf	2L	AGAP005853	22608607	22610192			cyclin-dependent kinase 10 [Source:VB External Description;Acc:AGAP005851]
G_Abf	2L	AGAP005854	22610196	22610683			mitochondrial ribosomal protein L42 [Source:VB External Description;Acc:AGAP005852]
G_Abf	2L	AGAP005855	22610800	22613327			four way stop [Source:VB External Description;Acc:AGAP005853]
G_Abf	2L	AGAP005856	22614786	22615653			
G_Abf	2L	AGAP005857	22622057	22624685			
G_Abf	2L	AGAP005858	22624877	22628768			nodal modulator 2 [Source:VB External Description;Acc:AGAP005856]
G_Abf	2L	AGAP005859	22632771	22634748			actin-related protein 6 [Source:VB External Description;Acc:AGAP005857]
G_Abf	2L	AGAP005860	22634962	22635971			protein lin-7 homolog C [Source:VB External Description;Acc:AGAP005858]
G_Abf	2L	AGAP005861	22636990	22637797			
G_Abf	2L	AGAP005862	22638513	22640734			phosphoglucomutase [Source:VB External Description;Acc:AGAP005860]

G_Abf	2L	AGAP005863	22641732	22643038			translocon-associated protein subunit beta [Source:VB External Description;Acc:AGAP005861]
G_Abf	2L	AGAP005864	22643135	22644145			
G_Abf	2L	AGAP005865	22645345	22648522			N-alpha-acetyltransferase 35, NatC auxiliary subunit [Source:VB External Description;Acc:AGAP005863]
G_Abf	2L	AGAP005866	22649439	22654222			
G_Abf	2L	AGAP005869	22654574	22656498			fumarylacetoacetase [Source:VB External Description;Acc:AGAP005865]
G_Abf	2L	AGAP005870	22659643	22674320			glutamate decarboxylase [Source:VB External Description;Acc:AGAP005866]
G_Abf	2L	AGAP005871	22677296	22684106			
G_Abf	2L	AGAP005872	22686596	22707992			
G_Abf	2L	AGAP005873	22708657	22712387			ribosome biogenesis protein BMS1 [Source:VB External Description;Acc:AGAP005871]
G_Abf	2L	AGAP005874	22713695	22715763			
G_Abf	2L	AGAP005880	22716169	22716812			DNA-directed RNA polymerases I, II, and III subunit RPABC2 [Source:VB External Description;Acc:AGAP005873]
G_Abf	2L	AGAP005881	22716848	22718746			Protein downstream neighbor of son homolog [Source:VB External Description;Acc:AGAP005874]

G_Abf	2L	AGAP005882	23112887	23121632			
G_Abf	2L	AGAP005883	23123719	23131205			sentrin-specific protease 7 [Source:VB External Description;Acc:AGAP005881]
G_Abf	2L	AGAP005884	23132983	23134544			
G_Abf	2L	AGAP005885	23136307	23138051			coiled-coil domain-containing protein 6 [Source:VB External Description;Acc:AGAP005883]
G_Abf	2L	AGAP005886	23144468	23152286			sphingomyelin synthase-related 1 [Source:VB External Description;Acc:AGAP005884]
G_Abf	2L	AGAP005887	23153912	23155200			
G_Abf	2L	AGAP005888	23164762	23171338			
G_Abf	2L	AGAP005889	23173125	23175930			
G_Abf	2L	AGAP005890	23177221	23177796			
G_Abf	2L	AGAP005891	23180993	23181795			
G_Abf	2L	AGAP005892	23184934	23185692			
G_Abf	2L	AGAP005893	23191393	23209482			coronin homolog [Source:VB External Description;Acc:AGAP005891]

G_Abf	2L	AGAP005894	23218990	23223867			importin beta-2 [Source:VB External Description;Acc:AGAP005892]
G_Abf	2L	AGAP005895	23224936	23225955			unconventional SNARE in the endoplasmic reticulum protein 1 [Source:VB External Description;Acc:AGAP005893]
G_Abf	2L	AGAP005896	23226447	23229089			electron-transferring-flavoprotein dehydrogenase [Source:VB External Description;Acc:AGAP005894]
G_Abf	2L	AGAP005897	23267845	23273093			
G_Abf	2L	AGAP005898	23294510	23314550			
G_Abf	2L	AGAP005899	23352311	23357446			ubiquitin-protein ligase E3 B [Source:VB External Description;Acc:AGAP005897]
G_Abf	2L	AGAP006192	23359155	23430017			nemo like kinase [Source:VB External Description;Acc:AGAP005898]
G_Abf	2L	AGAP006193	23382399	23383765			
G_Abf	2L	AGAP006194	28210040	28211706			chymotrypsin B chain C [Source:VB External Description;Acc:AGAP006192]
G_Abf	2L	AGAP006195	28212028	28212829			
G_Abf	2L	AGAP006196	28213429	28214272			
G_Abf	2L	AGAP006197	28215110	28215991			

G_Abf	2L	AGAP006198	28216227	28217474			
G_Abf	2L	AGAP006199	28218544	28219386			
G_Abf	2L	AGAP006200	28220346	28221163			
G_Abf	2L	AGAP006201	28222220	28222916			
G_Abf	2L	AGAP006202	28224499	28225391			
G_Abf	2L	AGAP006203	28226038	28226846			
G_Abf	2L	AGAP006204	28228128	28228839			
G_Abf	2L	AGAP006205	28229846	28231437			F-box protein 28 [Source:VB External Description;Acc:AGAP006203]
G_Abf	2L	AGAP006206	28232378	28233172			
G_Abf	2L	AGAP006207	28233793	28238829			ribosome biogenesis ATPase [Source:VB External Description;Acc:AGAP006205]
G_Abf	2L	AGAP006208	28239196	28243323			carboxypeptidase B [Source:VB External Description;Acc:AGAP006206]
G_Abf	2L	AGAP006209	28254825	28256356			carboxypeptidase B [Source:VB External Description;Acc:AGAP006207]

G_Abf	2L	AGAP006210	28256766	28258289			carboxypeptidase B [Source:VB External Description;Acc:AGAP006208]
G_Abf	2L	AGAP006211	28258831	28260544			carboxypeptidase B [Source:VB External Description;Acc:AGAP006209]
G_Abf	2L	AGAP006212	28265164	28266108			carboxypeptidase B [Source:VB External Description;Acc:AGAP006210]
G_Abf	2L	AGAP006213	28324182	28325583			
G_Abf	2L	AGAP006214	28332449	28360060			
G_Abf	2L	AGAP006215	28338172	28350797			
G_Abf	2L	AGAP006216	28459338	28460276			
G_Abf	2L	AGAP006217	28464790	28466912	GPRMTH1		methuselah receptor 1 [Source:VB Community Annotation;Acc:AGAP006215]
G_Abf	2L	AGAP006218	28468559	28472431	GPRMTH2		methuselah receptor 2 [Source:VB Community Annotation;Acc:AGAP006216]
G_Abf	2L	AGAP006219	28475349	28476095			
G_Abf	2L	AGAP006220	28476341	28490868	GPRMTH4		methuselah receptor 4 [Source:VB Community Annotation;Acc:AGAP006218]
G_Abf	2L	AGAP006221	28504771	28507510			receptor tyrosine kinase-like orphan receptor 1 [Source:VB External Description;Acc:AGAP006219]

G_Abf	2L	AGAP006222	28512602	28517680			aldehyde oxidase [Source:VB External Description;Acc:AGAP006220]
G_Abf	2L	AGAP006223	28519457	28523860			aldehyde oxidase [Source:VB External Description;Acc:AGAP006221]
G_Abf	2L	AGAP006224	28524284	28526141			glucosyl/glucuronosyl transferases [Source:VB External Description;Acc:AGAP006222]
G_Abf	2L	AGAP006225	28526654	28528179			glucosyl/glucuronosyl transferases [Source:VB External Description;Acc:AGAP006223]
G_Abf	2L	AGAP006226	28528882	28533013			aldehyde oxidase [Source:VB External Description;Acc:AGAP006224]
G_Abf	2L	AGAP006227	28534732	28539416			aldehyde oxidase [Source:VB External Description;Acc:AGAP006225]
G_Abf	2L	AGAP006228	28540651	28545294	Aldehyde_oxidase		xanthine dehydrogenase/oxidase [Source:VB External Description;Acc:AGAP006226]
G_Abf	2L	AGAP006229	28545568	28547787			alpha esterase [Source:VB External Description;Acc:AGAP006227]
G_Abf	2L	AGAP006231	28548433	28550748	COEAE2F		carboxylesterase [Source:VB Community Annotation;Acc:AGAP006228]
G_Abf	2L	AGAP006232	28550814	28552032			charged multivesicular body protein 6 [Source:VB External Description;Acc:AGAP006229]
G_Abf	2L	AGAP006233	28554773	28560186			serine/threonine-protein phosphatase dullard homolog [Source:VB External Description;Acc:AGAP006231]
G_Abf	2L	AGAP006234	28563646	28565368			peroxin-14 [Source:VB External Description;Acc:AGAP006232]

G_Abf	2L	AGAP006235	28565968	28567026			
G_Abf	2L	AGAP006236	28567535	28569087			protein SHQ1 [Source:VB External Description;Acc:AGAP006234]
G_Abf	2L	AGAP006237	28569164	28572971			
G_Abf	2L	AGAP006238	28573531	28574496			
G_Abf	2L	AGAP006239	28574752	28575648			Negative elongation factor E [Source:VB External Description;Acc:AGAP006237]
G_Abf	2L	AGAP006240	28576341	28579600			ubiquitin-conjugating enzyme E2 C [Source:VB External Description;Acc:AGAP006238]
G_Abf	2L	AGAP006241	28579834	28581250			Protein TSSC1 [Source:VB External Description;Acc:AGAP006239]
G_Abf	2L	AGAP006242	28581656	28584133			splicing factor 3B subunit 2 [Source:VB External Description;Acc:AGAP006240]
G_Abf	2L	AGAP006243	28585064	28586748			Innexin inx2 [Source:VB External Description;Acc:AGAP006241]
G_Abf	2L	AGAP006244	28587919	28588453			
G_Abf	2L	AGAP006245	28590349	28593745			phosphatidylinositol-4,5-bisphosphate 4-phosphatase [Source:VB External Description;Acc:AGAP006243]
G_Abf	2L	AGAP006246	28597433	28601266			CTL-like protein 1 [Source:VB External Description;Acc:AGAP006244]

G_Abf	2L	AGAP006247	28601810	28602615			Zinc finger matrin-type protein 2 [Source:VB External Description;Acc:AGAP006245]
G_Abf	2L	AGAP006248	28604122	28605603			Sorcin [Source:VB External Description;Acc:AGAP006246]
G_Abf	2L	AGAP006249	28607828	28609169			Survival of motor neuron-related-splicing factor 30 [Source:VB External Description;Acc:AGAP006247]
G_Abf	2L	AGAP006250	28609342	28610052			Mediator of RNA polymerase II transcription subunit 10 [Source:VB External Description;Acc:AGAP006248]
G_Abf	2L	AGAP006251	28611340	28614271			solute carrier family 12 (potassium/chloride transporters), member 8 [Source:VB External Description;Acc:AGAP006249]
G_Abf	2L	AGAP006252	28614984	28616576			Eukaryotic elongation factor, selenocysteine-tRNA-specific [Source:VB External Description;Acc:AGAP006250]
G_Abf	2L	AGAP006253	28617304	28622296			syntaxin 6 [Source:VB External Description;Acc:AGAP006251]
G_Abf	2L	AGAP006254	28619719	28620098			Cysteine-rich venom protein [Source:VB External Description;Acc:AGAP006252]
G_Abf	2L	AGAP006255	28620618	28621149			Cysteine-rich venom protein [Source:VB External Description;Acc:AGAP006253]
G_Abf	2L	AGAP006256	28624363	28643664			polypeptide N-acetylglucosaminyltransferase [Source:VB External Description;Acc:AGAP006254]
G_Abf	2L	AGAP006257	28644377	28647388			
G_Abf	2L	AGAP006258	28650212	28663145			Cad74A [Source:VB External Description;Acc:AGAP006256]

G_Abf	2L	AGAP006259	28684406	28688740			
G_Abf	2L	AGAP006260	28702474	28705612	PPO2	PPO2	prophenoloxidase [Source:VB Community Annotation;Acc:AGAP006258]
G_Abf	2L	AGAP006261	28705998	28706261			
G_Abf	2L	AGAP006271	28709029	28740710			Z band alternatively spliced PDZ-motif protein 66, isoform B [Source:VB External Description;Acc:AGAP006260]
G_Abf	2L	AGAP006272	28743187	28746274	CPR135		cuticular protein 135 RR-2 family [Source:VB Community Annotation;Acc:AGAP006261]
G_Abf	2L	AGAP006273	28931170	29014318			fyn-related kinase [Source:VB External Description;Acc:AGAP006270]
G_Abf	2L	AGAP006274	28964413	28983730			
G_Abf	2L	AGAP006275	29019477	29020812			
G_Abf	2L	AGAP006343	29021062	29023548	ABCB3		ATP-binding cassette, subfamily B (MDR/TAP), member 8 [Source:VB External Description;Acc:AGAP006273]
G_Abf	2L	AGAP006344	29080921	29116487			
G_Abf	2L	AGAP006345	29082536	29083876			
G_Abf	2L	AGAP006346	29929534	29961616			misshapen/NIK-related kinase [Source:VB External Description;Acc:AGAP006340]

G_Abf	2L	AGAP006347	29973455	29974430	PGRPS2	PGRPS2	peptidoglycan recognition protein (short) [Source:VB Community Annotation;Acc:AGAP006343]
G_Abf	2L	AGAP007200	29976298	29977639			RAG1-activating protein 1-like protein [Source:VB External Description;Acc:AGAP006344]
G_Abf	2L	AGAP007199	30093249	30098316			
G_Abf	2L	AGAP007100	30127818	30152476			Protein spinster homolog 2 [Source:VB External Description;Acc:AGAP006346]
G_Abf	2L	AGAP007101	30175822	30340409			potassium voltage-gated channel KQT-like subfamily, invertebrate [Source:VB External Description;Acc:AGAP006347]
G_Abf	2L	AGAP007102	44248847	44249053	DEF5	DEF5	defensin anti-microbial peptide [Source:VB Community Annotation;Acc:AGAP007200]
G_Abf	2L	AGAP007103	44247303	44247506	DEF3	DEF3	defensin anti-microbial peptide [Source:VB Community Annotation;Acc:AGAP007199]
G_Abf	2L	AGAP007104	42583659	42623914			
G_Abf	2L	AGAP007105	42676356	42683998			
G_Abf	2L	AGAP007106	42685570	42687946			
G_Abf	2L	AGAP007107	42688304	42690072			CWF19-like protein 1 homolog [Source:VB External Description;Acc:AGAP007102]
G_Abf	2L	AGAP007108	42690394	42780336			Calsyntenin-1 [Source:VB External Description;Acc:AGAP007103]

G_Abf	2L	AGAP007109	42784519	42792836			farnesyl diphosphate synthase [Source:VB External Description;Acc:AGAP007104]
G_Abf	2L	AGAP007110	42795728	42798687			
G_Abf	2L	AGAP007111	42800362	42817607			ubiquitin carboxyl-terminal hydrolase 47 [Source:VB External Description;Acc:AGAP007106]
G_Abf	2L	AGAP007112	42819885	42821706			DnaJ homolog subfamily B member 4 [Source:VB External Description;Acc:AGAP007107]
G_Abf	2L	AGAP007113	42825338	42829315			multiple PDZ domain protein [Source:VB External Description;Acc:AGAP007108]
G_Abf	2L	AGAP007114	42860665	42862101			
G_Abf	2L	AGAP007115	42914490	42939104			protein vein [Source:VB External Description;Acc:AGAP007110]
G_Abf	2L	AGAP007116	42952626	42955131			uracil phosphoribosyltransferase [Source:VB External Description;Acc:AGAP007111]
G_Abf	2L	AGAP007117	42955322	42957554			Pescadillo homolog [Source:VB External Description;Acc:AGAP007112]
G_Abf	2L	AGAP007118	42957994	42965130			1-acyl-sn-glycerol-3-phosphate acyltransferase gamma [Source:VB External Description;Acc:AGAP007113]
G_Abf	2L	AGAP007119	42980745	42991016			RING finger and CCCH-type zinc finger domain-containing protein [Source:VB External Description;Acc:AGAP007114]
G_Abf	2L	AGAP007120	43020195	43022049			

G_Abf	2L	AGAP007121	43022683	43024117			
G_Abf	2L	AGAP007122	43026304	43028115			
G_Abf	2L	AGAP007123	43031102	43039124			
G_Abf	2L	AGAP007124	43040522	43043135			Sideroflexin 1,2,3 [Source:VB External Description;Acc:AGAP007119]
G_Abf	2L	AGAP007178	43043577	43044650			nucleoside-diphosphate kinase [Source:VB External Description;Acc:AGAP007120]
G_Abf	2L	AGAP007180	43045845	43049930			cytochrome b5 protein [Source:VB External Description;Acc:AGAP007121]
G_Abf	2L	AGAP007181	43050145	43051673			Tubulin, alpha 1 [Source:VB External Description;Acc:AGAP007122]
G_Abf	2L	AGAP007182	43053485	43057667			sarcosine dehydrogenase [Source:VB External Description;Acc:AGAP007123]
G_Abf	2L	AGAP007184	43058730	43063265			
G_Abf	2L	AGAP007185	43909028	43910731			
G_Abf	2L	AGAP007186	44029784	44052643			
G_Abf	2L	AGAP007187	44060524	44070813			supervillin [Source:VB External Description;Acc:AGAP007181]

G_Abf	2L	AGAP007188	44081860	44083237			
G_Abf	2L	AGAP007189	44101034	44101495			
G_Abf	2L	AGAP007190	44103459	44106496			
G_Abf	2L	AGAP007191	44107541	44122327			
G_Abf	2L	AGAP007192	44166429	44166695			
G_Abf	2L	AGAP007193	44168370	44168636			
G_Abf	2L	AGAP007194	44170128	44170394			
G_Abf	2L	AGAP007195	44172071	44172337			
G_Abf	2L	AGAP007196	44177174	44177431			
G_Abf	2L	AGAP007197	44180300	44180557			
G_Abf	2L	AGAP007198	44183630	44183887			
G_Abf	2L	AGAP007201	44185149	44185376			

G_Abf	2L	AGAP007202	44188749	44189000			
G_Abf	2L	AGAP007203	44191299	44191583			
G_Abf	2L	AGAP007204	44192386	44192868		ML11	Niemann-Pick Type C-2 [Source:VB External Description;Acc:AGAP007197]
G_Abf	2L	AGAP007205	44193776	44200750			
G_Abf	2L	AGAP007206	44268905	44269838	TRX2		thioredoxin [Source:VB Community Annotation;Acc:AGAP007201]
G_Abf	2L	AGAP007207	44269904	44270752			
G_Abf	2L	AGAP007208	44275491	44300623			DE-cadherin [Source:VB External Description;Acc:AGAP007203]
G_Abf	2L	AGAP007209	44280294	44284218			E3 ubiquitin-protein ligase MARCH6 [Source:VB External Description;Acc:AGAP007204]
G_Abf	2L	AGAP007210	44284959	44286158			RAT1-interacting protein [Source:VB External Description;Acc:AGAP007205]
G_Abf	2L	AGAP007211	44286271	44287612			
G_Abf	2L	AGAP007212	44307059	44312519			DE-cadherin [Source:VB External Description;Acc:AGAP007207]
G_Abf	2L	AGAP007213	44327781	44328755			NADH dehydrogenase (ubiquinone) 1 alpha subcomplex 11 [Source:VB External Description;Acc:AGAP007208]

G_Abf	2L	AGAP007214	44331116	44343426			
G_Abf	2L	AGAP007215	44345057	44360698			
G_Abf	2L	AGAP007216	44361226	44363081			RNA (guanine-9-)-methyltransferase domain-containing protein 1 [Source:VB External Description;Acc:AGAP007211]
G_Abf	2L	AGAP007217	44362765	44366980			ATP-dependent RNA helicase DHX8/PRP22 [Source:VB External Description;Acc:AGAP007212]
G_Abf	2L	AGAP007218	44367385	44367839			Mitogen-activated protein-binding protein-interacting protein [Source:VB External Description;Acc:AGAP007213]
G_Abf	2L	AGAP007220	44367893	44369257			
G_Abf	2L	AGAP007221	44369741	44371801			phosphoacetylglucosamine mutase [Source:VB External Description;Acc:AGAP007215]
G_Abf	2L	AGAP007223	44372106	44376380			DE-cadherin [Source:VB External Description;Acc:AGAP007216]
G_Abf	2L	AGAP007224	44379193	44381232			pre-mRNA-processing factor 19 [Source:VB External Description;Acc:AGAP007217]
G_Abf	2L	AGAP007225	44381398	44383519			Eukaryotic translation initiation factor 2, subunit 2 beta, 38kDa [Source:VB External Description;Acc:AGAP007218]
G_Abf	2L	AGAP007226	44383538	44384474			
G_Abf	2L	AGAP007227	44384829	44389094			DNA-directed RNA polymerase III subunit RPC9 [Source:VB External Description;Acc:AGAP007220]

G_Abf	2L	AGAP007228	44391214	44398585			
G_Abf	2L	AGAP007229	44408537	44408800			
G_Abf	2L	AGAP007230	44409733	44410056			
G_Abf	2L	AGAP007231	44410493	44410744			
G_Abf	2L	AGAP007232	44412534	44412731			
G_Abf	2L	AGAP007233	44413209	44413406			
G_Abf	2L	AGAP007234	44413898	44414305			
G_Abf	2L	AGAP007235	44415630	44415902			
G_Abf	2L	AGAP007236	44416174	44416437			
G_Abf	2L	AGAP007238	44418169	44418366			
G_Abf	2L	AGAP007239	44420311	44420565			
G_Abf	2L	AGAP007240	44421401	44421682			

G_Abf	2L	AGAP007241	44422950	44423201			
G_Abf	2L	AGAP007242	44434229	44434426			
G_Abf	2L	AGAP007243	44436278	44436475			
G_Abf	2L	AGAP007244	44505488	44506731			Acyl-coenzyme A thioesterase 13 [Source:VB External Description;Acc:AGAP007238]
G_Abf	2L	AGAP007245	44506991	44509042			
G_Abf	2L	AGAP007246	44509304	44510154			Enkurin, TRPC channel interacting protein [Source:VB External Description;Acc:AGAP007240]
G_Abf	2L	AGAP007247	44511157	44512706			
G_Abf	2L	AGAP007248	44511854	44515421			cleavage and polyadenylation specificity factor subunit 5 [Source:VB External Description;Acc:AGAP007242]
G_Abf	2L	AGAP007249	44515927	44517239			26S protease regulatory subunit 8 [Source:VB External Description;Acc:AGAP007243]
G_Abf	2L	AGAP006342	44517438	44519115			Ribosome biogenesis protein WDR12 homolog [Source:VB External Description;Acc:AGAP007244]
G_Abf	2L	AGAP005821	44519402	44519897			
G_Abf	2L	AGAP005876	44520107	44520752			small nuclear ribonucleoprotein D1 [Source:VB External Description;Acc:AGAP007246]

G_Abf	2L	AGAP013557	44523757	44628840			Hippocalcin-like protein 1 [Source:VB External Description;Acc:AGAP007247]
G_Abf	2L	AGAP007222	44577826	44610983			Neuronal calcium sensor 2 [Source:VB External Description;Acc:AGAP007248]
G_Abf	2L	AGAP028260	44638197	44642288	Flightin		Flightin [Source:VB External Description;Acc:AGAP007249]
G_Abf	2L	AGAP005827	29969584	29970150	PGRPS3	PGRPS3	peptidoglycan recognition protein (short) [Source:VB Community Annotation;Acc:AGAP006342]
G_Abf	2R	AGAP028290	1214536	1215158			
G_Abf	2R	AGAP028294	1215908	1232126			
G_Abf	2R	AGAP006341	10771840	10785393			
G_Abf	2R	AGAP005868	10837462	10839379			Tetratricopeptide repeat domain 26 [Source:VB External Description;Acc:AGAP001809]
G_Abf	2R	AGAP013647	10851535	10853577	IR75h.1		ionotropic receptor IR75h.1 [Source:VB Community Annotation;Acc:AGAP001811]
G_Abf	2R	AGAP005867	10855568	10857858	IR75h.2		ionotropic receptor IR75h.2 [Source:VB Community Annotation;Acc:AGAP001812]
G_Abf	2R	AGAP005875	10859312	10865032			Cytosolic carboxypeptidase 6 [Source:VB External Description;Acc:AGAP001814]
G_Abf	2R	AGAP005157	10867621	10868082			

G_Abf	2R	AGAP005156	10869932	10870919			
G_Abf	2R	AGAP005807	10886723	10887414			
G_Abf	2R	AGAP006270	10902267	10903524			V-type H+-transporting ATPase subunit G [Source:VB External Description;Acc:AGAP001823]
G_Abf	2R	AGAP006340	10900129	10901647			
G_Abf	2R	AGAP007099	10871574	10878925			TATA-binding protein-associated factor [Source:VB External Description;Acc:AGAP001820]
G_Abf	2R	AGAP007219	10867987	10869000			Homeobox prox 1 [Source:VB External Description;Acc:AGAP001818]
G_Abf	2R	AGAP001194	10866302	10867306			Homeobox prox 1 [Source:VB External Description;Acc:AGAP001816]
G_Abf	2R	AGAP001806	10865042	10866073			
G_Abf	2R	AGAP001809	10860116	10862659			histone H3 [Source:VB External Description;Acc:AGAP001813]
G_Abf	2R	AGAP001811	10841634	10844181			DnaJ homolog subfamily B [Source:VB External Description;Acc:AGAP001810]
G_Abf	2R	AGAP001812	10790866	10805553	GPRGPH		putative glycoprotein hormone gph-like receptor [Source:VB Community Annotation;Acc:AGAP001807]
G_Abf	2R	AGAP001814	10846334	10848560	IR75g		ionotropic receptor IR75g [Source:VB Community Annotation;Acc:AGAP013085]

G_Abf	2R	AGAP001817	10897668	10898832			
G_Abf	2R	AGAP001819	11021083	11022159			salivary lipase [Source:VB External Description;Acc:AGAP001825]
G_Abf	2R	AGAP013470	10911118	11032919			
G_Abf	2R	AGAP001823	1249000	1255302			
G_Abf	2R	AGAP001822	1238210	1257658			Nuclear cap-binding protein subunit 1 [Source:VB External Description;Acc:AGAP001195]
G_Abf	2R	AGAP001820	1257984	1259194			Enn protein [Source:VB External Description;Acc:AGAP001196]
G_Abf	2R	AGAP001818	1270412	1271785			
G_Abf	2R	AGAP001816	1275455	1276464			chymotrypsin [Source:VB External Description;Acc:AGAP001198]
G_Abf	2R	AGAP001815	1278912	1280352			serine protease [Source:VB Community Annotation;Acc:AGAP001199]
G_Abf	2R	AGAP001813	1284944	1291277			glycogen debranching enzyme [Source:VB External Description;Acc:AGAP001200]
G_Abf	2R	AGAP001810	1402899	1404898			Organic cation transporter [Source:VB External Description;Acc:AGAP001202]
G_Abf	2R	AGAP001807	1496600	1497238			

G_Abf	2R	AGAP013085	1297008	1344393			defective proboscis extension response [Source:VB External Description;Acc:AGAP001201]
G_Abf	2R	AGAP001821	1274224	1284558			DNA polymerase zeta [Source:VB External Description;Acc:AGAP013386]
G_Abf	2R	AGAP001825	1501390	1514018			chitin synthase [Source:VB External Description;Acc:AGAP001205]
G_Abf	2R	AGAP001824	1560058	1564399			COMM domain-containing protein 4 [Source:VB External Description;Acc:AGAP001207]
G_Abf	2R	AGAP013523	1564839	1569129			
G_Abf	2R	AGAP001195	1585468	1589997			Ras-related protein Rab-8A [Source:VB External Description;Acc:AGAP001211]
G_Abf	2R	AGAP001196	1593354	1595399	PGRPLB	PGRPLB	peptidoglycan recognition protein (Long) [Source:VB Community Annotation;Acc:AGAP001212]
G_Abf	2R	AGAP013230	1599878	1603974			
G_Abf	2R	AGAP001198	1605327	1606439			
G_Abf	2R	AGAP001199	1611163	1611839			
G_Abf	2R	AGAP001200	1621913	1624294			Tubulin alpha-4A chain [Source:VB External Description;Acc:AGAP001219]
G_Abf	2R	AGAP001202	1635844	1637291			

G_Abf	2R	AGAP001203	1637107	1637388			SRA stem-loop-interacting RNA-binding protein, mitochondrial precursor [Source:VB External Description;Acc:AGAP013048]
G_Abf	2R	AGAP001201	1639768	1641840			cleavage and polyadenylation specificity factor subunit 3 [Source:VB External Description;Acc:AGAP001224]
G_Abf	2R	AGAP013386	1648880	1652299			gamma-tubulin complex component 5 [Source:VB External Description;Acc:AGAP001227]
G_Abf	2R	AGAP001205	1653342	1658336			dynein light chain Tctex-type 1 [Source:VB External Description;Acc:AGAP001229]
G_Abf	2R	AGAP001207	1745953	1747762			alpha-1,3/alpha-1,6-mannosyltransferase [Source:VB External Description;Acc:AGAP001232]
G_Abf	2R	AGAP001208	1663908	1735427			
G_Abf	2R	AGAP001211	1747738	1749534			
G_Abf	2R	AGAP001212	1730409	1745786			
G_Abf	2R	AGAP001213	1652312	1652910			DNA-directed RNA polymerase II subunit RPB4 [Source:VB External Description;Acc:AGAP001228]
G_Abf	2R	AGAP001214	1647691	1648722			
G_Abf	2R	AGAP013543	1642948	1646465			
G_Abf	2R	AGAP001219	1637507	1639524			ATP-dependent RNA helicase DDX55/SPB4 [Source:VB External Description;Acc:AGAP001223]

G_Abf	2R	AGAP001222	1625814	1635009			NAD-dependent deacetylase sirtuin 7 [Source:VB External Description;Acc:AGAP001220]
G_Abf	2R	AGAP013048	1617935	1620320			Tubulin alpha-4A chain [Source:VB External Description;Acc:AGAP001218]
G_Abf	2R	AGAP001224	1615070	1616976			soluble calcium-activated nucleotidase 1 [Source:VB External Description;Acc:AGAP001217]
G_Abf	2R	AGAP001227	1608204	1613085			Tetratricopeptide repeat protein 39C [Source:VB External Description;Acc:AGAP001215]
G_Abf	2R	AGAP001229	1590486	1592093			A-kinase anchoring protein AKAP120 [Source:VB External Description;Acc:AGAP013011]
G_Abf	2R	AGAP001232	1570811	1583778			ubiquitin carboxyl-terminal hydrolase 6/32 [Source:VB External Description;Acc:AGAP001209]
G_Abf	2R	AGAP013012	1560741	1562260			
G_Abf	2R	AGAP001233	1527421	1529058			
G_Abf	2R	AGAP001231	1750144	1757210			Activating signal cointegrator 1 complex subunit 3 [Source:VB External Description;Acc:AGAP001234]
G_Abf	2R	AGAP001228	1770522	1772729			Sugar transporter ERD6-like 6 [Source:VB External Description;Acc:AGAP001236]
G_Abf	2R	AGAP001226	1779496	1815088			Ras-specific guanine nucleotide-releasing factor 2 [Source:VB External Description;Acc:AGAP001238]
G_Abf	2R	AGAP001225	1882633	1884715	SP11372		Thymus-specific serine protease [Source:VB External Description;Acc:AGAP001240]

G_Abf	2R	AGAP001223	1905684	1906697			Eupolytin [Source:VB External Description;Acc:AGAP001241]
G_Abf	2R	AGAP001220	1934306	1938456			
G_Abf	2R	AGAP001218	1970271	1973082			Defective proboscis extension response [Source:VB External Description;Acc:AGAP001242]
G_Abf	2R	AGAP001217	1982566	1986438			
G_Abf	2R	AGAP001215	1988251	1990704			
G_Abf	2R	AGAP013011	1840884	1864559			Defective proboscis extension response [Source:VB External Description;Acc:AGAP001239]
G_Abf	2R	AGAP001209	1772749	1773959			Mediator of RNA polymerase II transcription subunit 29 [Source:VB External Description;Acc:AGAP001237]
G_Abf	2R	AGAP013518	1757771	1764254			phosphatidylserine decarboxylase [Source:VB External Description;Acc:AGAP001235]
G_Abf	2R	AGAP001206	2031648	2032691			Eupolytin [Source:VB External Description;Acc:AGAP001246]
G_Abf	2R	AGAP001234	2037107	2038136			Eupolytin [Source:VB External Description;Acc:AGAP001249]
G_Abf	2R	AGAP001236	2038458	2039707			Eupolytin [Source:VB External Description;Acc:AGAP001250]
G_Abf	2R	AGAP001238	2046107	2053275			

G_Abf	2R	AGAP001240	2082467	2084221			
G_Abf	2R	AGAP001241	2089321	2091433			L-caldesmon [Source:VB External Description;Acc:AGAP001261]
G_Abf	2R	AGAP013332	2091916	2093494			Plasma glutamate carboxypeptidase [Source:VB External Description;Acc:AGAP013443]
G_Abf	2R	AGAP001242	2094039	2095241			Plasma glutamate carboxypeptidase precursor [Source:VB External Description;Acc:AGAP013078]
G_Abf	2R	AGAP001582	2095727	2097478			Plasma glutamate carboxypeptidase [Source:VB External Description;Acc:AGAP001264]
G_Abf	2R	AGAP001243	2125310	2132140			Adaptor-related protein complex 2, beta 1 subunit [Source:VB External Description;Acc:AGAP001267]
G_Abf	2R	AGAP001239	2140536	2145097			
G_Abf	2R	AGAP001237	2148670	2158897			pre-mRNA cleavage complex 2 protein Pcf11 [Source:VB External Description;Acc:AGAP001271]
G_Abf	2R	AGAP001235	2176280	2180464			Karyopherin (importin) alpha 4 [Source:VB External Description;Acc:AGAP001273]
G_Abf	2R	AGAP001246	2185354	2186002	Rps15		40S ribosomal protein S15 [Source:VB Community Annotation;Acc:AGAP001274]
G_Abf	2R	AGAP001249	2187230	2188894			asparaginyl-tRNA synthetase [Source:VB External Description;Acc:AGAP001276]
G_Abf	2R	AGAP001250	2195493	2197228			Cysteine-rich hydrophobic domain 2 [Source:VB External Description;Acc:AGAP001278]

G_Abf	2R	AGAP001255	2206679	2207523			
G_Abf	2R	AGAP001259	2217740	2222956			protein phosphatase 3, catalytic subunit [Source:VB External Description;Acc:AGAP001279]
G_Abf	2R	AGAP001261	2189194	2190072			
G_Abf	2R	AGAP013443	2186061	2186808			
G_Abf	2R	AGAP013078	2161807	2167475			
G_Abf	2R	AGAP001264	2146078	2147348			
G_Abf	2R	AGAP001267	2132454	2133880			
G_Abf	2R	AGAP001269	2101260	2106211			solute carrier family 7 (cationic amino acid transporter), member 14 [Source:VB External Description;Acc:AGAP001265]
G_Abf	2R	AGAP001271	2066367	2067177			
G_Abf	2R	AGAP001273	2065249	2066185			small VCP/p97-interacting protein [Source:VB External Description;Acc:AGAP013220]
G_Abf	2R	AGAP001274	2059771	2065317			UTP--glucose-1-phosphate uridylyltransferase [Source:VB External Description;Acc:AGAP001257]
G_Abf	2R	AGAP001276	2053330	2059076			3'-phosphoadenosine 5'-phosphosulfate synthase [Source:VB External Description;Acc:AGAP001256]

G_Abf	2R	AGAP001278	2043489	2044772			
G_Abf	2R	AGAP013159	2041741	2042734			Eupolytin [Source:VB External Description;Acc:AGAP001252]
G_Abf	2R	AGAP001279	2040018	2041312			Eupolytin [Source:VB External Description;Acc:AGAP001251]
G_Abf	2R	AGAP001277	2034986	2035967			Eupolytin [Source:VB External Description;Acc:AGAP001248]
G_Abf	2R	AGAP001275	2033356	2034363			Eupolytin [Source:VB External Description;Acc:AGAP001247]
G_Abf	2R	AGAP001272	2029478	2030464			Eupolytin [Source:VB External Description;Acc:AGAP001245]
G_Abf	2R	AGAP001270	2026789	2027870			Eupolytin [Source:VB External Description;Acc:AGAP001244]
G_Abf	2R	AGAP001268	2263694	2269072			potassium inwardly-rectifying channel subfamily J [Source:VB External Description;Acc:AGAP001280]
G_Abf	2R	AGAP001265	2268140	2274752			Potassium inwardly-rectifying channel subfamily J [Source:VB External Description;Acc:AGAP001281]
G_Abf	2R	AGAP001258	2276105	2279562			Potassium inwardly-rectifying channel subfamily J [Source:VB External Description;Acc:AGAP001283]
G_Abf	2R	AGAP013220	2280076	2281706			Potassium inwardly-rectifying channel subfamily J [Source:VB External Description;Acc:AGAP001284]
G_Abf	2R	AGAP001257	2466313	2468758			

G_Abf	2R	AGAP001256	2472438	2475513			integrator complex subunit 4 [Source:VB External Description;Acc:AGAP001286]
G_Abf	2R	AGAP001253	2476050	2498876			
G_Abf	2R	AGAP001252	2470907	2472085			charged multivesicular body protein 2A [Source:VB External Description;Acc:AGAP001285]
G_Abf	2R	AGAP001251	2616403	2618742			
G_Abf	2R	AGAP001248	2623887	2626235			
G_Abf	2R	AGAP001247	2628767	2644802			E3 ubiquitin-protein ligase TRIP12 [Source:VB External Description;Acc:AGAP001296]
G_Abf	2R	AGAP001245	2619883	2623094			
G_Abf	2R	AGAP001244	2539595	2571510			zinc finger protein ZIC, invertebrate [Source:VB External Description;Acc:AGAP001291]
G_Abf	2R	AGAP001280	2505659	2508881			replication factor C subunit 1 [Source:VB External Description;Acc:AGAP001290]
G_Abf	2R	AGAP001281	30978462	30979823			TNF-receptor-associated factor [Source:VB External Description;Acc:AGAP003004]
G_Abf	2R	AGAP001283	30955842	30966819			
G_Abf	2R	AGAP001284	30975847	30977909			tyrosyl-tRNA synthetase [Source:VB External Description;Acc:AGAP003003]

G_Abf	2R	AGAP012950	30954842	30975549			ribosome assembly protein 1 [Source:VB External Description;Acc:AGAP003001]
G_Abf	2R	AGAP001286	30969683	30972642			AdoMet-dependent rRNA methyltransferase [Source:VB External Description;Acc:AGAP003002]
G_Abf	2R	AGAP001287	30962953	30964508			
G_Abf	2R	AGAP001285	30985240	31002993			serine/threonine-protein kinase SIK [Source:VB External Description;Acc:AGAP003005]
G_Abf	2R	AGAP001292	31018898	31020483			serine/threonine-protein kinase SIK [Source:VB External Description;Acc:AGAP013439]
G_Abf	2R	AGAP001294	31011967	31042325			26S proteasome regulatory subunit T3 [Source:VB External Description;Acc:AGAP003008]
G_Abf	2R	AGAP001296	31149927	31152536			SP71, isoform A [Source:VB External Description;Acc:AGAP003012]
G_Abf	2R	AGAP001293	31171219	31175606			fasciculation and elongation protein zeta 2 (zygin II) [Source:VB External Description;Acc:AGAP003014]
G_Abf	2R	AGAP001291	31179112	31180748			argininosuccinate synthase [Source:VB External Description;Acc:AGAP003015]
G_Abf	2R	AGAP001290	31182545	31184166			mesencephalic astrocyte-derived neurotrophic factor homolog [Source:VB External Description;Acc:AGAP003016]
G_Abf	2R	AGAP003004	31199556	31201234			serine/threonine-protein phosphatase 6 catalytic subunit [Source:VB External Description;Acc:AGAP003017]
G_Abf	2R	AGAP013545	31205281	31207750			solute carrier family 2, facilitated glucose transporter member 8 [Source:VB External Description;Acc:AGAP003020]

G_Abf	2R	AGAP003003	31208394	31219116			clathrin heavy chain [Source:VB External Description;Acc:AGAP003021]
G_Abf	2R	AGAP003001	31230560	31232558			
G_Abf	2R	AGAP003002	31234647	31236284			chimerin (chimaerin) 2 [Source:VB External Description;Acc:AGAP003026]
G_Abf	2R	AGAP013105	31239097	31243757			dumpy-like protein [Source:VB External Description;Acc:AGAP003027]
G_Abf	2R	AGAP003005	31010380	31011662			
G_Abf	2R	AGAP013439	31037870	31039151			
G_Abf	2R	AGAP003008	31050937	31053197			
G_Abf	2R	AGAP003012	31084129	31093710			
G_Abf	2R	AGAP003014	31158130	31166515			euchromatic histone-lysine N-methyltransferase [Source:VB External Description;Acc:AGAP003013]
G_Abf	2R	AGAP003015	31185533	31199122			dynamin GTPase [Source:VB External Description;Acc:AGAP003018]
G_Abf	2R	AGAP003016	31201266	31204342			cleavage stimulation factor subunit 3 [Source:VB External Description;Acc:AGAP003019]
G_Abf	2R	AGAP003017	31221318	31223249			

G_Abf	2R	AGAP003020	31226418	31230265			syntaxin-binding protein 1 [Source:VB External Description;Acc:AGAP003023]
G_Abf	2R	AGAP003021	31232794	31234277	Rplp2		60S ribosomal protein LP2 [Source:VB Community Annotation;Acc:AGAP003025]
G_Abf	2R	AGAP003024	31245928	31248261			Ras-related protein Rab-35 [Source:VB External Description;Acc:AGAP003028]
G_Abf	2R	AGAP003026	31248644	31252239			
G_Abf	2R	AGAP003027	31258092	31259052			
G_Abf	2R	AGAP003006	31260172	31262154			
G_Abf	2R	AGAP003007	31267869	31269484			
G_Abf	2R	AGAP003009	31269599	31271110			
G_Abf	2R	AGAP003010	31252286	31254127			pyruvate dehydrogenase E1 component subunit alpha [Source:VB External Description;Acc:AGAP003030]
G_Abf	2R	AGAP003013	1272611	1273259	GALE10	GALE10	galectin [Source:VB Community Annotation;Acc:AGAP001197]
G_Abf	2R	AGAP003018	1686238	1691977			
G_Abf	3L	AGAP003019	13830846	13849498			transcription initiation factor TFIID TATA-box-binding protein [Source:VB External Description;Acc:AGAP010958]

G_Abf	3L	AGAP003022	13837570	13839124			
G_Abf	3L	AGAP003023	13839175	13841038	CYP6AK1		cytochrome P450 [Source:VB Community Annotation;Acc:AGAP010961]
G_Abf	3L	AGAP003025	13888287	13889383			
G_Abf	3L	AGAP003028	13892906	13902774			protein N-terminal asparagine amidohydrolase [Source:VB External Description;Acc:AGAP010963]
G_Abf	3L	AGAP003029	13921398	13922370			
G_Abf	3L	AGAP013077	13925679	13926588			
G_Abf	3L	AGAP003031	13964171	13966158	CYP6AJ1		cytochrome P450 [Source:VB Community Annotation;Acc:AGAP010966]
G_Abf	3L	AGAP003032	13970019	13987819			Pickpocket [Source:VB External Description;Acc:AGAP010967]
G_Abf	3L	AGAP013505	14047820	14062527			Roundabout 1 [Source:VB External Description;Acc:AGAP010969]
G_Abf	3L	AGAP003030	14136670	14153767			Roundabout, axon guidance receptor, homolog 2 (Drosophila) [Source:VB External Description;Acc:AGAP010970]
G_Abf	3L	AGAP001197	35849053	35850604			
G_Abf	3L	AGAP001230	14000015	14001312	CLIPA9	CLIPA9	Clip-Domain Serine Protease [Source:VB Community Annotation;Acc:AGAP010968]

G_Abf	2L	AGAP028328	21839672	21839758			
G_Abf	3L	AGAP001193	35732988	35734762			
G_Abf	3L	AGAP010960	35903035	35966106			
G_Abf	3L	AGAP010961	35714877	35717719	SCRC1	SCRC1	Class C Scavenger Receptor (Sushi/SCR/CCP and Somatomedin B domains). [Source:VB Community Annotation;Acc:AGAP011974]
G_Abf	3L	AGAP010962	35857409	35858296			
G_Abf	3L	AGAP010963	35942172	35943468			Lysosomal acid lipase, [Source:VB External Description;Acc:AGAP011992]
G_Abf	3L	AGAP010964	35726987	35728695			
G_Abf	3L	AGAP010965	35831183	35834412			
G_Abf	3L	AGAP010966	35881138	35889962			twist [Source:VB External Description;Acc:AGAP011985]
G_Abf	3L	AGAP010967	35826957	35829735			
G_Abf	3L	AGAP010969	35870317	35872354			UDP-N-acetyl-alpha-D-galactosamine:polypeptide N-acetylgalactosaminyltransferase 20 [Source:VB External Description;Acc:AGAP011984]
G_Abf	3L	AGAP010970	35814701	35816121	Or60		odorant receptor [Source:VB Community Annotation;Acc:AGAP011979]

G_Abf	3L	AGAP011982	35792480	35793875	Or62		odorant receptor [Source:VB Community Annotation;Acc:AGAP011978]
G_Abf	3L	AGAP010968	35934433	35935859	Or64		odorant receptor [Source:VB Community Annotation;Acc:AGAP011990]
G_Abf	3L	AGAP011977	35923244	35924671	Or63		odorant receptor [Source:VB Community Annotation;Acc:AGAP011989]
G_Abf	3L	AGAP011988	35717978	35720109			Ufm1-specific protease 2 [Source:VB External Description;Acc:AGAP011975]
G_Abf	3L	AGAP011983	35896365	35899236			Fas apoptotic inhibitory molecule [Source:VB External Description;Acc:AGAP011987]
G_Abf	3L	AGAP011992	35936167	35937569	Or61		odorant receptor [Source:VB Community Annotation;Acc:AGAP011991]
G_Abf	3L	AGAP011976	35722320	35724163			
G_Abf	3L	AGAP011981	35742517	35744752			
G_Abf	2L	AGAP011985	22777748	22777820			tRNA-Lys [Source:VB RNA Description;Acc:AGAP005876]
G_Abf	2L	AGAP011980	44242678	44242784			U6 spliceosomal RNA [Source: RFAM 9.0] [Source:VB RNA Description;Acc:AGAP013557]
G_Abf	2L	AGAP011984	44400916	44400997			tRNA-Ser [Source:VB RNA Description;Acc:AGAP007222]
G_Abf	2L	AGAP011979	23189286	23189439			

G_Abf	2L	AGAP011978	22061211	22061311			tRNA-Tyr [Source:VB RNA Description;Acc:AGAP005827]
G_Abf	2L	AGAP011990	43033828	43033923			
G_Abf	2L	AGAP011989	21839678	21839753			
G_Abf	2L	AGAP011975	29942173	29942245			tRNA-Val [Source:VB RNA Description;Acc:AGAP006341]
G_Abf	2L	AGAP011987	22670812	22670884			tRNA-Ala [Source:VB RNA Description;Acc:AGAP005868]
G_Abf	3L	AGAP011991	35896805	35896886			tRNA-Ser [Source:VB RNA Description;Acc:AGAP011986]
G_Abf	2L	AGAP028193	11039420	11039522			
G_Abf	2R	AGAP028130	31232208	31232288			
G_Abf	2L	AGAP011986	22668532	22668604			tRNA-Ala [Source:VB RNA Description;Acc:AGAP005867]
G_Abf	2L	AGAP010958	22734332	22734404			tRNA-Ala [Source:VB RNA Description;Acc:AGAP005875]
G_Abf	2L	AGAP011974	10738148	10738220			tRNA-Lys [Source:VB RNA Description;Acc:AGAP005157]
Ac_Abf	2L	AGAP006077	26129377	26130091	OBP51		odorant binding protein [Source:VB Community Annotation;Acc:AGAP006077]

Ac_Abf	2L	AGAP006012	24654152	24654694	CPR32		cuticular protein RR-1 family (CPR32) [Source:VB Community Annotation;Acc:AGAP006012]
Ac_Abf	2L	AGAP006013	24658517	24659081	CPR33		cuticular protein RR-1 family (CPR33) [Source:VB Community Annotation;Acc:AGAP006013]
Ac_Abf	2L	AGAP006014	24665045	24666509			
Ac_Abf	2L	AGAP006015	24671856	24674367			decaprenyl-diphosphate synthase subunit 2 [Source:VB External Description;Acc:AGAP006015]
Ac_Abf	2L	AGAP006016	24676009	24679680			decaprenyl-diphosphate synthase subunit 2 [Source:VB External Description;Acc:AGAP006016]
Ac_Abf	2L	AGAP006017	24690401	24703431			serine/threonine-protein phosphatase 6 regulatory subunit 3 [Source:VB External Description;Acc:AGAP006017]
Ac_Abf	2L	AGAP006018	24713099	24845318			
Ac_Abf	2L	AGAP006019	24773211	24775285			maltase [Source:VB External Description;Acc:AGAP006019]
Ac_Abf	2L	AGAP006025	25161003	25166641			Ras-like protein family member [Source:VB External Description;Acc:AGAP006025]
Ac_Abf	2L	AGAP006026	25174728	25195703			
Ac_Abf	2L	AGAP006027	25272296	25314781			glutamate receptor, ionotropic, AMPA 4b [Source:VB External Description;Acc:AGAP006027]
Ac_Abf	2L	AGAP006028	25363652	25434556			GABA-gated chloride channel subunit [Source:VB External Description;Acc:AGAP006028]

Ac_Abf	2L	AGAP006029	25447418	25448405			
Ac_Abf	2L	AGAP006030	25450808	25461067			mitoferrin [Source:VB External Description;Acc:AGAP006030]
Ac_Abf	2L	AGAP006031	25462491	25466768			nuclear pore complex protein Nup54 [Source:VB External Description;Acc:AGAP006031]
Ac_Abf	2L	AGAP006032	25462778	25463951			
Ac_Abf	2L	AGAP006033	25466906	25468254			
Ac_Abf	2L	AGAP006034	25469312	25473092			
Ac_Abf	2L	AGAP006035	25514443	25516430			Ras-related protein Rab-36 [Source:VB External Description;Acc:AGAP006035]
Ac_Abf	2L	AGAP006036	25516573	25518865			axonemal dynein intermediate chain inner arm i1 [Source:VB External Description;Acc:AGAP006036]
Ac_Abf	2L	AGAP006037	25521114	25523716	Rpl24		60S ribosomal protein L24 [Source:VB Community Annotation;Acc:AGAP006037]
Ac_Abf	2L	AGAP006038	25524455	25544365			serine/arginine repetitive matrix protein 2 [Source:VB External Description;Acc:AGAP006038]
Ac_Abf	2L	AGAP006039	25526369	25528702			
Ac_Abf	2L	AGAP006040	25546090	25548795			peroxisomal membrane protein 2 [Source:VB External Description;Acc:AGAP006040]

Ac_Abf	2L	AGAP006041	25554043	25554891			E3 ubiquitin-protein ligase RNF5 [Source:VB External Description;Acc:AGAP006041]
Ac_Abf	2L	AGAP006042	25557922	25567942			
Ac_Abf	2L	AGAP006043	25568752	25573092			Cop-coated vesicle membrane protein P24 [Source:VB External Description;Acc:AGAP006043]
Ac_Abf	2L	AGAP006044	25573237	25576590			serine/threonine kinase 3 [Source:VB External Description;Acc:AGAP006044]
Ac_Abf	2L	AGAP006045	25588281	25619543			protein yorkie [Source:VB External Description;Acc:AGAP006045]
Ac_Abf	2L	AGAP006046	25627062	25632169			mediator of RNA polymerase II transcription subunit 23 [Source:VB External Description;Acc:AGAP006046]
Ac_Abf	2L	AGAP006047	25632214	25633880	CYP4J9		cytochrome P450 [Source:VB Community Annotation;Acc:AGAP006047]
Ac_Abf	2L	AGAP006048	25634411	25636099	CYP4J5		cytochrome P450 [Source:VB Community Annotation;Acc:AGAP006048]
Ac_Abf	2L	AGAP006049	25636420	25638630	CYP4J10		cytochrome P450 [Source:VB Community Annotation;Acc:AGAP006049]
Ac_Abf	2L	AGAP006050	25640105	25642170			AarF domain containing kinase 5 [Source:VB External Description;Acc:AGAP006050]
Ac_Abf	2L	AGAP006051	25642608	25644768			pentatricopeptide repeat domain 1 [Source:VB External Description;Acc:AGAP006051]
Ac_Abf	2L	AGAP006052	25646621	25660433			protein phosphatase 1, regulatory (inhibitor) subunit 3 [Source:VB External Description;Acc:AGAP006052]

Ac_Abf	2L	AGAP006053	25660981	25662299			
Ac_Abf	2L	AGAP006054	25664197	25666124			
Ac_Abf	2L	AGAP006055	25666334	25671923			NF-kappa-B inhibitor-like protein 2 [Source:VB External Description;Acc:AGAP006055]
Ac_Abf	2L	AGAP006056	25672651	25673946			
Ac_Abf	2L	AGAP006057	25674004	25674468			multiple coagulation factor deficiency 2 [Source:VB External Description;Acc:AGAP006057]
Ac_Abf	2L	AGAP006058	25676498	25719836			heparan sulfate 2-o-sulfotransferase [Source:VB External Description;Acc:AGAP006058]
Ac_Abf	2L	AGAP006059	25801800	25856226			
Ac_Abf	2L	AGAP006060	25928498	25928942			
Ac_Abf	2L	AGAP006061	25930982	25935080			
Ac_Abf	2L	AGAP006062	25935512	25940149			
Ac_Abf	2L	AGAP006063	25950088	25975600			
Ac_Abf	2L	AGAP006064	25976910	25977149			bladder cancer-associated protein [Source:VB External Description;Acc:AGAP006064]

Ac_Abf	2L	AGAP006065	25977898	25979619			DNA primase small subunit [Source:VB External Description;Acc:AGAP006065]
Ac_Abf	2L	AGAP006066	25980384	25983852			
Ac_Abf	2L	AGAP006067	25983910	25985391			
Ac_Abf	2L	AGAP006068	25987093	25997823			
Ac_Abf	2L	AGAP006069	26002375	26016906			
Ac_Abf	2L	AGAP006070	26053755	26055333			prefoldin 2 [Source:VB External Description;Acc:AGAP006070]
Ac_Abf	2L	AGAP006071	26055839	26056556			B9 domain-containing protein 1 [Source:VB External Description;Acc:AGAP006071]
Ac_Abf	2L	AGAP006072	26056657	26062439			molybdenum cofactor biosynthesis protein [Source:VB External Description;Acc:AGAP006072]
Ac_Abf	2L	AGAP006073	26097305	26100112			
Ac_Abf	2L	AGAP006074	26101764	26135649			
Ac_Abf	2L	AGAP006076	26104148	26104931	OBP50		odorant binding protein [Source:VB Community Annotation;Acc:AGAP006076]
Ac_Abf	2L	AGAP006075	26103215	26103894	OBP49		odorant binding protein [Source:VB Community Annotation;Acc:AGAP006075]

Ac_Abf	2L	AGAP006079	26131618	26132453	OBP53		odorant binding protein [Source:VB Community Annotation;Acc:AGAP006079]
Ac_Abf	2L	AGAP006080	26133006	26133968	OBP54		odorant binding protein [Source:VB Community Annotation;Acc:AGAP006080]
Ac_Abf	2L	AGAP006081	26134275	26135119	OBP55		odorant binding protein [Source:VB Community Annotation;Acc:AGAP006081]
Ac_Abf	2L	AGAP006082	26136547	26145914	CYP301A1		cytochrome P450 [Source:VB Community Annotation;Acc:AGAP006082]
Ac_Abf	2L	AGAP006083	26149370	26156793			frazzled protein [Source:VB External Description;Acc:AGAP006083]
Ac_Abf	2L	AGAP006078	26130285	26131425	OBP52		odorant binding protein [Source:VB Community Annotation;Acc:AGAP006078]
Ac_Abf	2R	AGAP013678	21852309	21854748			cleavage and polyadenylation specificity factor subunit 2 [Source:VB External Description;Acc:AGAP002474]
Ac_Abf	2R	AGAP002474	21850803	21851824			V-type proton ATPase subunit F [Source:VB External Description;Acc:AGAP002473]
Ac_Abf	2R	AGAP002473	21972922	21974640			
Ac_Abf	2R	AGAP002491	21969237	21973289			transcriptional regulator ATRX [Source:VB External Description;Acc:AGAP002490]
Ac_Abf	2R	AGAP002490	19227606	19229860			
Ac_Abf	2R	AGAP002313	19229445	19230679			

Ac_Abf	2R	AGAP002314	19225564	19227118			
Ac_Abf	2R	AGAP002312	19074789	19135191			protocadherin-15 [Source:VB External Description;Acc:AGAP002310]
Ac_Abf	2R	AGAP002316	19235646	19265831			
Ac_Abf	2R	AGAP002317	19444357	19446105	Alpha_amylase		alpha-amylase [Source:VB External Description;Acc:AGAP002317]
Ac_Abf	2R	AGAP002318	19449770	19451260			alpha-amylase [Source:VB External Description;Acc:AGAP002318]
Ac_Abf	2R	AGAP002320	19483679	19484648			isochorismatase domain-containing protein [Source:VB External Description;Acc:AGAP002320]
Ac_Abf	2R	AGAP002321	19518880	19532204			
Ac_Abf	2R	AGAP002322	19538683	19541190			
Ac_Abf	2R	AGAP002324	19567983	19574991			mitochondrial sodium/hydrogen exchanger NHA2 [Source:VB External Description;Acc:AGAP002324]
Ac_Abf	2R	AGAP002326	19723884	19724691			
Ac_Abf	2R	AGAP002325	19610696	19658751			
Ac_Abf	2R	AGAP002323	19547045	19553216			

Ac_Abf	2R	AGAP012947	19890611	19892029			
Ac_Abf	2R	AGAP002328	19896041	19897138			
Ac_Abf	2R	AGAP013459	19915255	19916259			
Ac_Abf	2R	AGAP013245	19916950	19917597			
Ac_Abf	2R	AGAP002332	19974032	19974823			39S ribosomal protein L11, mitochondrial [Source:VB External Description;Acc:AGAP002332]
Ac_Abf	2R	AGAP002334	19977776	19994401	SPAST_ANOGA		Spastin [Source:UniProtKB/Swiss-Prot;Acc:Q7QBW0]
Ac_Abf	2R	AGAP002333	19974751	19975789			
Ac_Abf	2R	AGAP002331	19954166	19956783			sodium-independent sulfate anion transporter [Source:VB External Description;Acc:AGAP002331]
Ac_Abf	2R	AGAP002330	19952102	19952729			60S ribosome subunit biogenesis protein NIP7 [Source:VB External Description;Acc:AGAP002330]
Ac_Abf	2R	AGAP002329	19947532	19951883			carnitine O-octanoyltransferase [Source:VB External Description;Acc:AGAP002329]
Ac_Abf	2R	AGAP013359	19949335	19950027			
Ac_Abf	2R	AGAP013453	19945134	19946693			

Ac_Abf	2R	AGAP002327	19895009	19898969			glucosyl/glucuronosyl transferases [Source:VB External Description;Acc:AGAP002327]
Ac_Abf	2R	AGAP002336	20216981	20220319			
Ac_Abf	2R	AGAP002335	20003872	20007544			nucleolysin TIA-1/TIAR [Source:VB External Description;Acc:AGAP002335]
Ac_Abf	2R	AGAP002338	20277667	20278503			vacuolar protein sorting 29 homolog [Source:VB External Description;Acc:AGAP002338]
Ac_Abf	2R	AGAP002340	20284397	20288304			eukaryotic translation initiation factor 3 subunit A [Source:VB External Description;Acc:AGAP002340]
Ac_Abf	2R	AGAP002344	20487928	20492035			brain tumor protein [Source:VB External Description;Acc:AGAP002344]
Ac_Abf	2R	AGAP002342	20376396	20387809			
Ac_Abf	2R	AGAP002341	20288825	20290349			
Ac_Abf	2R	AGAP002339	20278838	20279921			AN1-type zinc finger protein 2B [Source:VB External Description;Acc:AGAP002339]
Ac_Abf	2R	AGAP002337	20274998	20277322			eukaryotic translation initiation factor 3 subunit D [Source:VB External Description;Acc:AGAP002337]
Ac_Abf	2R	AGAP002345	20500138	20502586			anaphase-promoting complex subunit 4 [Source:VB External Description;Acc:AGAP002345]
Ac_Abf	2R	AGAP002349	20508179	20510102	PBD1		piggyBac-derived 1 [Source:VB Community Annotation;Acc:AGAP002349]

Ac_Abf	2R	AGAP002350	20517932	20530180			troponin T, fast skeletal muscle [Source:VB External Description;Acc:AGAP002350]
Ac_Abf	2R	AGAP002352	20538788	20546515			
Ac_Abf	2R	AGAP002353	20547215	20548780			lipase 3 [Source:VB External Description;Acc:AGAP002353]
Ac_Abf	2R	AGAP002354	20571876	20577183			EVI5-like protein [Source:VB External Description;Acc:AGAP002354]
Ac_Abf	2R	AGAP002355	20583976	20591576			glutamine synthetase [Source:VB External Description;Acc:AGAP002355]
Ac_Abf	2R	AGAP002357	20595150	20596781			vesicle transport protein GOT1B [Source:VB External Description;Acc:AGAP002357]
Ac_Abf	2R	AGAP002359	20604485	20608709			carbonic anhydrase [Source:VB External Description;Acc:AGAP002359]
Ac_Abf	2R	AGAP013402	20614585	20615699			Carbonic anhydrase I [Source:VB External Description;Acc:AGAP013402]
Ac_Abf	2R	AGAP002360	20617383	20618411			carbonic anhydrase III [Source:VB External Description;Acc:AGAP002360]
Ac_Abf	2R	AGAP002366	20672967	20677672			high affinity choline transporter [Source:VB External Description;Acc:AGAP002366]
Ac_Abf	2R	AGAP002369	20736414	20738177			vesicular acetylcholine transporter [Source:VB External Description;Acc:AGAP002369]
Ac_Abf	2R	AGAP002367	20684469	20687088			

Ac_Abf	2R	AGAP013375	20657806	20658645			
Ac_Abf	2R	AGAP002365	20650893	20653223			
Ac_Abf	2R	AGAP002364	20646222	20650102			
Ac_Abf	2R	AGAP002363	20644572	20646085			
Ac_Abf	2R	AGAP002362	20643276	20644364			ribonuclease P protein subunit p20 [Source:VB External Description;Acc:AGAP002362]
Ac_Abf	2R	AGAP013174	20642978	20643918			
Ac_Abf	2R	AGAP002361	20620164	20636209			
Ac_Abf	2R	AGAP002358	20597739	20600249			ADP,ATP carrier protein 2 [Source:VB External Description;Acc:AGAP002358]
Ac_Abf	2R	AGAP002356	20592831	20594830			parvin, beta [Source:VB External Description;Acc:AGAP002356]
Ac_Abf	2R	AGAP002351	20530881	20537832			nuclear pore complex protein Nup98-Nup96 [Source:VB External Description;Acc:AGAP002351]
Ac_Abf	2R	AGAP002348	20506394	20507830			exosome complex component RRP45 [Source:VB External Description;Acc:AGAP002348]
Ac_Abf	2R	AGAP002347	20503869	20505783			N-acetylglucosamine-6-phosphate deacetylase [Source:VB External Description;Acc:AGAP002347]

Ac_Abf	2R	AGAP002346	20502709	20503435	Rps14-2		40S ribosomal protein S14 [Source:VB Community Annotation;Acc:AGAP002346]
Ac_Abf	2R	AGAP002370	20754759	20758354			choline O-acetyltransferase [Source:VB External Description;Acc:AGAP002370]
Ac_Abf	2R	AGAP002378	20815983	20817794			adenylosuccinate lyase [Source:VB External Description;Acc:AGAP002378]
Ac_Abf	2R	AGAP002382	20833274	20862118			
Ac_Abf	2R	AGAP002381	20866390	20869552			disintegrin and metalloproteinase domain-containing protein 17 [Source:VB External Description;Acc:AGAP002381]
Ac_Abf	2R	AGAP002387	20878224	20880447			acid phosphatase [Source:VB External Description;Acc:AGAP002387]
Ac_Abf	2R	AGAP002389	20881152	20881860			ubiquitin-like 4A [Source:VB External Description;Acc:AGAP002389]
Ac_Abf	2R	AGAP002390	20883327	20886049			
Ac_Abf	2R	AGAP002391	20888558	20898575	COEAE5O		carboxylesterase [Source:VB Community Annotation;Acc:AGAP002391]
Ac_Abf	2R	AGAP002392	20900072	20901310			TBC1 domain family, member 7 [Source:VB External Description;Acc:AGAP002392]
Ac_Abf	2R	AGAP002394	20902807	20904462			DNA-directed RNA polymerase III subunit RPC3 [Source:VB External Description;Acc:AGAP002394]
Ac_Abf	2R	AGAP002396	20906137	20909870			dolichyl-diphosphooligosaccharide--protein glycosyltransferase [Source:VB External Description;Acc:AGAP002396]

Ac_Abf	2R	AGAP002397	20913332	20915653			60kDa lysophospholipase [Source:VB External Description;Acc:AGAP002397]
Ac_Abf	2R	AGAP013414	20916795	20920399			
Ac_Abf	2R	AGAP002398	20924106	20925044			
Ac_Abf	2R	AGAP013481	20929602	20946193			
Ac_Abf	2R	AGAP002399	20946288	20949539			
Ac_Abf	2R	AGAP013137	20950475	20951200			
Ac_Abf	2R	AGAP002401	20955633	20957882			V-type H+-transporting ATPase subunit E [Source:VB External Description;Acc:AGAP002401]
Ac_Abf	2R	AGAP002403	20966774	20968437			Nucleoside diphosphate-linked moiety X motif 18 [Source:VB External Description;Acc:AGAP002403]
Ac_Abf	2R	AGAP002404	20970024	20973127			cullin 5 [Source:VB External Description;Acc:AGAP002404]
Ac_Abf	2R	AGAP002406	20974838	20975905			COMM domain-containing protein 2 [Source:VB External Description;Acc:AGAP002406]
Ac_Abf	2R	AGAP002408	20976895	20978276			
Ac_Abf	2R	AGAP002372	20776828	20785488			homeo domain only family, other [Source:VB External Description;Acc:AGAP002372]

Ac_Abf	2R	AGAP002386	20872914	20877180			DnaJ homolog subfamily C member 14 [Source:VB External Description;Acc:AGAP002386]
Ac_Abf	2R	AGAP002385	20871484	20872178			trafficking protein particle complex 6B [Source:VB External Description;Acc:AGAP002385]
Ac_Abf	2R	AGAP002384	20869591	20871377			tRNA (guanine10-N2)-methyltransferase [Source:VB External Description;Acc:AGAP002384]
Ac_Abf	2R	AGAP002383	20864135	20866090			methionyl-tRNA synthetase [Source:VB External Description;Acc:AGAP002383]
Ac_Abf	2R	AGAP002379	20818085	20844958			
Ac_Abf	2R	AGAP002377	20804723	20812644			fatty-acid amide hydrolase 2 [Source:VB External Description;Acc:AGAP002377]
Ac_Abf	2R	AGAP013161	20797580	20802621			Fatty-acid amide hydrolase 2 [Source:VB External Description;Acc:AGAP013161]
Ac_Abf	2R	AGAP002376	20795402	20797041			
Ac_Abf	2R	AGAP002375	20794114	20794866			DNA-directed RNA polymerase I subunit RPA12 [Source:VB External Description;Acc:AGAP002375]
Ac_Abf	2R	AGAP002374	20789812	20793640			heterogeneous nuclear ribonucleoprotein A1/A3 [Source:VB External Description;Acc:AGAP002374]
Ac_Abf	2R	AGAP002371	20761175	20770172			
Ac_Abf	2R	AGAP002388	20880469	20882947			endonuclease III [Source:VB External Description;Acc:AGAP002388]

Ac_Abf	2R	AGAP002393	20901504	20902732			solute carrier family 35 (GDP-fucose transporter), member C1 [Source:VB External Description;Acc:AGAP002393]
Ac_Abf	2R	AGAP002395	20904484	20905565	Rpl10-2		60S ribosomal protein L10-2 [Source:VB Community Annotation;Acc:AGAP002395]
Ac_Abf	2R	AGAP013405	20951244	20952908			
Ac_Abf	2R	AGAP002400	20953620	20955114			Mitochondrial ribosomal protein L37 [Source:VB External Description;Acc:AGAP002400]
Ac_Abf	2R	AGAP002402	20960261	20961211			copper homeostasis protein [Source:VB External Description;Acc:AGAP002402]
Ac_Abf	2R	AGAP002405	20973233	20974140			
Ac_Abf	2R	AGAP002407	20975933	20976550			Mitochondrial ribosomal protein S18A [Source:VB External Description;Acc:AGAP002407]
Ac_Abf	2R	AGAP002409	20978294	20979782			tRNA pseudouridine38-40 synthase [Source:VB External Description;Acc:AGAP002409]
Ac_Abf	2R	AGAP002411	20980896	21020204			regulator of G-protein signaling [Source:VB External Description;Acc:AGAP002411]
Ac_Abf	2R	AGAP002413	21022307	21031277			Basic leucine zipper and W2 domain-containing protein 1 [Source:VB External Description;Acc:AGAP002413]
Ac_Abf	2R	AGAP002415	21045662	21047271			
Ac_Abf	2R	AGAP002416	21047645	21049457	CYP4K2		cytochrome P450 [Source:VB Community Annotation;Acc:AGAP002416]

Ac_Abf	2R	AGAP002418	21054655	21057484	CYP4D15		cytochrome P450 [Source:VB Community Annotation;Acc:AGAP002418]
Ac_Abf	2R	AGAP012957	21058285	21060905	CYP4D17		cytochrome P450 [Source:VB Community Annotation;Acc:AGAP012957]
Ac_Abf	2R	AGAP013241	21061611	21063654	CYP4D16		cytochrome P450 [Source:VB Community Annotation;Acc:AGAP013241]
Ac_Abf	2R	AGAP002419	21065272	21067725	CYP4D22		cytochrome P450 [Source:VB Community Annotation;Acc:AGAP002419]
Ac_Abf	2R	AGAP002420	21070040	21071555			alpha-1,2-glucosyltransferase [Source:VB External Description;Acc:AGAP002420]
Ac_Abf	2R	AGAP002423	21086838	21088551			
Ac_Abf	2R	AGAP002424	21135939	21203685			Sema domain, seven thrombospondin repeats (type 1 and type 1-like), transmembrane domain [Source:VB External Description;Acc:AGAP002424]
Ac_Abf	2R	AGAP002425	21205238	21207556			Cysteine sulfinic acid decarboxylase [Source:VB External Description;Acc:AGAP002425]
Ac_Abf	2R	AGAP002427	21209294	21224334			kinesin family member 3/17 [Source:VB External Description;Acc:AGAP002427]
Ac_Abf	2R	AGAP002429	21226460	21228741	CYP314A1		cytochrome P450 [Source:VB Community Annotation;Acc:AGAP002429]
Ac_Abf	2R	AGAP002428	21210652	21220711			
Ac_Abf	2R	AGAP002426	21207617	21208856			Protein OPI10 homolog [Source:VB External Description;Acc:AGAP002426]

Ac_Abf	2R	AGAP002422	21083023	21084584	CLIPD1	CLIPD1	Clip-Domain Serine Protease [Source:VB Community Annotation;Acc:AGAP002422]
Ac_Abf	2R	AGAP002421	21072562	21077555			
Ac_Abf	2R	AGAP002417	21049463	21051719	CYP4AR1		cytochrome P450 [Source:VB Community Annotation;Acc:AGAP002417]
Ac_Abf	2R	AGAP002414	21032955	21045056			carboxypeptidase D [Source:VB External Description;Acc:AGAP002414]
Ac_Abf	2R	AGAP002412	21020810	21021993			39S ribosomal protein L45 [Source:VB External Description;Acc:AGAP002412]
Ac_Abf	2R	AGAP002430	21260057	21261659	AKH2		adipokinetic hormone 2 [Source:VB Community Annotation;Acc:AGAP002430]
Ac_Abf	2R	AGAP002434	21353080	21375362			centrosomin [Source:VB External Description;Acc:AGAP002434]
Ac_Abf	2R	AGAP002444	21477474	21489405	GPROP12		pteropsin [Source:VB Community Annotation;Acc:AGAP002444]
Ac_Abf	2R	AGAP002439	21421576	21422028			
Ac_Abf	2R	AGAP002431	21309978	21325380			
Ac_Abf	2R	AGAP002432	21336793	21337749			Chymotrypsin-like protease [Source:VB External Description;Acc:AGAP002432]
Ac_Abf	2R	AGAP013182	21343359	21344048			

Ac_Abf	2R	AGAP002433	21350389	21352590			
Ac_Abf	2R	AGAP002435	21353540	21354223			
Ac_Abf	2R	AGAP002436	21377985	21379909			Kip1 ubiquitination-promoting complex protein 2 [Source:VB External Description;Acc:AGAP002436]
Ac_Abf	2R	AGAP002437	21381905	21383668	Rps8		40S ribosomal protein S8 [Source:VB Community Annotation;Acc:AGAP002437]
Ac_Abf	2R	AGAP002438	21390291	21415159			tyrosine-protein phosphatase non-receptor type 11 [Source:VB External Description;Acc:AGAP002438]
Ac_Abf	2R	AGAP002440	21424814	21429766			Cdc42 homolog [Source:VB External Description;Acc:AGAP002440]
Ac_Abf	2R	AGAP002441	21430613	21434861			
Ac_Abf	2R	AGAP002442	21444856	21446093			
Ac_Abf	2R	AGAP002443	21458418	21468816	GPROP11		pteropsin [Source:VB Community Annotation;Acc:AGAP002443]
Ac_Abf	2R	AGAP002449	21520244	21530048			3-OH androgenic UDPGT [Source:VB External Description;Acc:AGAP002449]
Ac_Abf	2R	AGAP013339	21549427	21550044			
Ac_Abf	2R	AGAP002453	21558960	21561069			

Ac_Abf	2R	AGAP002455	21562869	21563906			
Ac_Abf	2R	AGAP002460	21674481	21675692			forkhead box protein, other [Source:VB External Description;Acc:AGAP002460]
Ac_Abf	2R	AGAP002461	21727428	21729313			
Ac_Abf	2R	AGAP013297	21634430	21635740			
Ac_Abf	2R	AGAP002459	21603585	21606936			
Ac_Abf	2R	AGAP013018	21598626	21600572			Abhydrolase domain-containing protein FAM108B1 [Source:VB External Description;Acc:AGAP013018]
Ac_Abf	2R	AGAP002458	21595989	21598094			
Ac_Abf	2R	AGAP002457	21584335	21587320			chitinase [Source:VB External Description;Acc:AGAP002457]
Ac_Abf	2R	AGAP013166	21582376	21583879			Chitinase-3-like protein 1 [Source:VB External Description;Acc:AGAP013166]
Ac_Abf	2R	AGAP013120	21578831	21580283			Chitotriosidase precursor [Source:VB External Description;Acc:AGAP013120]
Ac_Abf	2R	AGAP013496	21576775	21578276			Chitinase-3-like protein 3 precursor [Source:VB External Description;Acc:AGAP013496]
Ac_Abf	2R	AGAP013260	21573458	21575079			Acidic mammalian chitinase precursor [Source:VB External Description;Acc:AGAP013260]

Ac_Abf	2R	AGAP002456	21565035	21572465			
Ac_Abf	2R	AGAP002454	21561263	21562598			golgi SNAP receptor complex member 1 [Source:VB External Description;Acc:AGAP002454]
Ac_Abf	2R	AGAP002489	21967027	21968685			
Ac_Abf	2R	AGAP002448	21523963	21524437			
Ac_Abf	2R	AGAP002447	21523256	21523658			
Ac_Abf	2R	AGAP012970	21518839	21519156			Cysteine-rich venom protein [Source:VB External Description;Acc:AGAP012970]
Ac_Abf	2R	AGAP002445	21511763	21512161			Cysteine-rich venom protein [Source:VB External Description;Acc:AGAP002445]
Ac_Abf	2R	AGAP002446	21515255	21515776			
Ac_Abf	2R	AGAP002462	21814022	21815246	GPROP7		long wavelength sensitive opsin [Source:VB Community Annotation;Acc:AGAP002462]
Ac_Abf	2R	AGAP002463	21817458	21821369			ubiquitin associated and SH3 domain-containing protein B [Source:VB External Description;Acc:AGAP002463]
Ac_Abf	2R	AGAP002465	21825402	21827293			ferritin heavy chain [Source:VB External Description;Acc:AGAP002465]
Ac_Abf	2R	AGAP002466	21828303	21829656			potassium channel, subfamily K, member 9 [Source:VB External Description;Acc:AGAP002466]

Ac_Abf	2R	AGAP002467	21830960	21833199			LMBR1 domain-containing protein 2 homolog [Source:VB External Description;Acc:AGAP002467]
Ac_Abf	2R	AGAP013273	21830588	21830896			
Ac_Abf	2R	AGAP002468	21835953	21836716	Rpl26		60S ribosomal protein L26 [Source:VB Community Annotation;Acc:AGAP002468]
Ac_Abf	2R	AGAP002469	21839444	21842815			AP2-associated kinase [Source:VB External Description;Acc:AGAP002469]
Ac_Abf	2R	AGAP002471	21845638	21846268			ADP-ribosylation factor-like protein 16 [Source:VB External Description;Acc:AGAP002471]
Ac_Abf	2R	AGAP002472	21846490	21850734			DNA damage-binding protein 1 [Source:VB External Description;Acc:AGAP002472]
Ac_Abf	2R	AGAP002464	21823645	21825022			secreted ferritin G subunit [Source:VB External Description;Acc:AGAP002464]
Ac_Abf	2R	AGAP013320	21836748	21838155			
Ac_Abf	2R	AGAP002470	21844846	21845340			mitochondrial 39S ribosomal protein L27 [Source:VB External Description;Acc:AGAP002470]
Ac_Abf	2R	AGAP002495	22010753	22012608			
Ac_Abf	2R	AGAP002496	22012891	22013624			Von Hippel-Lindau disease tumor suppressor [Source:VB External Description;Acc:AGAP002496]
Ac_Abf	2R	AGAP002501	22050381	22053158			serine/threonine-protein phosphatase 4 regulatory subunit 2 [Source:VB External Description;Acc:AGAP002501]

Ac_Abf	2R	AGAP002506	22094643	22110151			runt-related transcription factor, other [Source:VB External Description;Acc:AGAP002506]
Ac_Abf	2R	AGAP002507	22112400	22114363			peroxisomal biogenesis factor 3 [Source:VB External Description;Acc:AGAP002507]
Ac_Abf	2R	AGAP002509	22129049	22133349			
Ac_Abf	2R	AGAP002512	22169828	22170782			protein FRG1 [Source:VB External Description;Acc:AGAP002512]
Ac_Abf	2R	AGAP002514	22175893	22177036			
Ac_Abf	2R	AGAP002515	22177211	22178562			renal tumor antigen [Source:VB External Description;Acc:AGAP002515]
Ac_Abf	2R	AGAP002517	22183278	22184548			
Ac_Abf	2R	AGAP002505	22070155	22090671			voltage-dependent calcium channel alpha 1, invertebrate [Source:VB External Description;Acc:AGAP002505]
Ac_Abf	2R	AGAP002504	22066592	22069024			tRNA (cytosine34-C5)-methyltransferase [Source:VB External Description;Acc:AGAP002504]
Ac_Abf	2R	AGAP002503	22051162	22066256			4-coumarate:CoA ligase [Source:VB External Description;Acc:AGAP002503]
Ac_Abf	2R	AGAP002502	22055523	22063775			translation initiation factor 4G [Source:VB External Description;Acc:AGAP002502]
Ac_Abf	2R	AGAP002500	22049520	22050219			monothiol glutaredoxin [Source:VB External Description;Acc:AGAP002500]

Ac_Abf	2R	AGAP002499	22045705	22048873			methylmalonate-semialdehyde dehydrogenase (acylating), mitochondrial [Source:VB External Description;Acc:AGAP002499]
Ac_Abf	2R	AGAP002498	22042257	22045491			Vam6/Vps39-like protein isoform 1 [Source:VB External Description;Acc:AGAP002498]
Ac_Abf	2R	AGAP002497	22014945	22018620			
Ac_Abf	2R	AGAP002494	22006351	22008336			defective proboscis extension response [Source:VB External Description;Acc:AGAP002494]
Ac_Abf	2R	AGAP002508	22123544	22127039			protease m1 zinc metalloprotease [Source:VB External Description;Acc:AGAP002508]
Ac_Abf	2R	AGAP002511	22134638	22143589			
Ac_Abf	2R	AGAP002510	22138179	22139972			sarcolemmal associated protein [Source:VB External Description;Acc:AGAP002510]
Ac_Abf	2R	AGAP002513	22172281	22175751			
Ac_Abf	2R	AGAP002516	22179222	22182465			
Ac_Abf	2R	AGAP002518	22184936	22193619			delta-1-pyrroline-5-carboxylate synthetase [Source:VB External Description;Acc:AGAP002518]
Ac_Abf	2R	AGAP002519	22204377	22206308	GPRTYR		putative tyramine receptor [Source:VB Community Annotation;Acc:AGAP002519]
Ac_Abf	2R	AGAP002520	22321323	22322311			short-chain dehydrogenease/reductase [Source:VB External Description;Acc:AGAP002520]

Ac_Abf	2R	AGAP002522	22323584	22325386			cell cycle checkpoint control protein RAD9A [Source:VB External Description;Acc:AGAP002522]
Ac_Abf	2R	AGAP002525	22360892	22363476			eukaryotic translation initiation factor 2A [Source:VB External Description;Acc:AGAP002525]
Ac_Abf	2R	AGAP002527	22364288	22371320			
Ac_Abf	2R	AGAP002528	22372972	22373483			trafficking protein particle complex subunit 2 [Source:VB External Description;Acc:AGAP002528]
Ac_Abf	2R	AGAP002526	22363492	22363828			
Ac_Abf	2R	AGAP002524	22353696	22354918			
Ac_Abf	2R	AGAP002523	22342137	22352687			mediator of RNA polymerase II transcription subunit 12 [Source:VB External Description;Acc:AGAP002523]
Ac_Abf	2R	AGAP013013	22340983	22341716			
Ac_Abf	2R	AGAP013234	22326623	22328161			
Ac_Abf	2R	AGAP002521	22322243	22323397			hydroxybutyrate dehydrogenase [Source:VB External Description;Acc:AGAP002521]
Ac_Abf	2R	AGAP002549	22672709	22675715			nicalin homolog [Source:VB External Description;Acc:AGAP002549]
Ac_Abf	2R	AGAP002550	22698065	22699065			

Ac_Abf	2R	AGAP002552	22718447	22723370			glucose dehydrogenase (acceptor) [Source:VB External Description;Acc:AGAP002552]
Ac_Abf	2R	AGAP002551	22702149	22704094			glucose dehydrogenase (acceptor) [Source:VB External Description;Acc:AGAP002551]
Ac_Abf	2R	AGAP002553	22774444	22776503			
Ac_Abf	2R	AGAP002555	22785584	22787760	CYP325K1		cytochrome P450 [Source:VB Community Annotation;Acc:AGAP002555]
Ac_Abf	2R	AGAP013111	22796149	22796539			
Ac_Abf	2R	AGAP002563	22870786	22871836			Ras-like protein family member 10B precursor [Source:VB External Description;Acc:AGAP002563]
Ac_Abf	2R	AGAP002564	22874863	22892403			fructose-bisphosphate aldolase, class I [Source:VB External Description;Acc:AGAP002564]
Ac_Abf	2R	AGAP002566	22968003	22970561	GPRHIS		putative histamine receptor [Source:VB Community Annotation;Acc:AGAP002566]
Ac_Abf	2R	AGAP002567	22993406	22997891			hormone-sensitive lipase [Source:VB External Description;Acc:AGAP002567]
Ac_Abf	2R	AGAP002560	22849252	22858650	Or7		odorant receptor [Source:VB Community Annotation;Acc:AGAP002560]
Ac_Abf	2R	AGAP002559	22829180	22838504			alpha-tocopherol transfer protein-like protein [Source:VB External Description;Acc:AGAP002559]
Ac_Abf	2R	AGAP002558	22823983	22825656	Or40		odorant receptor [Source:VB Community Annotation;Acc:AGAP002558]

Ac_Abf	2R	AGAP002557	22796675	22816458			glucose dehydrogenase (acceptor) [Source:VB External Description;Acc:AGAP002557]
Ac_Abf	2R	AGAP013222	22793963	22794362			
Ac_Abf	2R	AGAP002556	22787889	22792798			
Ac_Abf	2R	AGAP002554	22780368	22782949		PASHA	DiGeorge syndrome critical region gene 8 [Source:VB External Description;Acc:AGAP002554]
Ac_Abf	2R	AGAP002568	22999014	23000671			Nat13 protein [Source:VB External Description;Acc:AGAP002568]
Ac_Abf	2R	AGAP002569	23000992	23003522			Serine incorporator 1 [Source:VB External Description;Acc:AGAP002569]
Ac_Abf	2R	AGAP002571	23005557	23007902			solute carrier family 35 (adenosine 3'-phospho 5'-phosphosulfate transporter) [Source:VB External Description;Acc:AGAP002571]
Ac_Abf	2R	AGAP002573	23016855	23092994			GTPase-activating Rap/Ran-GAP domain-like protein 3 [Source:VB External Description;Acc:AGAP002573]
Ac_Abf	2R	AGAP002578	23163895	23198838			
Ac_Abf	2R	AGAP002577	23132008	23146452			Voltage-dependent p/q type calcium channel [Source:VB External Description;Acc:AGAP002577]
Ac_Abf	2R	AGAP002576	23114859	23126509			
Ac_Abf	2R	AGAP002575	23096751	23107410			

Ac_Abf	2R	AGAP002572	23075482	23077568			
Ac_Abf	2R	AGAP002570	23003440	23005305			glutamyl-tRNA synthetase [Source:VB External Description;Acc:AGAP002570]
Ac_Abf	2R	AGAP013206	23262183	23264345			
Ac_Abf	2R	AGAP002579	23266440	23272082			
Ac_Abf	2R	AGAP002582	23278594	23279723			
Ac_Abf	2R	AGAP002585	23282878	23290569			
Ac_Abf	2R	AGAP002583	23280868	23282316			
Ac_Abf	2R	AGAP002589	23411485	23412341			dynein light intermediate chain 1, cytosolic [Source:VB External Description;Acc:AGAP002589]
Ac_Abf	2R	AGAP002580	23272473	23275129			DNA helicase MCM8 [Source:VB External Description;Acc:AGAP002580]
Ac_Abf	2R	AGAP002581	23275989	23278271			
Ac_Abf	2R	AGAP002586	23292023	23296228			glycogen(starch) synthase [Source:VB External Description;Acc:AGAP002586]
Ac_Abf	2R	AGAP002587	23306923	23309356			

Ac_Abf	2R	AGAP002588	23314050	23314901			
Ac_Abf	2R	AGAP002591	23569476	23656656			
Ac_Abf	2R	AGAP002592	23674824	23677382			outer membrane lipoprotein Blc [Source:VB External Description;Acc:AGAP002592]
Ac_Abf	2R	AGAP013318	23665044	23665873			Outer membrane lipoprotein Blc [Source:VB External Description;Acc:AGAP013318]
Ac_Abf	2R	AGAP013229	23672936	23673764			Outer membrane lipoprotein BLC precursor [Source:VB External Description;Acc:AGAP013229]
Ac_Abf	2R	AGAP002593	23677600	23678609			outer membrane lipoprotein Blc [Source:VB External Description;Acc:AGAP002593]
Ac_Abf	2R	AGAP002594	23681002	23682727			Apolipoprotein D [Source:VB External Description;Acc:AGAP002594]
Ac_Abf	2R	AGAP002596	23723071	23724325			
Ac_Abf	2R	AGAP013451	23669361	23670068			Outer membrane lipoprotein Blc (Precursor) [Source:VB External Description;Acc:AGAP013451]
Ac_Abf	2R	AGAP002595	23695505	23696886			outer mitochondrial translocase subunit [Source:VB External Description;Acc:AGAP002595]
Ac_Abf	2R	AGAP013190	23757468	23766169			
Ac_Abf	2R	AGAP002598	23777702	23779447			

Ac_Abf	2R	AGAP002600	23784014	23785836			tRNA nucleotidyltransferase (CCA-adding enzyme) [Source:VB External Description;Acc:AGAP002600]
Ac_Abf	2R	AGAP002601	23818836	23820416			nervous fingers [Source:VB External Description;Acc:AGAP002601]
Ac_Abf	2R	AGAP002602	23823922	23825471			
Ac_Abf	2R	AGAP002603	23826316	23830836			elongation factor 1 alpha-like protein [Source:VB External Description;Acc:AGAP002603]
Ac_Abf	2R	AGAP012994	23827848	23828853			
Ac_Abf	2R	AGAP002605	23831914	23835963			DNA-repair protein XRCC1 [Source:VB External Description;Acc:AGAP002605]
Ac_Abf	2R	AGAP002607	23836783	23841399			
Ac_Abf	2R	AGAP013336	23845513	23846011			
Ac_Abf	2R	AGAP002609	23847727	23849797			
Ac_Abf	2R	AGAP002608	23841728	23843238			ribokinase [Source:VB External Description;Acc:AGAP002608]
Ac_Abf	2R	AGAP002606	23835373	23836583			26S proteasome regulatory subunit N12 [Source:VB External Description;Acc:AGAP002606]
Ac_Abf	2R	AGAP013156	23833514	23834366			

Ac_Abf	2R	AGAP002604	23830883	23831679			
Ac_Abf	2R	AGAP013296	23825464	23827161			Peptidyl-prolyl cis-trans isomerase NIMA-interacting 4 [Source:VB External Description;Acc:AGAP013296]
Ac_Abf	2R	AGAP002599	23779841	23783717			polyubiquitin [Source:VB External Description;Acc:AGAP002599]
Ac_Abf	2R	AGAP002597	23769059	23776505			proteasome activator subunit 4 [Source:VB External Description;Acc:AGAP002597]
Ac_Abf	2R	AGAP002488	21962023	21965934			REST corepressor [Source:VB External Description;Acc:AGAP002488]
Ac_Abf	2R	AGAP002610	24041704	24057080			
Ac_Abf	2R	AGAP002628	24496842	24528705			opioid binding protein/cell adhesion molecule-like [Source:VB External Description;Acc:AGAP002628]
Ac_Abf	2R	AGAP002629	24564879	24567474			
Ac_Abf	2R	AGAP002631	24621991	24622170			
Ac_Abf	2R	AGAP002633	24694665	24698605	Gr53		gustatory receptor [Source:VB Community Annotation;Acc:AGAP002633]
Ac_Abf	2R	AGAP002632	24622462	24622880			
Ac_Abf	2R	AGAP002630	24619825	24620932			NADH dehydrogenase (ubiquinone) 1 beta subcomplex 2 [Source:VB External Description;Acc:AGAP002630]

Ac_Abf	2R	AGAP002634	24773120	24781524			membrane dipeptidase [Source:VB External Description;Acc:AGAP002634]
Ac_Abf	2R	AGAP002635	24811173	24812613	Gr13		gustatory receptor [Source:VB Community Annotation;Acc:AGAP002635]
Ac_Abf	2R	AGAP002636	24820728	24821113			
Ac_Abf	2R	AGAP002637	24821628	24821897			
Ac_Abf	2R	AGAP002638	24844985	24847793			ABC protein, subfamily ABCH [Source:VB External Description;Acc:AGAP002638]
Ac_Abf	2R	AGAP002639	24850239	24851846	Or39		odorant receptor [Source:VB Community Annotation;Acc:AGAP002639]
Ac_Abf	2R	AGAP002640	24857474	24859095	Or38		odorant receptor [Source:VB Community Annotation;Acc:AGAP002640]
Ac_Abf	2R	AGAP002642	24891704	24894264			DNA mismatch repair protein MSH5 [Source:VB External Description;Acc:AGAP002642]
Ac_Abf	2R	AGAP002644	24919689	24940588			phospholipid-translocating ATPase [Source:VB External Description;Acc:AGAP002644]
Ac_Abf	2R	AGAP013264	24948720	24949426			
Ac_Abf	2R	AGAP013050	24949912	24950590			
Ac_Abf	2R	AGAP013113	24950967	24951681			

Ac_Abf	2R	AGAP013369	24953935	24954646			
Ac_Abf	2R	AGAP013448	24955085	24955774			
Ac_Abf	2R	AGAP002646	24959689	24961156			cyclin-dependent kinase 7 [Source:VB External Description;Acc:AGAP002646]
Ac_Abf	2R	AGAP002647	24961740	24973933			phosphorylase kinase gamma subunit [Source:VB External Description;Acc:AGAP002647]
Ac_Abf	2R	AGAP002645	24944159	24959244			septin 2 [Source:VB External Description;Acc:AGAP002645]
Ac_Abf	2R	AGAP002641	24889907	24890303			
Ac_Abf	2R	AGAP013316	24888935	24889563			
Ac_Abf	2R	AGAP013247	24887231	24887946			
Ac_Abf	2R	AGAP013484	24881361	24882076			
Ac_Abf	2R	AGAP013110	24877895	24878576			
Ac_Abf	2R	AGAP013353	24876664	24877349			
Ac_Abf	2R	AGAP013322	24875495	24876175			

Ac_Abf	2R	AGAP013225	24872733	24873411			
Ac_Abf	2R	AGAP013456	24871016	24871694			
Ac_Abf	2R	AGAP013086	24869480	24870154			
Ac_Abf	2R	AGAP013517	24867791	24868460			
Ac_Abf	2R	AGAP013045	24822272	24822694			
Ac_Abf	2R	AGAP002643	24908246	24909052			
Ac_Abf	2R	AGAP002648	25077385	25088084			rapsynoid [Source:VB External Description;Acc:AGAP002648]
Ac_Abf	2R	AGAP002650	25130272	25131563			
Ac_Abf	2R	AGAP002652	25163895	25166904			
Ac_Abf	2R	AGAP002655	25188318	25195541			
Ac_Abf	2R	AGAP002656	25196705	25203337			general transcription factor 3C polypeptide 1 [Source:VB External Description;Acc:AGAP002656]
Ac_Abf	2R	AGAP002658	25205095	25205361			small nuclear ribonucleoprotein polypeptide F [Source:VB External Description;Acc:AGAP002658]

Ac_Abf	2R	AGAP002661	25208503	25209884			delta(3,5)-Delta(2,4)-dienoyl-CoA isomerase [Source:VB External Description;Acc:AGAP002661]
Ac_Abf	2R	AGAP002662	25210173	25213087			CDP-diacylglycerol--glycerol-3-phosphate 3-phosphatidyltransferase [Source:VB External Description;Acc:AGAP002662]
Ac_Abf	2R	AGAP002659	25205541	25208321			solute carrier family 10 (sodium/bile acid cotransporter) [Source:VB External Description;Acc:AGAP002659]
Ac_Abf	2R	AGAP002657	25203303	25204572			
Ac_Abf	2R	AGAP002654	25181331	25187768			
Ac_Abf	2R	AGAP002653	25166906	25168623			phenylalanyl-tRNA synthetase alpha chain [Source:VB External Description;Acc:AGAP002653]
Ac_Abf	2R	AGAP002651	25142459	25161648		IAP6	baculoviral IAP repeat-containing protein 6 (apollon) [Source:VB External Description;Acc:AGAP002651]
Ac_Abf	2R	AGAP013321	25110055	25135569			
Ac_Abf	2R	AGAP002649	25095636	25102149			
Ac_Abf	2R	AGAP013344	25175993	25176786			
Ac_Abf	2R	AGAP002663	25251748	25252905			
Ac_Abf	2R	AGAP002665	25255484	25259257			

Ac_Abf	2R	AGAP002667	25262177	25264178			translationally-controlled tumor protein homolog [Source:VB External Description;Acc:AGAP002667]
Ac_Abf	2R	AGAP002668	25264714	25266144			
Ac_Abf	2R	AGAP013131	25265715	25266044			
Ac_Abf	2R	AGAP002670	25271138	25276775			
Ac_Abf	2R	AGAP002671	25281239	25287524			beta-1,3-galactosyltransferase 1 [Source:VB External Description;Acc:AGAP002671]
Ac_Abf	2R	AGAP013200	25394913	25397951			
Ac_Abf	2R	AGAP002674	25378949	25391048			dolichyl-phosphate-mannose-protein mannosyltransferase [Source:VB External Description;Acc:AGAP002674]
Ac_Abf	2R	AGAP002672	25293700	25307724			
Ac_Abf	2R	AGAP002669	25266143	25268478			flap endonuclease GEN [Source:VB External Description;Acc:AGAP002669]
Ac_Abf	2R	AGAP002666	25260024	25261685			dolichyldiphosphatase [Source:VB External Description;Acc:AGAP002666]
Ac_Abf	2R	AGAP002664	25253791	25255045			mediator of RNA polymerase II transcription subunit 27 [Source:VB External Description;Acc:AGAP002664]
Ac_Abf	2R	AGAP002677	25392238	25556374			coiled-coil domain-containing protein lobo homolog [Source:VB External Description;Acc:AGAP002677]

Ac_Abf	2R	AGAP002679	25576295	25578207	GPRNNA6		putative GPCR class a orphan receptor 6 [Source:VB Community Annotation;Acc:AGAP002679]
Ac_Abf	2R	AGAP002681	25601816	25603575			
Ac_Abf	2R	AGAP002682	25604227	25609445			lysine-specific demethylase 3 [Source:VB External Description;Acc:AGAP002682]
Ac_Abf	2R	AGAP002684	25611523	25614470			ribosomal RNA-processing protein 1 [Source:VB External Description;Acc:AGAP002684]
Ac_Abf	2R	AGAP002686	25617892	25620182			5'-AMP-activated protein kinase, catalytic alpha subunit [Source:VB External Description;Acc:AGAP002686]
Ac_Abf	2R	AGAP013116	25568803	25572676			
Ac_Abf	2R	AGAP002688	25624636	25638337			
Ac_Abf	2R	AGAP013006	25627867	25629534			
Ac_Abf	2R	AGAP002687	25620254	25624299			ATP-dependent RNA helicase DHX37/DHR1 [Source:VB External Description;Acc:AGAP002687]
Ac_Abf	2R	AGAP002685	25614644	25617611	APG8	APG8	autophagy related gene [Source:VB Community Annotation;Acc:AGAP002685]
Ac_Abf	2R	AGAP002683	25609516	25611208			dolichol kinase [Source:VB External Description;Acc:AGAP002683]
Ac_Abf	2R	AGAP002680	25597969	25601420			serologically defined colon cancer antigen 1 [Source:VB External Description;Acc:AGAP002680]

Ac_Abf	2R	AGAP002678	25558873	25562578			
Ac_Abf	2R	AGAP002711	25936374	25944762			
Ac_Abf	2R	AGAP002712	26014517	26044178			stardust, isoform B [Source:VB External Description;Acc:AGAP002711]
Ac_Abf	2R	AGAP002715	26053186	26054334			
Ac_Abf	2R	AGAP002717	26150873	26163737			
Ac_Abf	2R	AGAP002719	26166839	26169646			ATP-dependent permease MDL1 [Source:VB External Description;Acc:AGAP002717]
Ac_Abf	2R	AGAP002720	26205131	26227733			potassium voltage-gated channel Eag-related subfamily H, invertebrate [Source:VB External Description;Acc:AGAP002719]
Ac_Abf	2R	AGAP002718	26232458	26234417			cathepsin O [Source:VB External Description;Acc:AGAP002720]
Ac_Abf	2R	AGAP002713	26170969	26182520			4-coumarate:CoA ligase isoform 2 [Source:VB External Description;Acc:AGAP002718]
Ac_Abf	2R	AGAP002710	26054432	26055142			mitochondrial 39S ribosomal protein L49 [Source:VB External Description;Acc:AGAP002713]
Ac_Abf	2R	AGAP002709	26006547	26012382			
Ac_Abf	2R	AGAP002487	26001233	26004244			

Ac_Abf	2R	AGAP002742	21939648	21956160			
Ac_Abf	2R	AGAP002748	26448416	26563250			histone-lysine N-methyltransferase MLL1 [Source:VB External Description;Acc:AGAP002741]
Ac_Abf	2R	AGAP002751	26565615	26566673			dynactin 3 [Source:VB External Description;Acc:AGAP002742]
Ac_Abf	2R	AGAP002752	26644368	26657285			novel protein kinase C [Source:VB External Description;Acc:AGAP002748]
Ac_Abf	2R	AGAP002754	26667682	26669121			
Ac_Abf	2R	AGAP002757	26670074	26672699			DnaJ (Hsp40) homolog, subfamily C, member 3 [Source:VB External Description;Acc:AGAP002752]
Ac_Abf	2R	AGAP002756	26674578	26675826	Rpl35a		60S ribosomal protein L35a [Source:VB Community Annotation;Acc:AGAP002754]
Ac_Abf	2R	AGAP002755	26717517	26747494			
Ac_Abf	2R	AGAP002753	26729415	26730635			
Ac_Abf	2R	AGAP002747	26718948	26720234			
Ac_Abf	2R	AGAP002745	26673293	26674190			
Ac_Abf	2R	AGAP013160	26637244	26637783			

Ac_Abf	2R	AGAP002744	26611084	26612442			
Ac_Abf	2R	AGAP013298	26597596	26599494			
Ac_Abf	2R	AGAP002743	26587691	26589824			
Ac_Abf	2R	AGAP013025	26577451	26583298			
Ac_Abf	2R	AGAP002758	26567142	26568059			
Ac_Abf	2R	AGAP002760	26616737	26618119			
Ac_Abf	2R	AGAP002762	26775064	26778865			E3 ubiquitin-protein ligase RNF115/126 [Source:VB External Description;Acc:AGAP002758]
Ac_Abf	2R	AGAP013363	26782298	26787306			topoisomerase (DNA) II binding protein 1 [Source:VB External Description;Acc:AGAP002760]
Ac_Abf	2R	AGAP013285	26790354	26793054			T-complex protein 1 subunit eta [Source:VB External Description;Acc:AGAP002762]
Ac_Abf	2R	AGAP002763	26793376	26795314	IR7i		ionotropic receptor IR7i [Source:VB Community Annotation;Acc:AGAP013363]
Ac_Abf	2R	AGAP013416	26795525	26797440	IR7u		ionotropic receptor IR7u [Source:VB Community Annotation;Acc:AGAP013285]
Ac_Abf	2R	AGAP002764	26797736	26799713	IR7t		ionotropic receptor IR7t [Source:VB Community Annotation;Acc:AGAP002763]

Ac_Abf	2R	AGAP002770	26799941	26801942	IR7w		ionotropic receptor IR7w [Source:VB Community Annotation;Acc:AGAP013416]
Ac_Abf	2R	AGAP002769	26829604	26831375			
Ac_Abf	2R	AGAP002767	26856741	26858441			tubulin, alpha 1 [Source:VB External Description;Acc:AGAP002770]
Ac_Abf	2R	AGAP002766	26852633	26854309			C-4 methylsterol oxidase [Source:VB External Description;Acc:AGAP002769]
Ac_Abf	2R	AGAP002765	26839004	26848674			C-4 methylsterol oxidase [Source:VB External Description;Acc:AGAP002767]
Ac_Abf	2R	AGAP013026	26834132	26835745			C-4 methylsterol oxidase [Source:VB External Description;Acc:AGAP002766]
Ac_Abf	2R	AGAP002761	26832458	26833605			
Ac_Abf	2R	AGAP002759	26823707	26824588			
Ac_Abf	2R	AGAP002484	26787557	26789781			3-methylcrotonyl-CoA carboxylase beta subunit [Source:VB External Description;Acc:AGAP002761]
Ac_Abf	2R	AGAP002483	26779138	26781519			T-complex protein 1 subunit gamma [Source:VB External Description;Acc:AGAP002759]
Ac_Abf	2R	AGAP002482	21883063	21884163			epidermal retinal dehydrogenase [Source:VB External Description;Acc:AGAP002484]
Ac_Abf	2R	AGAP002481	21881646	21882666			ketohexokinase [Source:VB External Description;Acc:AGAP002483]

Ac_Abf	2R	AGAP003917	21877534	21879254			lysophosphatidylglycerol acyltransferase 1 [Source:VB External Description;Acc:AGAP002482]
Ac_Abf	2R	AGAP003920	21870599	21873614			26S proteasome regulatory subunit N1 [Source:VB External Description;Acc:AGAP002481]
Ac_Abf	2R	AGAP003923	46108009	46246976			
Ac_Abf	2R	AGAP003925	46255351	46258013			peptide alpha-N-acetyltransferase [Source:VB External Description;Acc:AGAP003917]
Ac_Abf	2R	AGAP013418	46267089	46267859			
Ac_Abf	2R	AGAP003926	46293559	46295520			Histone-arginine methyltransferase CARMER [Source:VB External Description;Acc:AGAP003923]
Ac_Abf	2R	AGAP003927	46338988	46354919			kinesin family member 1/13/14 [Source:VB External Description;Acc:AGAP003925]
Ac_Abf	2R	AGAP003930	46358979	46361681			
Ac_Abf	2R	AGAP003931	46361954	46364584			
Ac_Abf	2R	AGAP003929	46365499	46366232			Insulin-like peptide 5 [Source:VB External Description;Acc:AGAP003927]
Ac_Abf	2R	AGAP003928	46389527	46391890			
Ac_Abf	2R	AGAP013479	46405340	46434655			

Ac_Abf	2R	AGAP003924	46370360	46374845			Matrix metallopeptidase 16 (membrane-inserted) [Source:VB External Description;Acc:AGAP003929]
Ac_Abf	2R	AGAP003922	46366613	46368408			alpha-1,3-glucosyltransferase [Source:VB External Description;Acc:AGAP003928]
Ac_Abf	2R	AGAP003921	46320056	46321262			
Ac_Abf	2R	AGAP003919	46300383	46315784			
Ac_Abf	2R	AGAP003918	46290565	46291708			
Ac_Abf	2R	AGAP003933	46267922	46284492			Voltage-gated ion channel [Source:VB External Description;Acc:AGAP003921]
Ac_Abf	2R	AGAP003935	46265509	46266319			
Ac_Abf	2R	AGAP003940	46261308	46263981			
Ac_Abf	2R	AGAP013032	46512709	46515515			
Ac_Abf	2R	AGAP003942	46543806	46544911			20S proteasome subunit alpha 1 [Source:VB External Description;Acc:AGAP003935]
Ac_Abf	2R	AGAP003944	46587892	46593828			
Ac_Abf	2R	AGAP003945	46603720	46606516			

Ac_Abf	2R	AGAP003943	46608775	46610857			
Ac_Abf	2R	AGAP003941	46668190	46684617			
Ac_Abf	2R	AGAP003939	46708274	46742083			olypyrimidine tract-binding protein 2 [Source:VB External Description;Acc:AGAP003945]
Ac_Abf	2R	AGAP003938	46613341	46620432			regulatory factor X 1/2/3 [Source:VB External Description;Acc:AGAP003943]
Ac_Abf	2R	AGAP003936	46607896	46608567			LYR motif-containing protein 5 [Source:VB External Description;Acc:AGAP003941]
Ac_Abf	2R	AGAP003934	46558397	46565027			
Ac_Abf	2R	AGAP002480	46554946	46556602			
Ac_Abf	2R	AGAP002477	46544899	46545455			small nuclear ribonucleoprotein D2 [Source:VB External Description;Acc:AGAP003936]
Ac_Abf	2R	AGAP003937	46532070	46537664			battenin [Source:VB External Description;Acc:AGAP003934]
Ac_Abf	2R	AGAP002451	21870041	21870523			
Ac_Abf	2R	AGAP002492	21861926	21862637			single-stranded DNA-binding protein, mitochondrial [Source:VB External Description;Acc:AGAP002477]
Ac_Abf	2R	AGAP002493	46545896	46551286			

Ac_Abf	2R	AGAP002315	21532053	21540998	SCRB1	SCRB1	Class B Scavenger Receptor (CD36 domain). [Source:VB Community Annotation;Acc:AGAP002451]
Ac_Abf	2R	AGAP002475	21977203	21982865			nuclear respiratory factor 1 [Source:VB External Description;Acc:AGAP002492]
Ac_Abf	2R	AGAP002476	21991493	21999397			
Ac_Abf	2R	AGAP002478	19231025	19483421	APG16L	APG16L	autophagy related gene [Source:VB Community Annotation;Acc:AGAP002315]
Ac_Abf	2R	AGAP002485	21854891	21856897			
Ac_Abf	2R	AGAP013525	21857345	21861615			
Ac_Abf	2R	AGAP013486	21863492	21865841			cyclin B [Source:VB External Description;Acc:AGAP002478]
Ac_Abf	2R	AGAP013007	21893980	21896055			
Ac_Abf	2R	AGAP002486	21897775	21900484			
Ac_Abf	2R	AGAP013595	21901266	21903188			
Ac_Abf	2R	AGAP013657	21919565	21923099			
Ac_Abf	2R	AGAP013684	21925672	21927097			

Ac_Abf	2R	AGAP002750	26027297	26027390			
Ac_Abf	2R	AGAP002368	26218104	26218195			
Ac_Abf	2L	AGAP002561	25309069	25309151			
Ac_Abf	2R	AGAP002562	23887765	23887850			
Ac_Abf	2R	AGAP002673	26666080	26666161			tRNA-Ser [Source:VB RNA Description;Acc:AGAP002750]
Ac_Abf	2R	AGAP002660	20698736	20698817			tRNA-Ser [Source:VB RNA Description;Acc:AGAP002368]
Ac_Abf	2R	AGAP002676	22854518	22854590			tRNA-Ala [Source:VB RNA Description;Acc:AGAP002561]
Ac_Abf	2R	AGAP002749	22868372	22868444			tRNA-Ala [Source:VB RNA Description;Acc:AGAP002562]
Ac_Abf	2R	AGAP002746	25327854	25327925			tRNA-Thr [Source:VB RNA Description;Acc:AGAP002673]
Ac_Abf	2R	AGAP002590	25207247	25207318			tRNA-Glu [Source:VB RNA Description;Acc:AGAP002660]
Ac_Abf	2R	AGAP002310	25510326	25510421			tRNA-Tyr [Source:VB RNA Description;Acc:AGAP002676]
Ac_Abf	2R	AGAP002708	26665624	26665705			tRNA-Ser [Source:VB RNA Description;Acc:AGAP002749]

Ac_Abf	2R	AGAP002741	26626314	26626389			tRNA-Pseudo [Source:VB RNA Description;Acc:AGAP002746]
Ac_Abf	2R	AGAP003914	23459367	23459439			tRNA-Ala [Source:VB RNA Description;Acc:AGAP002590]
Ac_Ag	2L	AGAP005831	22279213	22283130			E3 ubiquitin-protein ligase Topors [Source:VB External Description;Acc:AGAP005831]
Ac_Ag	2L	AGAP005832	22284707	22295257			
Ac_Ag	2L	AGAP005833	22295976	22297899	COEJHE1E		carboxylesterase juvenile hormone esterase [Source:VB Community Annotation;Acc:AGAP005833]
Ac_Ag	2L	AGAP005834	22298997	22304146	COEJHE2E		carboxylesterase [Source:VB Community Annotation;Acc:AGAP005834]
Ac_Ag	2L	AGAP005835	22310958	22312826	COEJHE3E		carboxylesterase juvenile hormone esterase [Source:VB Community Annotation;Acc:AGAP005835]
Ac_Ag	2L	AGAP005836	22313684	22315544	COEJHE4E		carboxylesterase juvenile hormone esterase [Source:VB Community Annotation;Acc:AGAP005836]
Ac_Ag	2L	AGAP005837	22316476	22318579	COEJHE5E		carboxylesterase [Source:VB Community Annotation;Acc:AGAP005837]
Ac_Ag	2L	AGAP005838	22321985	22327760			
Ac_Ag	2L	AGAP005839	22337247	22358013			MFS transporter, FLVCR family, feline leukemia virus subgroup C receptor-relat [Source:VB External Description;Acc:AGAP005839]
Ac_Ag	2L	AGAP005840	22376630	22417899			

Ac_Ag	2L	AGAP005841	22418105	22419345			
Ac_Ag	2L	AGAP005842	22420222	22420962			
Ac_Ag	2L	AGAP005843	22422914	22423937			
Ac_Ag	2L	AGAP005844	22424221	22425368			
Ac_Ag	2L	AGAP005845	22427237	22434841			V-type H+-transporting ATPase subunit C [Source:VB External Description;Acc:AGAP005845]
Ac_Ag	2L	AGAP006272	28931170	29014318			fyn-related kinase [Source:VB External Description;Acc:AGAP006270]
Ac_Ag	2L	AGAP006273	29019477	29020812			
Ac_Ag	2L	AGAP006274	29021062	29023548	ABCB3		ATP-binding cassette, subfamily B (MDR/TAP), member 8 [Source:VB External Description;Acc:AGAP006273]
Ac_Ag	2L	AGAP006275	29080921	29116487			
Ac_Ag	2L	AGAP006276	29082536	29083876			
Ac_Ag	2L	AGAP006277	29156992	29168076			
Ac_Ag	2L	AGAP006278	29181553	29215450			

Ac_Ag	2L	AGAP007104	29235061	29236536			
Ac_Ag	2L	AGAP007105	42690394	42780336			Calsyntenin-1 [Source:VB External Description;Acc:AGAP007103]
Ac_Ag	2L	AGAP007106	42784519	42792836			farnesyl diphosphate synthase [Source:VB External Description;Acc:AGAP007104]
Ac_Ag	2L	AGAP007107	42795728	42798687			
Ac_Ag	2L	AGAP007108	42800362	42817607			ubiquitin carboxyl-terminal hydrolase 47 [Source:VB External Description;Acc:AGAP007106]
Ac_Ag	2L	AGAP007109	42819885	42821706			DnaJ homolog subfamily B member 4 [Source:VB External Description;Acc:AGAP007107]
Ac_Ag	2L	AGAP007110	42825338	42829315			multiple PDZ domain protein [Source:VB External Description;Acc:AGAP007108]
Ac_Ag	2L	AGAP007111	42860665	42862101			
Ac_Ag	2L	AGAP007112	42914490	42939104			protein vein [Source:VB External Description;Acc:AGAP007110]
Ac_Ag	2L	AGAP007113	42952626	42955131			uracil phosphoribosyltransferase [Source:VB External Description;Acc:AGAP007111]
Ac_Ag	2L	AGAP007114	42955322	42957554			Pescadillo homolog [Source:VB External Description;Acc:AGAP007112]
Ac_Ag	2L	AGAP007115	42957994	42965130			1-acyl-sn-glycerol-3-phosphate acyltransferase gamma [Source:VB External Description;Acc:AGAP007113]

Ac_Ag	2L	AGAP007116	42980745	42991016			RING finger and CCCH-type zinc finger domain-containing protein [Source:VB External Description;Acc:AGAP007114]
Ac_Ag	2L	AGAP007117	43020195	43022049			
Ac_Ag	2L	AGAP007118	43022683	43024117			
Ac_Ag	2L	AGAP007119	43026304	43028115			
Ac_Ag	2L	AGAP007120	43031102	43039124			
Ac_Ag	2L	AGAP007121	43040522	43043135			Sideroflexin 1,2,3 [Source:VB External Description;Acc:AGAP007119]
Ac_Ag	2L	AGAP007122	43043577	43044650			nucleoside-diphosphate kinase [Source:VB External Description;Acc:AGAP007120]
Ac_Ag	2L	AGAP007123	43045845	43049930			cytochrome b5 protein [Source:VB External Description;Acc:AGAP007121]
Ac_Ag	2L	AGAP007124	43050145	43051673			Tubulin, alpha 1 [Source:VB External Description;Acc:AGAP007122]
Ac_Ag	2L	AGAP007125	43053485	43057667			sarcosine dehydrogenase [Source:VB External Description;Acc:AGAP007123]
Ac_Ag	2L	AGAP007126	43058730	43063265			
Ac_Ag	2L	AGAP007127	43064656	43066267			Glutamate-rich WD repeat-containing protein 1 [Source:VB External Description;Acc:AGAP007125]

Ac_Ag	2L	AGAP028290	43066288	43069315			DNA mismatch repair protein PMS2 [Source:VB External Description;Acc:AGAP007126]
Ac_Ag	2L	AGAP006270	43076933	43098986			regulator of G-protein signaling [Source:VB External Description;Acc:AGAP007127]
Ac_Ag	2R	AGAP007103	40596519	40621367			long-chain acyl-CoA synthetase [Source:VB External Description;Acc:AGAP003623]
Ac_Ag	2R	AGAP003624	40641932	40643027			
Ac_Ag	2R	AGAP003625	40674640	40683555	CTL8	CTL8	C-Type Lectin (CTL) [Source:VB Community Annotation;Acc:AGAP003625]
Ac_Ag	2R	AGAP013153	40685112	40685944			
Ac_Ag	2R	AGAP013221	40688706	40690136			
Ac_Ag	2R	AGAP012946	40692804	40694168			
Ac_Ag	2R	AGAP003627	40695309	40696459			
Ac_Ag	2R	AGAP003630	40723859	40724443			
Ac_Ag	2R	AGAP003631	40725964	40738059	GPRGRP2		putative gastrin/bombesin receptor 2 [Source:VB Community Annotation;Acc:AGAP003631]
Ac_Ag	2R	AGAP003629	40698086	40705049			5'-nucleotidase [Source:VB External Description;Acc:AGAP003629]

Ac_Ag	2R	AGAP003626	40687126	40688303			
Ac_Ag	2R	AGAP003635	40795993	40800819			
Ac_Ag	2R	AGAP003636	40803578	40805894			inositol oxygenase [Source:VB External Description;Acc:AGAP003636]
Ac_Ag	2R	AGAP003632	40782890	40785367			U3 small nucleolar RNA-associated protein 14 [Source:VB External Description;Acc:AGAP003632]
Ac_Ag	2R	AGAP003633	40786307	40793705			
Ac_Ag	2R	AGAP003874	44897794	44910947			uridine kinase [Source:VB External Description;Acc:AGAP003874]
Ac_Ag	2R	AGAP003875	44918572	44919063			
Ac_Ag	2R	AGAP003876	44970189	44971520			bHLH factor, other [Source:VB External Description;Acc:AGAP003876]
Ac_Ag	2R	AGAP013059	45076118	45078303			
Ac_Ag	2R	AGAP003878	45078840	45081167			
Ac_Ag	2R	AGAP003880	45240521	45241732			
Ac_Ag	2R	AGAP003877	45069739	45071073			

Ac_Ag	2R	AGAP003879	45082311	45083822			V-type H+-transporting ATPase S1 subunit [Source:VB External Description;Acc:AGAP003879]
Ac_Ag	2R	AGAP004030	47930721	47970933			intron-binding protein aquarius [Source:VB External Description;Acc:AGAP004028]
Ac_Ag	2R	AGAP004031	47972284	47973328			dynein light intermediate chain, axonemal [Source:VB External Description;Acc:AGAP004030]
Ac_Ag	2R	AGAP004029	47973189	47975013			Mitochondrial electron transfer flavoprotein subunit alpha [Source:VB External Description;Acc:AGAP004031]
Ac_Ag	2R	AGAP004026	47971044	47972122			DNA excision repair protein ERCC-1 [Source:VB External Description;Acc:AGAP004029]
Ac_Ag	2R	AGAP004033	47949596	47963509	GPRMTH6		methuselah receptor 6 [Source:VB Community Annotation;Acc:AGAP004026]
Ac_Ag	2R	AGAP004034	48125098	48149667			
Ac_Ag	2R	AGAP013324	48168169	48176891	GPRNNA4		putative GPCR class a orphan receptor 4 [Source:VB Community Annotation;Acc:AGAP004034]
Ac_Ag	2R	AGAP004035	48217344	48233118			putative G-protein coupled receptor GPCR [Source:VB External Description;Acc:AGAP013324]
Ac_Ag	2R	AGAP004032	48240411	48249362	GPRFSH		putative glyco-protein hormone fsh-like receptor [Source:VB Community Annotation;Acc:AGAP004035]
Ac_Ag	2R	AGAP003623	48015213	48044827			alpha-mannosidase [Source:VB External Description;Acc:AGAP004032]
Ac_Ag	3R	AGAP004028	45853445	45854470	GSTMS3		glutathione transferase microsomal [Source:VB Community Annotation;Acc:AGAP009946]

Ac_Ag	3R	AGAP009946	45880431	45902599			Beat protein [Source:VB External Description;Acc:AGAP009947]
Ac_Ag	3R	AGAP009947	46015350	46015969			signal recognition particle subunit SRP19 [Source:VB External Description;Acc:AGAP009948]
Ac_Ag	3R	AGAP009948	46040593	46042994			oxidoreductase GLYR1 homolog [Source:VB External Description;Acc:AGAP009949]
Ac_Ag	3R	AGAP009949	46097218	46105196			
Ac_Ag	3R	AGAP009950	46148454	46164104			
Ac_Ag	3R	AGAP009951	46164412	46166463			ELAV (embryonic lethal, abnormal vision, Drosophila)-like 1 [Source:VB External Description;Acc:AGAP009952]
Ac_Ag	3R	AGAP009952	46187605	46206053			guanine nucleotide-binding protein G(I)/G(S)/G(O) subunit gamma-13 [Source:VB External Description;Acc:AGAP009953]
Ac_Ag	3R	AGAP009953	46297393	46302538			Ankyrin repeat domain-containing protein 13C [Source:VB External Description;Acc:AGAP009954]
Ac_Ag	3R	AGAP009954	46304184	46318858			
Ac_Ag	3R	AGAP009955	46320550	46322002			
Ac_Ag	3R	AGAP009956	46464354	46465412			transcription factor SOX1/3/14/21 (SOX group B) [Source:VB External Description;Acc:AGAP009957]
Ac_Ag	3R	AGAP009957	46570723	46574186			arginine and glutamate-rich protein 1 [Source:VB External Description;Acc:AGAP009958]

Ac_Ag	3R	AGAP009958	46576255	46583408			tubulin monoglycylase TTLL3/8 [Source:VB External Description;Acc:AGAP009959]
Ac_Ag	3R	AGAP009959	46585643	46588138			tubulin monoglycylase TTLL3/8 [Source:VB External Description;Acc:AGAP009960]
Ac_Ag	2L	AGAP009960	43033828	43033923			
G_Ag	2L	AGAP004708	2471997	2474401			arginyl-tRNA synthetase [Source:VB External Description;Acc:AGAP004708]
G_Ag	2L	AGAP004709	2482553	2483310			large subunit ribosomal protein L18 [Source:VB External Description;Acc:AGAP004709]
G_Ag	2L	AGAP004710	2483226	2483631			ubiquinol-cytochrome c reductase subunit 9 [Source:VB External Description;Acc:AGAP004710]
G_Ag	2L	AGAP004711	2487770	2489611			ATP-dependent RNA helicase DDX41 [Source:VB External Description;Acc:AGAP004711]
G_Ag	2L	AGAP004712	2506572	2507341			
G_Ag	2L	AGAP004713	2559360	2559808			
G_Ag	2L	AGAP004714	2573498	2574460			
G_Ag	2L	AGAP004715	2615657	2620722			Pyruvate dehydrogenase phosphatase regulatory subunit, mitochondrial [Source:VB External Description;Acc:AGAP004715]
G_Ag	2L	AGAP004716	2624121	2627818	Gr57		gustatory receptor [Source:VB Community Annotation;Acc:AGAP004716]

G_Ag	2L	AGAP004717	2643650	2679635			
G_Ag	2L	AGAP004718	2687938	2714108			
G_Ag	2L	AGAP004768	3288076	3322501			periodic tryptophan protein 1 [Source:VB External Description;Acc:AGAP004768]
G_Ag	2L	AGAP004769	3297616	3317823			Ras-related protein Rap-1b precursor [Source:VB External Description;Acc:AGAP004769]
G_Ag	2L	AGAP004770	3312046	3312961			female reproductive tract protease GLEANR_896 [Source:VB External Description;Acc:AGAP004770]
G_Ag	2L	AGAP004771	3328939	3340228			
G_Ag	2L	AGAP004772	3348417	3353159			SLIT-ROBO Rho GTPase activating protein [Source:VB External Description;Acc:AGAP004772]
G_Ag	2L	AGAP004773	3360197	3361330			pyruvate dehydrogenase E1 component subunit alpha, mitochondrial [Source:VB External Description;Acc:AGAP004773]
G_Ag	2L	AGAP004774	3389141	3399248			host cell factor [Source:VB External Description;Acc:AGAP004774]
G_Ag	2L	AGAP004775	3401014	3447379			Xaa-Pro dipeptidase [Source:VB External Description;Acc:AGAP004775]
G_Ag	2L	AGAP004776	3402582	3404685			pre-mRNA-processing factor SLU7 [Source:VB External Description;Acc:AGAP004776]
G_Ag	2L	AGAP004777	3405024	3407138			

G_Ag	2L	AGAP004813	3818251	3818511			
G_Ag	2L	AGAP004814	3825668	3826851			
G_Ag	2L	AGAP004815	3831551	3831951			
G_Ag	2L	AGAP004816	3839485	3840411			
G_Ag	2L	AGAP004817	3843984	3852663			protein lingerer [Source:VB External Description;Acc:AGAP004817]
G_Ag	2L	AGAP004818	3858864	3859471			28S ribosomal protein S16, mitochondrial [Source:VB External Description;Acc:AGAP004818]
G_Ag	2L	AGAP004819	3860781	3870396			receptor expression-enhancing protein 5 [Source:VB External Description;Acc:AGAP004819]
G_Ag	2L	AGAP004820	3870994	3872609			RNA 3'-terminal phosphate cyclase [Source:VB External Description;Acc:AGAP004820]
G_Ag	2L	AGAP004823	3915261	3917699			sprouty [Source:VB External Description;Acc:AGAP004823]
G_Ag	2L	AGAP004824	3953334	3982092			translation initiation factor 5B [Source:VB External Description;Acc:AGAP004824]
G_Ag	2L	AGAP004825	3992274	3996433			
G_Ag	2L	AGAP004826	4066369	4068651			

G_Ag	2L	AGAP004827	4120678	4142005			
G_Ag	2L	AGAP004828	4153261	4156465			Bardet-Biedl syndrome 4 protein [Source:VB External Description;Acc:AGAP004828]
G_Ag	2L	AGAP004829	4159876	4171227	GPRNNA11		putative GPCR class a orphan receptor 11 [Source:VB Community Annotation;Acc:AGAP004829]
G_Ag	2L	AGAP004830	4183099	4185754			
G_Ag	2L	AGAP004831	4201432	4202564			
G_Ag	2L	AGAP004832	4214235	4217585			
G_Ag	2L	AGAP004833	4233342	4239866			serine/threonine-protein kinase PRP4 [Source:VB External Description;Acc:AGAP004833]
G_Ag	2L	AGAP004834	4243691	4252291			
G_Ag	2L	AGAP004835	4302587	4323649			
G_Ag	2L	AGAP005070	9483269	9485404			zinc finger CCHC domain-containing protein 8 [Source:VB External Description;Acc:AGAP005070]
G_Ag	2L	AGAP005071	9486328	9493057			calcium release-activated calcium channel protein 1 [Source:VB External Description;Acc:AGAP005071]
G_Ag	2L	AGAP005072	9545863	9554248			

G_Ag	2L	AGAP005073	9564761	9567229			
G_Ag	2L	AGAP005074	9614343	9616139			
G_Ag	2L	AGAP005075	9642985	9651954			
G_Ag	2L	AGAP005076	9657060	9693793			bridging integrator [Source:VB External Description;Acc:AGAP005076]
G_Ag	2L	AGAP005159	10773905	10775953			Ras-related protein Rap-1b [Source:VB External Description;Acc:AGAP005159]
G_Ag	2L	AGAP005160	10785074	10811531			Ras homolog gene family, member A [Source:VB External Description;Acc:AGAP005160]
G_Ag	2L	AGAP005161	10811841	10816977			polynucleotide 5'-hydroxyl-kinase GRC3/NOL9 [Source:VB External Description;Acc:AGAP005161]
G_Ag	2L	AGAP005162	10820811	10847221			dystroglycan 1 [Source:VB External Description;Acc:AGAP005162]
G_Ag	2L	AGAP005163	10907702	10909701			Glucosyl/glucuronosyl transferases [Source:VB External Description;Acc:AGAP005163]
G_Ag	2L	AGAP005164	11054076	11119385			
G_Ag	2L	AGAP005165	11131877	11241906			
G_Ag	2L	AGAP005166	11186428	11190856			

G_Ag	2L	AGAP005167	11192031	11193411			Short chain dehydrogenase/3-oxoacyl-(acyl-carrier protein) reductase [Source:VB External Description;Acc:AGAP005167]
G_Ag	2L	AGAP005168	11195971	11200471			
G_Ag	2L	AGAP005169	11274226	11275949			
G_Ag	2L	AGAP005170	11284393	11334901			
G_Ag	2L	AGAP005171	11337707	11346317			Tctex1 domain-containing protein 4 [Source:VB External Description;Acc:AGAP005171]
G_Ag	2L	AGAP005172	11340609	11341921			
G_Ag	2L	AGAP005173	11368159	11374909			Px serine/threonine kinase [Source:VB External Description;Acc:AGAP005173]
G_Ag	2L	AGAP005174	11376450	11378030			nucleoporin SEH1 [Source:VB External Description;Acc:AGAP005174]
G_Ag	2L	AGAP005175	11378371	11405181			acetyl-CoA carboxylase / biotin carboxylase [Source:VB External Description;Acc:AGAP005175]
G_Ag	2L	AGAP005176	11407606	11409098			cell division control protein 6 [Source:VB External Description;Acc:AGAP005176]
G_Ag	2L	AGAP005177	11409421	11410687			Intraflagellar transport 46 homolog [Source:VB External Description;Acc:AGAP005177]
G_Ag	2L	AGAP005178	11410730	11414253			

G_Ag	2L	AGAP005179	11414718	11415633			
G_Ag	2L	AGAP005180	11415914	11416886			
G_Ag	2L	AGAP005181	11479150	11496824			
G_Ag	2L	AGAP005182	11685185	11686024	OBP41		odorant binding protein [Source:VB Community Annotation;Acc:AGAP005182]
G_Ag	2R	AGAP013620	10851535	10853577	IR75h.1		ionotropic receptor IR75h.1 [Source:VB Community Annotation;Acc:AGAP001811]
G_Ag	2R	AGAP004730	10855568	10857858	IR75h.2		ionotropic receptor IR75h.2 [Source:VB Community Annotation;Acc:AGAP001812]
G_Ag	2R	AGAP004746	10859312	10865032			Cytosolic carboxypeptidase 6 [Source:VB External Description;Acc:AGAP001814]
G_Ag	2R	AGAP004748	10867621	10868082			
G_Ag	2R	AGAP004756	10869932	10870919			
G_Ag	2R	AGAP004755	10886723	10887414			
G_Ag	2R	AGAP004734	10902267	10903524			V-type H+-transporting ATPase subunit G [Source:VB External Description;Acc:AGAP001823]
G_Ag	2R	AGAP004757	10900129	10901647			

G_Ag	2R	AGAP004725	10871574	10878925			TATA-binding protein-associated factor [Source:VB External Description;Acc:AGAP001820]
G_Ag	2R	AGAP013546	10867987	10869000			Homeobox prox 1 [Source:VB External Description;Acc:AGAP001818]
G_Ag	2R	AGAP004743	10866302	10867306			Homeobox prox 1 [Source:VB External Description;Acc:AGAP001816]
G_Ag	2R	AGAP004731	10865042	10866073			
G_Ag	2R	AGAP004744	10860116	10862659			histone H3 [Source:VB External Description;Acc:AGAP001813]
G_Ag	2R	AGAP004754	10846334	10848560	IR75g		ionotropic receptor IR75g [Source:VB Community Annotation;Acc:AGAP013085]
G_Ag	2R	AGAP004735	10897668	10898832			
G_Ag	2R	AGAP004733	11021083	11022159			salivary lipase [Source:VB External Description;Acc:AGAP001825]
G_Ag	2R	AGAP004753	10911118	11032919			
G_Ag	2R	AGAP004727	11116762	11163371	Lg		lipophorin [Source:VB Community Annotation;Acc:AGAP001826]
G_Ag	2R	AGAP004749	11276774	11280461			
G_Ag	2R	AGAP004724	11265311	11269057			hypoxia up-regulated 1 [Source:VB External Description;Acc:AGAP001827]

G_Ag	2R	AGAP004736	19723884	19724691			
G_Ag	2R	AGAP004732	19610696	19658751			
G_Ag	2R	AGAP004751	20487928	20492035			brain tumor protein [Source:VB External Description;Acc:AGAP002344]
G_Ag	2R	AGAP004758	20376396	20387809			
G_Ag	2R	AGAP004762	23163895	23198838			
G_Ag	2R	AGAP004745	23262183	23264345			
G_Ag	2R	AGAP004760	23266440	23272082			
G_Ag	2R	AGAP004737	23278594	23279723			
G_Ag	2R	AGAP004723	23282878	23290569			
G_Ag	2R	AGAP004722	23280868	23282316			
G_Ag	2R	AGAP004720	23272473	23275129			DNA helicase MCM8 [Source:VB External Description;Acc:AGAP002580]
G_Ag	2R	AGAP004726	23275989	23278271			

G_Ag	2R	AGAP004747	23292023	23296228			glycogen(starch) synthase [Source:VB External Description;Acc:AGAP002586]
G_Ag	2R	AGAP004763	23306923	23309356			
G_Ag	2R	AGAP004739	23314050	23314901			
G_Ag	2R	AGAP004721	24496842	24528705			opioid binding protein/cell adhesion molecule-like [Source:VB External Description;Acc:AGAP002628]
G_Ag	2R	AGAP004759	25936374	25944762			
G_Ag	2R	AGAP004741	26014517	26044178			stardust, isoform B [Source:VB External Description;Acc:AGAP002711]
G_Ag	2R	AGAP004750	26053186	26054334			
G_Ag	2R	AGAP004729	26150873	26163737			
G_Ag	2R	AGAP004767	26166839	26169646			ATP-dependent permease MDL1 [Source:VB External Description;Acc:AGAP002717]
G_Ag	2R	AGAP004738	26205131	26227733			potassium voltage-gated channel Eag-related subfamily H, invertebrate [Source:VB External Description;Acc:AGAP002719]
G_Ag	2R	AGAP004765	26239866	26241686	Or28		odorant receptor [Source:VB Community Annotation;Acc:AGAP002722]
G_Ag	2R	AGAP004752	26242045	26242891			

G_Ag	2R	AGAP004740	26246043	26247431			
G_Ag	2R	AGAP004764	26234853	26238591			tryptophan 2,3-dioxygenase [Source:VB External Description;Acc:AGAP002721]
G_Ag	2R	AGAP004728	26232458	26234417			cathepsin O [Source:VB External Description;Acc:AGAP002720]
G_Ag	2R	AGAP004761	26170969	26182520			4-coumarate:CoA ligase isoform 2 [Source:VB External Description;Acc:AGAP002718]
G_Ag	2R	AGAP004742	26054432	26055142			mitochondrial 39S ribosomal protein L49 [Source:VB External Description;Acc:AGAP002713]
G_Ag	2R	AGAP004766	26006547	26012382			
G_Ag	2R	AGAP004719	26001233	26004244			
G_Ag	2R	AGAP028129	26248500	26263468			
G_Ag	2R	AGAP004821	26282085	26283004	CPR9		cuticular protein 9 RR-1 family [Source:VB Community Annotation;Acc:AGAP002726]
G_Ag	2R	AGAP013647	26283345	26283945			
G_Ag	2R	AGAP001811	26285372	26286453			
G_Ag	2R	AGAP001812	26286947	26290237			isocitrate dehydrogenase (NAD+) [Source:VB External Description;Acc:AGAP002728]

G_Ag	2R	AGAP001814	26299185	26302081			protein prenyltransferase alpha subunit repeat containing protein 1 [Source:VB External Description;Acc:AGAP002731]
G_Ag	2R	AGAP001817	26314514	26332411			
G_Ag	2R	AGAP001819	26337577	26338896			
G_Ag	2R	AGAP013470	26339943	26341603			
G_Ag	2R	AGAP001823	26356725	26362523			
G_Ag	2R	AGAP001822	26367279	26395076			
G_Ag	2R	AGAP001820	26428070	26440703			
G_Ag	2R	AGAP001818	26441730	26443236			cleavage and polyadenylation specificity factor subunit 4 [Source:VB External Description;Acc:AGAP013044]
G_Ag	2R	AGAP001816	26443365	26444581			FAD synthetase [Source:VB External Description;Acc:AGAP002740]
G_Ag	2R	AGAP001815	26343487	26353678			histone acetyltransferase MYST4 [Source:VB External Description;Acc:AGAP002735]
G_Ag	2R	AGAP001813	26297612	26298794			iron-sulfur cluster assembly protein [Source:VB External Description;Acc:AGAP002730]
G_Ag	2R	AGAP013085	26291953	26296342			Ras GTPase-activating protein 1 [Source:VB External Description;Acc:AGAP002729]

G_Ag	2R	AGAP001821	26448416	26563250			histone-lysine N-methyltransferase MLL1 [Source:VB External Description;Acc:AGAP002741]
G_Ag	2R	AGAP001825	26565615	26566673			dynactin 3 [Source:VB External Description;Acc:AGAP002742]
G_Ag	2R	AGAP001824	26567142	26568059			
G_Ag	2R	AGAP001826	29198983	29204608			Control protein HCTL029 [Source:VB External Description;Acc:AGAP002909]
G_Ag	2R	AGAP001828	29216218	29216720			Salivary C-type lectin [Source:VB External Description;Acc:AGAP002910]
G_Ag	2R	AGAP001827	29217888	29218455	CTLMA9	CTLMA9	C-Type Lectin (CTL) - mannose binding [Source:VB Community Annotation;Acc:AGAP002911]
G_Ag	2R	AGAP002326	29219995	29220592			Salivary C-type lectin [Source:VB External Description;Acc:AGAP002912]
G_Ag	2R	AGAP002344	29228227	29230310			
G_Ag	2R	AGAP002342	29271073	29301565			galactokinase [Source:VB External Description;Acc:AGAP002914]
G_Ag	2R	AGAP013206	29304390	29399573			
G_Ag	2R	AGAP002579	55211938	55283047			Beat IIb [Source:VB External Description;Acc:AGAP004369]
G_Ag	2R	AGAP002582	55365327	55366257			transcription initiation factor TFIIA small subunit [Source:VB External Description;Acc:AGAP004370]

G_Ag	2R	AGAP002585	55366585	55368425			chondroitin 4-sulfotransferase 11 [Source:VB External Description;Acc:AGAP004371]
G_Ag	2R	AGAP002583	55372537	55394660			Elongation of very long chain fatty acids protein 1 [Source:VB External Description;Acc:AGAP004372]
G_Ag	2R	AGAP002580	56347496	56374324			
G_Ag	2R	AGAP002581	56364927	56366452			UDPglucose--hexose-1-phosphate uridylyltransferase [Source:VB External Description;Acc:AGAP004451]
G_Ag	2R	AGAP002586	56377985	56378218			LSM domain containing 1 [Source:VB External Description;Acc:AGAP013238]
G_Ag	2R	AGAP002587	56391403	56398232			
G_Ag	2R	AGAP002588	56438941	56447468			
G_Ag	2R	AGAP002628	56378236	56378647			
G_Ag	2R	AGAP002711	56483698	56565575	GPRDOP3		GPCR Dopamine Family [Source:VB Community Annotation;Acc:AGAP004453]
G_Ag	2R	AGAP002712	56677086	56677613			
G_Ag	2R	AGAP002715	56703770	56706974			ubiquitin-like 1-activating enzyme E1 A [Source:VB External Description;Acc:AGAP004459]
G_Ag	2R	AGAP002717	56712791	56713727	Rps25		40S ribosomal protein S25 [Source:VB Community Annotation;Acc:AGAP004462]

G_Ag	2R	AGAP002719	56715179	56717620			
G_Ag	2R	AGAP002722	56722803	56725057			centromere/kinetochore protein ZW10 [Source:VB External Description;Acc:AGAP004467]
G_Ag	2R	AGAP002723	56729698	56731889			STE24 endopeptidase [Source:VB External Description;Acc:AGAP004470]
G_Ag	2R	AGAP002724	56734479	56736544			
G_Ag	2R	AGAP002721	56736737	56740049			
G_Ag	2R	AGAP002720	56741249	56744267			
G_Ag	2R	AGAP002718	56740144	56740831			
G_Ag	2R	AGAP002713	56732011	56733549			
G_Ag	2R	AGAP002710	56727502	56729363			Phosphatidylinositol transfer protein, beta, like [Source:VB External Description;Acc:AGAP004469]
G_Ag	2R	AGAP002709	56725193	56726412			Phosducin-like protein [Source:VB External Description;Acc:AGAP004468]
G_Ag	2R	AGAP002725	56718931	56722472			
G_Ag	2R	AGAP002726	56717687	56718713			18S rRNA (adenine1779-N6/adenine1780-N6)-dimethyltransferase [Source:VB External Description;Acc:AGAP004465]

G_Ag	2R	AGAP013513	56713726	56714798			ribosomal RNA-processing protein 17 [Source:VB External Description;Acc:AGAP004463]
G_Ag	2R	AGAP002727	56709929	56712287			solute carrier family 30 (zinc transporter), member 5/7 [Source:VB External Description;Acc:AGAP004461]
G_Ag	2R	AGAP002728	56706871	56709022			sialic acid synthase [Source:VB External Description;Acc:AGAP004460]
G_Ag	2R	AGAP002731	56695814	56702772			Leucine-rich repeat-containing protein 58 [Source:VB External Description;Acc:AGAP004458]
G_Ag	2R	AGAP002732	56689964	56694425			Sugar transporter ERD6-like 4 [Source:VB External Description;Acc:AGAP004457]
G_Ag	2R	AGAP002733	56680939	56682732	GNBPB1	GNBPB1	3-Glucan Binding Protein (BGBP) [Source:VB Community Annotation;Acc:AGAP004455]
G_Ag	2R	AGAP002734	57707832	57709766			
G_Ag	2R	AGAP002736	57717791	57719238			
G_Ag	2R	AGAP002737	57711826	57725049			E3 ubiquitin-protein ligase RNF19A [Source:VB External Description;Acc:AGAP004573]
G_Ag	2R	AGAP002739	57739243	57751530			
G_Ag	2R	AGAP013044	57807624	57809597			
G_Ag	2R	AGAP002740	57853553	57861870	TWDL12		Cuticular protein 12 in TWDL family [Source:VB Community Annotation;Acc:AGAP004576]

G_Ag	2R	AGAP002735	57864434	57866591			
G_Ag	2R	AGAP002730	57877327	57880127			Alkaline phosphatase [Source:VB External Description;Acc:AGAP004578]
G_Ag	2R	AGAP002729	57950856	57952702			
G_Ag	2R	AGAP002741	57989423	57993690			Translin-associated factor X [Source:VB External Description;Acc:AGAP004585]
G_Ag	2R	AGAP002742	57869668	57870711			Vacuolar ATP synthase subunit d 1 [Source:VB External Description;Acc:AGAP013199]
G_Ag	2R	AGAP002743	57754698	57755823			
G_Ag	2R	AGAP002909	57863972	57890966			
G_Ag	2R	AGAP002910	57948151	57949597			cyclin-dependent kinase 2 [Source:VB External Description;Acc:AGAP004579]
G_Ag	2R	AGAP002911	57980100	57984881			
G_Ag	2R	AGAP002912	57956199	57957413			Heat shock protein 70kDa [Source:VB External Description;Acc:AGAP004581]
G_Ag	2R	AGAP002913	57969341	57972240			heat shock 70kDa protein [Source:VB External Description;Acc:AGAP004582]
G_Ag	2R	AGAP002914	57977978	57979236			Heat shock 70kDa protein [Source:VB External Description;Acc:AGAP004583]

G_Ag	2R	AGAP002915	58122901	58125331			
G_Ag	2R	AGAP004369	58125574	58128116			
G_Ag	2R	AGAP004370	58128136	58129364			
G_Ag	2R	AGAP004371	58129430	58130616			
G_Ag	2R	AGAP004372	58131078	58132909			acid phosphatase [Source:VB External Description;Acc:AGAP004591]
G_Ag	2R	AGAP004451	58143737	58163521			EH domain-containing protein 1 [Source:VB External Description;Acc:AGAP004593]
G_Ag	2R	AGAP013238	58230212	58238127	GPRGBB2		putative GABA-B receptor 2 [Source:VB Community Annotation;Acc:AGAP004595]
G_Ag	2R	AGAP004452	58102411	58117330			ADP-ribosylation factor related protein 1 [Source:VB External Description;Acc:AGAP004586]
G_Ag	2R	AGAP013508	58120393	58122482			
G_Ag	2R	AGAP013542	58135368	58142209			splicing factor, arginine/serine-rich 4/5/6 [Source:VB External Description;Acc:AGAP004592]
G_Ag	2R	AGAP004453	58174559	58175623			Cell division protein kinase 2 [Source:VB External Description;Acc:AGAP004594]
G_Ag	2R	AGAP004454	58245636	58251038			pyruvate kinase [Source:VB External Description;Acc:AGAP004596]

G_Ag	2R	AGAP004459	58257284	58258393			guanosine-3',5'-bis(diphosphate) 3'-pyrophosphohydrolase [Source:VB External Description;Acc:AGAP004597]
G_Ag	2R	AGAP004462	58263402	58263935			defense protein 3 [Source:VB External Description;Acc:AGAP004599]
G_Ag	2R	AGAP004464	58294035	58328776			
G_Ag	2R	AGAP004467	58338735	58339503			HYPK [Source:VB External Description;Acc:AGAP004606]
G_Ag	2R	AGAP004470	58346783	58354002			
G_Ag	2R	AGAP004472	58381084	58382774			prolyl 4-hydroxylase [Source:VB External Description;Acc:AGAP004611]
G_Ag	2R	AGAP004473	58391274	58391809			
G_Ag	2R	AGAP004474	58392105	58394400			phosphotransferase LOC123688 [Source:VB External Description;Acc:AGAP004612]
G_Ag	2R	AGAP013052	58410920	58427284	GPRDOP1		GPCR Dopamine Family [Source:VB Community Annotation;Acc:AGAP004613]
G_Ag	2R	AGAP004471	58374159	58390304			
G_Ag	2R	AGAP004469	58360124	58362066			signal recognition particle subunit SRP54 [Source:VB External Description;Acc:AGAP004610]
G_Ag	2R	AGAP004468	58356459	58358680			protein kinase C substrate 80K-H [Source:VB External Description;Acc:AGAP004609]

G_Ag	2R	AGAP004466	58339541	58341592			
G_Ag	2R	AGAP004465	58336575	58337779			zinc finger protein 830 [Source:VB External Description;Acc:AGAP004605]
G_Ag	2R	AGAP004463	58318633	58323306			ATP-binding cassette sub-family C member 12 [Source:VB External Description;Acc:AGAP004603]
G_Ag	2R	AGAP004461	58308421	58316282			ABC transporter family C protein ABCC2 [Source:VB External Description;Acc:AGAP004602]
G_Ag	2R	AGAP004460	58299669	58308241			
G_Ag	2R	AGAP004458	58257922	58259916			phosphoserine aminotransferase [Source:VB External Description;Acc:AGAP004598]
G_Ag	2R	AGAP004457	26395507	26405654	SCRB5	SCRB5	Class B Scavenger Receptor (CD36 domain). [Source:VB Community Annotation;Acc:AGAP002738]
G_Ag	2R	AGAP004455	56684663	56686049	GNBPB5	GNBPB5	3-Glucan Binding Protein (BGBP) [Source:VB Community Annotation;Acc:AGAP004456]
G_Ag	3L	AGAP004574	10908911	10910026		FREP19	
G_Ag	3L	AGAP004573	11180760	11181236	TEP18	TEP6	thioester-containing protein [Source:VB Community Annotation;Acc:AGAP010813]
G_Ag	3L	AGAP004575	11244116	11260285			
G_Ag	3L	AGAP013253	11283363	11288438	TEP11	TEP11	thioester-containing protein [Source:VB Community Annotation;Acc:AGAP010818]

G_Ag	3L	AGAP004576	11302054	11303186			
G_Ag	3L	AGAP013461	11334659	11337261			
G_Ag	3L	AGAP004578	11341631	11342833			
G_Ag	3L	AGAP004580	11443685	11449916			
G_Ag	3L	AGAP004585	11452625	11456200			
G_Ag	3L	AGAP013199	11496992	11498410			
G_Ag	3L	AGAP013469	11513355	11513727	CASPS10		caspase (short class) [Source:VB Community Annotation;Acc:AGAP010827]
G_Ag	3L	AGAP004577	11513998	11522239	CASPS9	CASPS9	Caspase (Short). [Source:VB Community Annotation;Acc:AGAP010828]
G_Ag	3L	AGAP004579	11524693	11531472	CASPS12	CASPS12	Caspase (Short). [Source:VB Community Annotation;Acc:AGAP010829]
G_Ag	3L	AGAP004584	11509509	11510123	CASPS13	CASPS13	Caspase (Short). [Source:VB Community Annotation;Acc:AGAP010826]
G_Ag	3L	AGAP004581	11202091	11206882	TEP1	TEP1	thioester-containing protein [Source:VB Community Annotation;Acc:AGAP010815]
G_Ag	3L	AGAP004582	11215246	11220064	TEP3	TEP3	thioester-containing protein [Source:VB Community Annotation;Acc:AGAP010816]

G_Ag	3L	AGAP004583	11001288	11007349	TEP4	TEP4	thioester-containing protein [Source:VB Community Annotation;Acc:AGAP010812]
G_Ag	3L	AGAP004588	11291103	11295788	TEP10	TEP10	thioester-containing protein [Source:VB Community Annotation;Acc:AGAP010819]
G_Ag	3L	AGAP004589	11185704	11190462	TEP6	TEP5	thioester-containing protein [Source:VB Community Annotation;Acc:AGAP010814]
G_Ag	3R	AGAP004590	28600501	28601320	GSTE7		glutathione S-transferase epsilon class [Source:VB Community Annotation;Acc:AGAP009196]
G_Ag	3R	AGAP013326	28611105	28612148			palmitoyltransferase ZDHHC24 [Source:VB External Description;Acc:AGAP009199]
G_Ag	3R	AGAP004591	28675320	28676719			Ankyrin repeat domain 39 [Source:VB External Description;Acc:AGAP009205]
G_Ag	3R	AGAP004593	28676926	28677635			
G_Ag	3R	AGAP004595	28743955	28745886			
G_Ag	3R	AGAP004586	28811997	28818217	SRPN6	SRPN6	Serine Protease Inhibitor (serpin) [Source:VB Community Annotation;Acc:AGAP009212]
G_Ag	3R	AGAP004587	28824548	28826209	SRPN16	SRPN16	Serine Protease Inhibitor (serpin) [Source:VB Community Annotation;Acc:AGAP009213]
G_Ag	3R	AGAP004592	28830471	28832415	CLIPB11	CLIPB11	Clip-Domain Serine Protease [Source:VB Community Annotation;Acc:AGAP009214]
G_Ag	3R	AGAP004594	28858149	28860047	SRPN5	SRPN5	Serine Protease Inhibitor (serpin) [Source:VB Community Annotation;Acc:AGAP009221]

G_Ag	3R	AGAP004596	28925352	28926128			
G_Ag	3R	AGAP004597	29051567	29053195			
G_Ag	3R	AGAP004599	29061644	29062525			
G_Ag	3R	AGAP004604	29091796	29093554			
G_Ag	3R	AGAP004606	28842176	28843507	CLIPB12	CLIPB12	Clip-Domain Serine Protease [Source:VB Community Annotation;Acc:AGAP009217]
G_Ag	3R	AGAP004608	28835295	28836687	CLIPB18	CLIPB18	Clip-Domain Serine Protease [Source:VB Community Annotation;Acc:AGAP009215]
G_Ag	2R	AGAP004611	26027297	26027390			
G_Ag	2L	AGAP013331	3439935	3440006			
G_Ag	2R	AGAP004612	26218104	26218195			
G_Ag	3L	AGAP004613	10994621	10994693			
G_Ag	3R	AGAP013073	29061165	29064000			Elongation factor Ts, mitochondrial [Source:VB External Description;Acc:AGAP009234]
G_Ag	3R	AGAP004610	28646812	28654237			collagen, type IV, alpha [Source:VB External Description;Acc:AGAP009201]

G_Ag	3R	AGAP004609	28613496	28620808			collagen, type IV, alpha [Source:VB External Description;Acc:AGAP009200]
G_Ag	3R	AGAP004607	29084469	29086834			Engulfment and cell motility protein [Source:VB External Description;Acc:AGAP009236]
G_Ag	3R	AGAP004605	28845073	28846244			
G_Ag	3R	AGAP004603	28870700	28889700			
G_Ag	3R	AGAP004602	29093874	29103367			RanBP-type and C3HC4-type zinc finger-containing protein 1 [Source:VB External Description;Acc:AGAP009239]
G_Ag	3R	AGAP004600	28607056	28610755			
G_Ag	3R	AGAP004598	28571277	28573222			Indanol dehydrogenase [Source:VB External Description;Acc:AGAP009187]
G_Ag	3R	AGAP002738	28897945	28901664			
G_Ag	3R	AGAP004456	28593714	28594762	GSTE6		glutathione S-transferase epsilon class [Source:VB Community Annotation;Acc:AGAP009191]
G_Ag	3R	AGAP013595	28601368	28602280	GSTE3		glutathione S-transferase epsilon class [Source:VB Community Annotation;Acc:AGAP009197]
G_Ag	3R	AGAP013657	28591663	28592475	GSTU4		glutathione S-transferase [Source:VB Community Annotation;Acc:AGAP009190]
G_Ag	3R	AGAP013615	28847921	28849015			

G_Ag	3R	AGAP002325	28809314	28811321			
G_Ag	3R	AGAP002578	28918210	28919685			
G_Ag	3R	AGAP002708	28595948	28596868	GSTE4		glutathione S-transferase epsilon class [Source:VB Community Annotation;Acc:AGAP009193]
G_Ag	3R	AGAP004450	28598871	28599816	GSTE1		glutathione S-transferase epsilon class [Source:VB Community Annotation;Acc:AGAP009195]
G_Ag	3R	AGAP013053	28594993	28595802	GSTE5		glutathione S-transferase epsilon class [Source:VB Community Annotation;Acc:AGAP009192]
G_Ag	3R	AGAP010811	28851788	28853341			
G_Ag	3R	AGAP010813	28573573	28575403			solute carrier family 39 (zinc transporter), member 9 [Source:VB External Description;Acc:AGAP009188]
G_Ag	3R	AGAP010817	28838651	28840291			Clip-domain serine protease [Source:VB External Description;Acc:AGAP009216]
G_Ag	3R	AGAP010818	28597652	28598640	GSTE2		glutathione S-transferase epsilon class [Source:VB Community Annotation;Acc:AGAP009194]
G_Ag	3R	AGAP010820	29087753	29091643			apoptotic chromatin condensation inducer in the nucleus [Source:VB External Description;Acc:AGAP009237]
G_Ag	3R	AGAP010821	29057154	29057744			
G_Ag	3R	AGAP010822	28697024	28745886			extracellular signal-regulated kinase 1/2 [Source:VB External Description;Acc:AGAP009207]

G_Ag	3R	AGAP010823	28673260	28674754			Eukaryotic translation initiation factor 3 subunit H [Source:VB External Description;Acc:AGAP009204]
G_Ag	3R	AGAP010824	28576092	28590073			
G_Ag	3R	AGAP010825	28891750	28893381			Dimeric dihydrodiol dehydrogenase [Source:VB External Description;Acc:AGAP009225]
G_Ag	3R	AGAP010827	28863347	28866812			DNA ligase 1 [Source:VB External Description;Acc:AGAP009222]
G_Ag	3R	AGAP010828	28659350	28670101			SPRY domain-containing SOCS box protein 3 [Source:VB External Description;Acc:AGAP009203]
G_Ag	3R	AGAP010829	28746535	28747439			DNA-directed RNA polymerase II subunit RPB11 [Source:VB External Description;Acc:AGAP009209]
G_Ag	3R	AGAP010826	28654700	28656232			selenoprotein T [Source:VB External Description;Acc:AGAP009202]
G_Ag	3R	AGAP010815	28747856	28807725			CAP-Gly domain-containing linker protein 1 [Source:VB External Description;Acc:AGAP009210]
G_Ag	3R	AGAP010816	28868750	28869684			
G_Ag	3R	AGAP010812	28658820	28659131			
G_Ag	3R	AGAP010819	29051094	29053709			
G_Ag	3R	AGAP010814	29056229	29056820			

G_Ag	3R	AGAP013706	29058175	29058856			
G_Ag	3R	AGAP009196	29059870	29060841			
G_Ag	3R	AGAP009199	29080457	29083273			
G_Ag	3R	AGAP009205	29061644	29062525			
G_Ag	2L	AGAP009206	2865742	2866766			Phospholipase A2, venom [Source:VB External Description;Acc:AGAP004730]
G_Ag	2L	AGAP009208	3030691	3033267			THO complex subunit 5 [Source:VB External Description;Acc:AGAP004746]
G_Ag	2L	AGAP009212	3037963	3038411			
G_Ag	2L	AGAP009213	3066808	3068314			F-box and WD-40 domain protein 4 [Source:VB External Description;Acc:AGAP004756]
G_Ag	2L	AGAP009214	3065637	3066950			Vacuolar protein-sorting-associated protein 36 [Source:VB External Description;Acc:AGAP004755]
G_Ag	2L	AGAP009221	2920492	2930688			PAX-interacting protein 1 [Source:VB External Description;Acc:AGAP004734]
G_Ag	2L	AGAP009228	3069282	3070456			
G_Ag	2L	AGAP009230	2797664	2801444			Eukaryotic translation initiation factor 3 subunit C [Source:VB External Description;Acc:AGAP004725]

G_Ag	2L	AGAP009235	3068708	3069527			
G_Ag	2L	AGAP009238	3020238	3021140			Transmembrane emp24 domain-containing protein [Source:VB External Description;Acc:AGAP004743]
G_Ag	2L	AGAP009217	2867519	2886486			secretory phospholipase A2 [Source:VB External Description;Acc:AGAP004731]
G_Ag	2L	AGAP009215	3021774	3025711			succinyl-CoA synthetase beta subunit [Source:VB External Description;Acc:AGAP004744]
G_Ag	2L	AGAP009234	3063116	3064911	CASPL2	CASPL2	caspase (Long) [Source:VB Community Annotation;Acc:AGAP004754]
G_Ag	2L	AGAP009201	2966120	2967485			
G_Ag	2L	AGAP009200	2917655	2919864			
G_Ag	2L	AGAP009236	3057997	3061847			
G_Ag	2L	AGAP009218	2812213	2814510	Gr25		gustatory receptor [Source:VB Community Annotation;Acc:AGAP004727]
G_Ag	2L	AGAP009224	3038604	3040277			coproporphyrinogen III oxidase [Source:VB External Description;Acc:AGAP004749]
G_Ag	2L	AGAP009239	2775211	2796481			Intraflagellar transport 74 homolog [Source:VB External Description;Acc:AGAP004724]
G_Ag	2L	AGAP009198	2968484	2969976			Mitochondrial GTPase 1 homolog [Source:VB External Description;Acc:AGAP004736]

G_Ag	2L	AGAP009226	2898242	2906165			
G_Ag	2L	AGAP009191	3052358	3056687			condensin-2 complex subunit D3 [Source:VB External Description;Acc:AGAP004751]
G_Ag	2L	AGAP009197	3070600	3072473			
G_Ag	2L	AGAP009190	3150315	3152338			Alpha-tocopherol transfer protein-like protein [Source:VB External Description;Acc:AGAP004762]
G_Ag	2L	AGAP009219	3026512	3030332			transcription elongation regulator 1 [Source:VB External Description;Acc:AGAP004745]
G_Ag	2L	AGAP009211	3080556	3081900			
G_Ag	2L	AGAP009227	2970597	2972774			Rhomboid-4, isoform B [Source:VB External Description;Acc:AGAP004737]
G_Ag	2L	AGAP009193	2756472	2760324			Chromobox protein homolog 1 [Source:VB External Description;Acc:AGAP004723]
G_Ag	2L	AGAP009195	2752424	2753362			Co-chaperone protein HscB, mitochondrial [Source:VB External Description;Acc:AGAP004722]
G_Ag	2L	AGAP009192	2727394	2742060			
G_Ag	2L	AGAP009220	2804809	2807762			Uncharacterized protein CG3556 [Source:VB External Description;Acc:AGAP004726]
G_Ag	2L	AGAP009188	3034074	3037695			Uncharacterized protein C05D11.1 [Source:VB External Description;Acc:AGAP004747]

G_Ag	2L	AGAP009216	3152721	3153806			
G_Ag	2L	AGAP009194	2976111	2977915			H/ACA ribonucleoprotein complex subunit 4 [Source:VB External Description;Acc:AGAP004739]
G_Ag	2L	AGAP009237	2749855	2752163			N-acetylglucosamine-6-sulfatase [Source:VB External Description;Acc:AGAP004721]
G_Ag	2L	AGAP028022	3075360	3076135			oligoribonuclease [Source:VB External Description;Acc:AGAP004759]
G_Ag	2L	AGAP009207	2997029	2998143			serine proteinase [Source:VB External Description;Acc:AGAP004741]
G_Ag	2L	AGAP009204	3041661	3052055			translation initiation factor 4G [Source:VB External Description;Acc:AGAP004750]
G_Ag	2L	AGAP009189	2844659	2847575			
G_Ag	2L	AGAP009225	3194035	3196599			
G_Ag	2L	AGAP009222	2972617	2974653			IK cytokine [Source:VB External Description;Acc:AGAP004738]
G_Ag	2L	AGAP009203	3156536	3159336			ATP-dependent RNA helicase DDX1 [Source:VB External Description;Acc:AGAP004765]
G_Ag	2L	AGAP009209	3056994	3057934			tRNA (guanine-N(7)-)-methyltransferase [Source:VB External Description;Acc:AGAP004752]
G_Ag	2L	AGAP009202	2982984	2983998			Serine collagenase 1 precursor [Source:VB External Description;Acc:AGAP004740]

G_Ag	2L	AGAP009210	3154590	3156095			
G_Ag	2L	AGAP009223	2824043	2831367			
G_Ag	2L	AGAP028058	3127125	3131071			
G_Ag	2L	AGAP028114	2998916	3008084			pyruvate carboxylase [Source:VB External Description;Acc:AGAP004742]
G_Ag	2L	AGAP009231	3163010	3178079			endophilin-A [Source:VB External Description;Acc:AGAP004766]
G_Ag	2L	AGAP028177	2714552	2719933	CLIPC9	CLIPC9	Clip-Domain Serine Protease [Source:VB Community Annotation;Acc:AGAP004719]
G_Ag	2L	AGAP009233	3158856	3159260			
G_Ag	3R	AGAP009232	29001981	29002063			
G_Ag	2R	AGAP028101	58375110	58375302			U2 spliceosomal RNA [Source: RFAM 9.0] [Source:VB RNA Description;Acc:AGAP013615]
G_Ag	3R	AGAP009229	29001980	29002062			
G_Ag	2L	AGAP028267	3876688	3876760			tRNA-Lys [Source:VB RNA Description;Acc:AGAP004821]
G_Ag	2L	AGAP009187	11039420	11039522			